AEDC TR-94-8

Description and Flow Characterization of Hypersonic Facilities

A. Anderson, R. K. Matthews, and J. R. Maus
Calspan Corporation/AEDC Operations

R. A. Crawford
University of Tennessee Space Institute

and

A. H. Boudreau
AEDC/USAF

August 1994

Final Report for Period July 1992 — July 1993

ARNOLD ENGINEERING DEVELOPMENT CENTER
ARNOLD AIR FORCE BASE, TENNESSEE
AIR FORCE MATERIEL COMMAND
UNITED STATES AIR FORCE

NOTICES

When U. S. Government drawings, specifications, or other data are used for any purpose other than a definitely related Government procurement operation, the Government thereby incurs no responsibility nor any obligation whatsoever, and the fact that the Government may have formulated, furnished, or in any way supplied the said drawings, specifications, or other data, is not to be regarded by implication or otherwise, or in any manner licensing the holder or any other person or corporation, or conveying any rights or permission to manufacture, use, or sell any patented invention that may in any way be related thereto.

Qualified users may obtain copies of this report from the Defense Technical Information Center.

References to named commercial products in this report are not to be considered in any sense as an endorsement of the product by the United States Air Force or the Government.

This report has been reviewed by the Office of Public Affairs (PA) and is releasable to the National Technical Information Service (NTIS). At NTIS, it will be available to the general public, including foreign nations.

APPROVAL STATEMENT

This report has been reviewed and approved.

Dennis N Huprich

DENNIS N. HUPRICH, Major, USAF
Space and Missile Systems Test Division

Approved for publication:

FOR THE COMMANDER

Conrad M Ritchey

CONRAD M. RITCHEY, Lt Col, USAF
Space and Missile Systems Test Division

REPORT DOCUMENTATION PAGE

Form Approved
OMB No. 0704-0188

1 AGENCY USE ONLY (Leave blank)	2. REPORT DATE	3. REPORT TYPE AND DATES COVERED
	August 1994	Final Report for July 1992 - July 1993

4. TITLE AND SUBTITLE

Description and Flow Characterization of Hypersonic Facilities

5. FUNDING NUMBERS

JN - 0979

6. AUTHOR(S)

Anderson, A., Matthews, R. K., and Maus, J. R., Calspan Corp./AEDC Operations: Crawford, R. A., Univ. of Tenn. Space Institute; and Boudreau, A. H., Arnold Engineering Development Center

7. PERFORMING ORGANIZATION NAME(S) AND ADDRESS(ES)

Arnold Engineering Development Center/DOF
Air Force Materiel Command
Arnold Air Force Base, TN 37389-4000

8 PERFORMING ORGANIZATION REPORT NUMBER

AEDC-TR-94-8

9. SPONSORING/MONITORING AGENCY NAMES(S) AND ADDRESS(ES)

Arnold Engineering Development Center/DOF
Air Force Materiel Command
Arnold Air Force Base, TN 37389-4000

10. SPONSORING/MONITORING AGENCY REPORT NUMBER

11 SUPPLEMENTARY NOTES

Available in Defense Technical Information Center (DTIC).

12a DISTRIBUTION/AVAILABILITY STATEMENT

Approved for public release; distribution is unlimited.

12b. DISTRIBUTION CODE

13 ABSTRACT (Maximum 200 words)

Hypersonic test facilities will continue to play a major role in the development of hypersonic vehicles. In the past, ground test facilities were often used to perform configuration parametric studies and/or to develop large databases. Future testing will emphasize understanding of fluid physics and validation of codes. Computational fluid dynamics (CFD) has made great progress in the past two decades, but the marriage of CFD and ground testing is clearly a reality today, and will become even more important in the future. One of the challenges for the experimentalist is to develop and utilize facilities that simulate hypersonic flight, and to provide the required data precision to validate CFD codes. This provides a brief review of facility fundamental considerations and simulation issues. It is clear that no one facility will meet the wide variety of test objectives; therefore, the test facilities span a range of size, run time, complexity, and operating cost. Representative facilities are described, as well as their test capabilities, flow quality, and deficiencies.

14 SUBJECT TERMS	15. NUMBER OF PAGES
computational fluid dynamics (CFD), ground testing, high-enthalpy facilities, aerodynamic testing, aerothermal testing	64
	16 PRICE CODE

17 SECURITY CLASSIFICATION OF REPORT	18 SECURITY CLASSIFICATION OF THIS PAGE	19. SECURITY CLASSIFICATION OF ABSTRACT	20 LIMITATION OF ABSTRACT
UNCLASSIFIED	UNCLASSIFIED	UNCLASSIFIED	SAME AS REPORT

FOREWORD

The hypersonic regime is the most severe of all flight regimes, and consequently demands smart utilization of ground testing and evaluation, flight testing, and computation/simulation methodologies. Because of this challenge, von Karman Institute (VKI) asked the Arnold Engineering Development Center (AEDC) to develop a comprehensive course to define the "Methodology of Hypersonic Testing." Seven American scientists and engineers, representing AEDC and the University of Tennessee Space Institute (UTSI), formulated this course from their background of over a century of combined experience in hypersonic testing.

The objective of the course was to present a comprehensive overview of the methods used in hypersonic testing and evaluation, and to explain the principles behind those test techniques. Topics covered include an introduction to hypersonic aerodynamics with descriptions of chemical and gas-dynamic phenomena associated with hypersonic flight; categories and application of various hypersonic ground test facilities; characterization of facility flow fields; measurement techniques (both intrusive and non-intrusive); hypersonic propulsion test principles and facilities; computational techniques and their integration into test programs; ground-test-to-flight data correlation methods; and test program planning. The Lecture Series begins at the introductory level and progressively increases in depth, culminating in a focus on special test and evaluation issues in hypersonics such as boundary-layer transition, shock interactions, electromagnetic wave testing, and propulsion integration test techniques.

To obtain a complete set of notes from this course write to:

Lecture Series Secretary
von Karman Institute
Charissie de Waterloo, 72
B-16409 Rhode-Saint-Genese (Belgium)

The information contained in this report is a subset of the work described above.

CONTENTS

AERODYNAMIC AND AEROTHERMAL FACILITIES I HYPERSONIC WIND TUNNELS

by
A. ANDERSON and R. K. MATTHEWS
Senior Staff Engineers
Calspan Corporation/AEDC Operations
Arnold Engineering Development Center

ABSTRACT

Hypersonic test facilities will continue to play a major role in the development of hypersonic vehicles. In the past, ground test facilities were often used to perform configuration parametric studies and/or to develop large databases. Future testing will emphasize understanding of fluid physics and validation of codes. Computational fluid dynamics (CFD) has made great progress in the past two decades, but the marriage of CFD and ground testing is clearly a reality today, and will become even more important in the future as computational and experimental researchers learn how to work together. One of the challenges for the experimentalist is to develop and utilize facilities that simulate hypersonic flight, and to provide the required data precision to validate CFD codes. This section provides a brief review of facility fundamental considerations and simulation issues. It is clear that no one facility will meet the wide variety of test objectives; therefore, the test facilities span a range of size, run time, complexity, and operating cost. Representative facilities are described, as well as their test capabilities and their shortfalls.

NOMENCLATURE

C_p	Pressure coefficient, $(P_w - P_\infty)/q_\infty$
L	Model length
M_∞	Free-stream Mach number
P_w	Model or wall surface pressure
P_t	Pitot pressure
P_o, P_T	Stilling chamber pressure
P	Static pressure
q	Dynamic pressure
Re	Reynolds number
T	Temperature
T_o, T_T	Stilling chamber temperature
U, V	Velocity
u	Local velocity
x	Axial distance
z	Lateral distance from tunnel centerline
α	Angle of attack
δ	Boundary layer thickness
ϱ	Density
μ	Viscosity
γ	Ratio of specific heats
Subscript	
∞	Free stream

INTRODUCTION

The role of the wind tunnel test in flight vehicle development has steadily changed in recent years from one of total dominance, to a sharing role in the process as both analytical methods and computational procedures have become more sophisticated (Fig. 1). All three disciplines have advantages and disadvantages, as shown in Figs. 2 through 4.

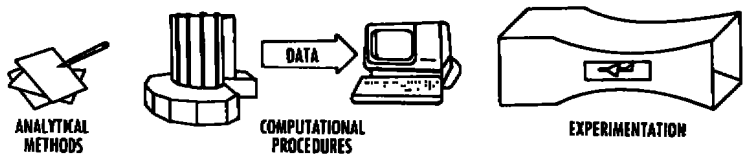

Figure 1. Tools for aerodynamic prediction.

ADVANTAGES	DISADVANTAGES
• CLOSED FORM SOLUTION (SIMILARITY RULES AND LAWS) • MINIMAL AMOUNT OF COMPUTER TIME	• RESTRICTIVE SIMPLIFYING ASSUMPTIONS • SIMPLISTIC CONFIGURATIONS • LIMITED AERODYNAMIC CHARACTERISTICS

Figure 2. Advantages and disadvantage of analytical methods.

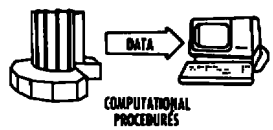

ADVANTAGES	DISADVANTAGES
• FEWEST RESTRICTIVE ASSUMPTIONS • OPTIMIZATION LINK POSSIBLE • COMPLETE FLOW FIELD DEFINITION • NO MACH NO. OR REYNOLDS NO. LIMITATIONS • COST EFFECTIVE	• INADEQUATE TURBULENCE MODELS • LACK OF COMPUTER STORAGE AND SPEED • ACCURACY OF FINITE - DIFFERENCE REPRESENTATIONS

Figure 3. Advantages and disadvantages of CFD.

ADVANTAGES	DISADVANTAGES
• REPRESENTATION OF ACTUAL CONFIGURATION • REPRESENTATIVE AERODYNAMIC DATA • OBSERVATION OF NEW FLOW PHENOMENA	• COSTLY MODELS AND TUNNEL TIME • TUNNEL DEPENDENT FLOW CONDITIONS (WALLS, IMPURITIES, TURBULENCE, DISTORTION) • LIMITED AMOUNT OF DATA • ACCURACY OF DATA OBTAINED • SCALING (VISCOUS EFFECTS, CHEMICAL NONEQUILIBRIUM, ETC.)

Figure 4. Advantage and disadvantages of wind tunnels.

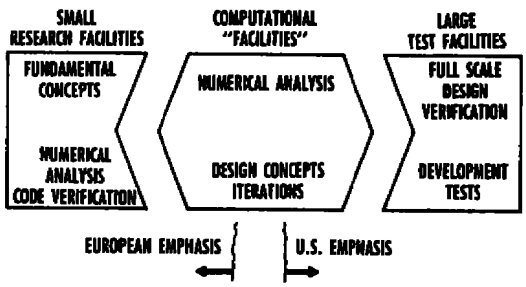

Figure 5. Role of aeronautical "tools."

Figure 5 emphasizes the use of computer codes in putting together the pieces of the puzzle. In a very general sense it may be said that in Europe, emphasis is placed on research and fundamental concepts using small facilities, while in the U.S., emphasis is placed on system development testing in large facilities.

The flow-field features around a body in a high-speed airstream are illustrated in Fig. 6, and the basic nomenclature of parameters simulating flight in the wind tunnel are shown in Fig. 7. Isentropic relationships between the total or stagnation properties and the static properties are typified by that given in Fig. 7 for total and static temperature as a function of Mach Number. The two most basic simulation parameters are Mach Number and Reynolds No. (Fig. 8). Geometric simulation (model fidelity) is, of course, important but is not always possible because of (small) model size. Altitude simulation is not often a test requirement, except in rarefied gas flow studies. Mach number, determines the general flow field around a body (Fig. 9), while Reynolds number

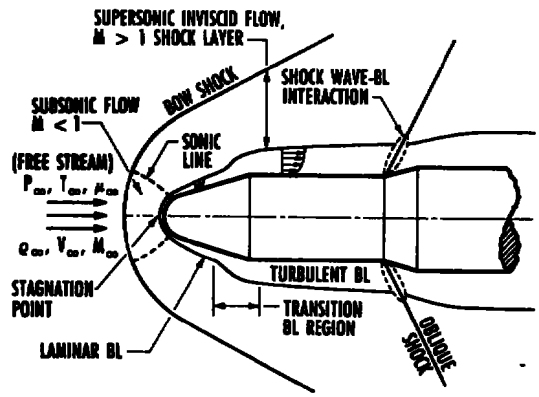

Figure 6. Typical missile configuration and flow field structure.

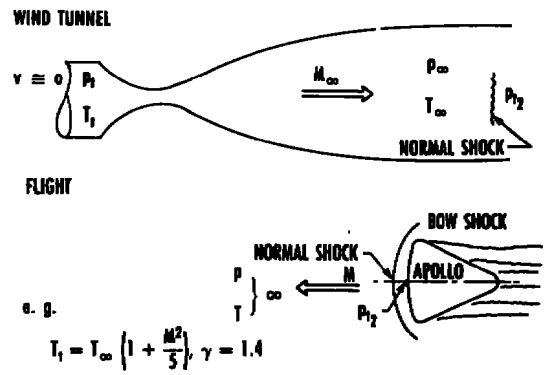

Figure 7. Basic nomenclature.

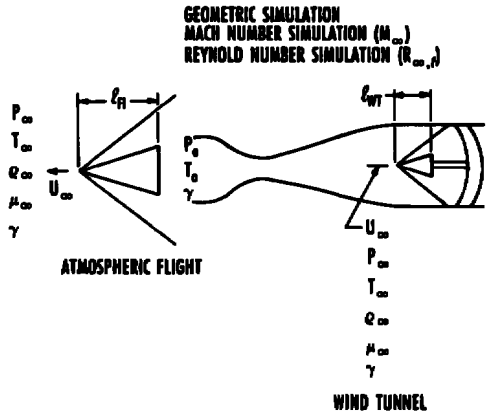

Figure 8. Basic simulation parameters.

- MACH NUMBER

  $M = \frac{V}{a}$ WHERE: V ~ VELOCITY
  a ~ SPEED OF SOUND
  $a = \sqrt{\gamma RT}$

  - DETERMINES
    - SHOCK SHAPE
    - FLOW FIELD
    - PRESSURE & HEATING DISTRIBUTIONS

- REYNOLDS NUMBER

  $Re = \frac{\rho V \ell}{\mu}$ WHERE: ρ ~ DENSITY
  V ~ VELOCITY
  $Re = \frac{\text{INERTIA FORCES}}{\text{VISCOUS FORCES}}$ ℓ ~ CHARACTERISTIC LENGTH
  μ ~ VISCOSITY

  - DETERMINES
    - BOUNDARY LAYER STATE
      LAMINAR FLOW $Re < 10^5$
      TURBULENT FLOW $Re > 10^7$
    - BOUNDARY LAYER THICKNESS, δ

Figure 9. Important simulation parameters.

determines viscous effects (the boundary-layer characteristics). The boundary layer growth on a body surface is illustrated in Fig. 10, which shows the laminar, transitional, and turbulent flow regions.

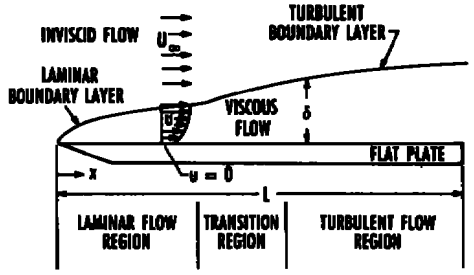

Figure 10. Boundary layer development.

1. IMPULSE (RUN TIME 1 SEC OR LESS)*
2. BLOWDOWN (RUN TIME SEVERAL MINUTES)
3. CONTINUOUS (RUN TIME SEVERAL HOURS)

Figure 11. Types of Hypersonic wind tunnels.

CONVENTIONAL HYPERSONIC WIND TUNNELS

Conventional hypersonic wind tunnels (i.e., not arc driven or shock tube-type)* are either continuous flow or intermittent (blowdown) type (Fig. 11). There are very few closed-circuit, continuous flow hypersonic tunnels in the world because the initial investment in plant facilities is very high. Delivering high-pressure air at a relatively high mass flow requires many stages of compression with all the attendant drive motors, valving, and coolers, etc. (Fig. 12). For example, the AEDC Mach 10 Tunnel C with a 1.28 m (50-in.) diameter test section uses nine stages of compression to supply 138 bar (2,000 psia) air at 29 Kgm/sec (64 lbm/sec), and consumes about 56 MW/hr or power. Some low-density tunnels which can operate for an hour or more are classified as continuous flow. These tunnels run with a stored high-pressure air supply and a vacuum plant. The primary advantage (Fig. 13) of the continuous flow tunnel is in data productivity, which can be very high, particularly when the tunnel is equipped with a model injection system which allows access to the model while the tunnel is running.

Blowdown, or intermittent, tunnels require rather simple plant capabilities (Fig. 14), including one or

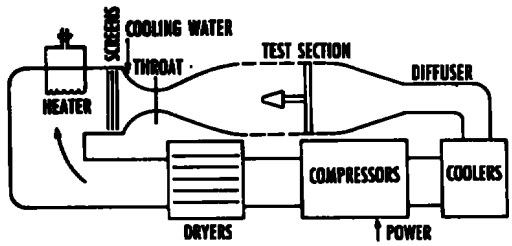

Figure 12. Schematic diagram of a continuous flow tunnel.

ADVANTAGES	DISADVANTAGES
• HIGHLY PRODUCTIVE	• LARGE INVESTMENT IN CAPITAL
• ABLE TO ACCOMMODATE MOST TEST TECHNIQUES	• LARGE INVESTMENT IN COMPRESSOR PLANT AND HEATERS
• STEADY FLOW FOR LONG PERIODS OF TIME	• LARGE INVESTMENT IN AUTOMATION
• EXACTLY REPEATABLE FLOW CONDITIONS	• HIGH OPERATING COST (POWER + PERSONNEL + MAINTENANCE)
	• LONG TIME TO GET ON TEST CONDITION (PUMP UP, ETC.)
	• ACCESS TO MODEL IS TIME CONSUMING (DOES NOT APPLY TO TUNNELS WITH INJECTION SYSTEM).

Figure 13. Continuous flow facilities.

* Impulse type facilities will be discussed in the next section.

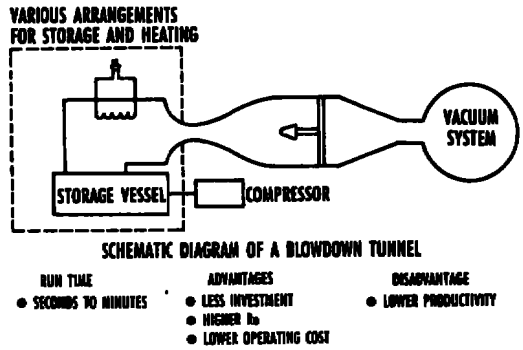

Figure 14. Blowdown facility.

OWNER	FACILITY NAME	TEST SECTION, DIAM, M	MACH NO.	TOTAL PRESSURE, ATMOSPHERES	TOTAL TEMP, °K
NASA AMES	3.5 HYPERSONIC WIND TUNNEL	1 1	5, 7, 10	135	1,920
NASA LANGLEY	8 FT HIGH TEMPERATURE TUNNEL	2.4	4-7.2	165	2,200
ARNOLD ENGINEERING DEVELOPMENT CENTER	HYPERSONIC WIND TUNNEL (B) HYPERSONIC WIND TUNNEL (C) AERODYNAMIC AND PROPULSION TEST UNIT (APTU)	1.3 1.3 0.8 - 0.96	6 or 8 4, 8, 10 2.2-4.1	60 138 11-20	720 1,250 1,100
NAVAL SURFACE WEAPONS CENTER	HYPERVELOCITY WIND TUNNEL NO. 9	1.6	8, 10, 14	1,380	1,780

Figure 15. Representative U. S. hypersonic wind tunnels.

more compressors to pump up a storage vessel of high-pressure air, and vacuum pumps if it exhausts to a vacuum. The tunnel may use ejectors instead of a vacuum tank, or it may exhaust to atmosphere, which requires very high tunnel supply pressures.

Hypersonic nozzles are generally conical or axisymmetric contoured. The conical nozzle does present problems, however, from a Mach number gradient prospective. The axisymmetric contoured nozzles of the AEDC Hypersonic Tunnel B and C were designed by the procedures outlined in Ref. 1.

All wind tunnels require air driers to avoid water vapor condensation during the expansion process. Hypersonic tunnels also require a heater to raise the air temperature above that at which air liquefaction can occur during the expansion process.

A listing of some of the more capable hypersonic conventional tunnels in the U.S. is given in Fig. 15, and schematic sketches of the tunnels are given in Figs. 16 through 20. A listing of non- U.S. wind tunnels is given in Fig. 21, and descriptive sketches of some of these are shown in Figs. 22 through 24. A comprehensive listing of hypersonic tunnels in the U.S. is given in Ref. 2 and the European tunnels are given in Ref. 3. Descriptions of the capabilities of selected hypersonic tunnels follow.

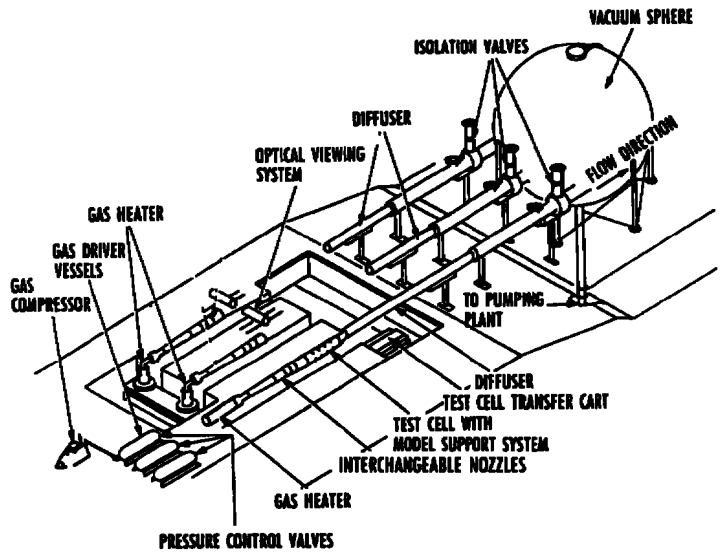

Figure 16. NSWC hypervelocity wind tunnel no. 9 (blowdown-type facility).

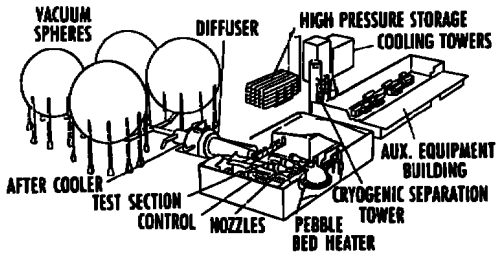

Figure 17. NASA-AMES 3.5 ft hypersonic tunnel.

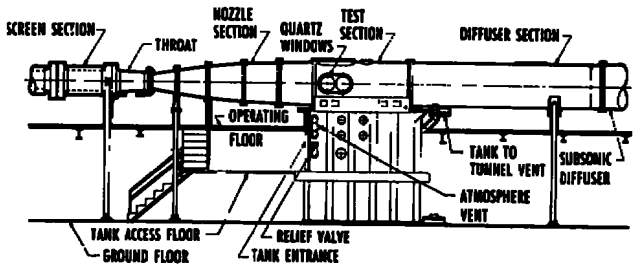

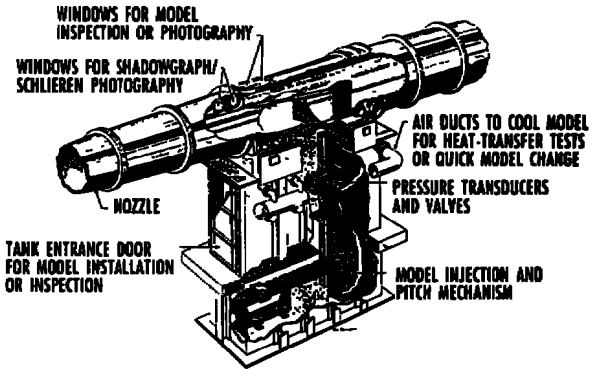

Figure 18. AEDC tunnel B.

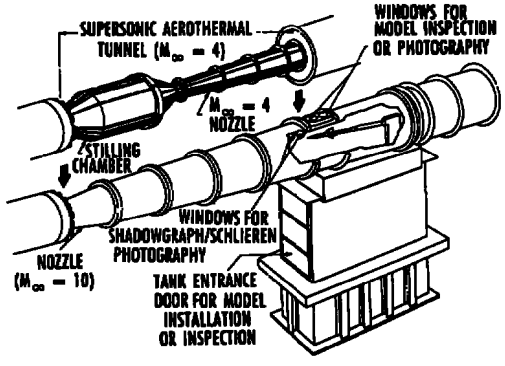

Figure 19. AEDC tunnel C.

NSWC Tunnel 9

The NSWC Tunnel 9 (Fig. 16) is a blowdown tunnel operating at Mach 8, 10, and 14 exhausting into a vacuum sphere. The nitrogen test gas at pressures up to 1,380 bars (20,000 psia) is heated by a graphite electric resistance heater to provide total temperatures up to 1,780°K (3,200°R). Cold, high-pressure gas is introduced behind the hot nitrogen to maintain constant reservoir conditions for the duration of the test run. The maximum test run is about 15 sec.

NASA LaRC 8-ft High Temperature Tunnel

The LaRC 8-ft High-Temperature tunnel is a blowdown tunnel exhausting to atmosphere. The nozzle is a conical-contoured axisymmetrical design with an 8-ft (2.46 m) exit diameter. Total temperatures up to 2,200°K (3,960°R) are obtained by burning methane in air and using the resulting combustion products as the test medium. The maximum total pressure is 166 bar (2,407 psia), and maximum run time is 120 sec.

NASA-AMES 3.5-ft Hypersonic Tunnel

The AMES 3.5-ft Hypersonic tunnel (Fig. 17) is a blowdown tunnel exhausting to vacuum spheres. Interchangeable, contoured axisymmetric nozzles provide Mach numbers of 5, 7, and 10. An alumina pebble bed heater, preheated by burning natural gas, provides total temperatures up to 1,920°K (3,460°R). The maximum total pressure is 135 bar (1,960 psia). Run times are from 0.5 to 4 min.

AEDC Tunnels B and C

The AEDC Tunnels B and C (Figs. 18 and 19) are continuous flow, closed-circuit, hypersonic wind tunnels with 50-in. (1.28m) diam test sections. Axisymmetric, contoured nozzles for Mach 6 and 8 are available in Tunnel B, and similar contoured nozzles for Mach 4, 8, and 10 are available in Tunnel C. The Mach 4 and 8 nozzles in Tunnel C are open jet with 25-in. (0.64m)-diam exits. A nine-stage compressor system with a total installed horsepower of 92,500 provides a wide range of mass flows and total pressures up to 138 bar (2,000 psia) at Mach 10. A gas-fired combustion heater provides total temperatures up to 750°K in Tunnel B, and the gas-fired heater, in conjunction with an electric resistance heater, provides temperatures up to

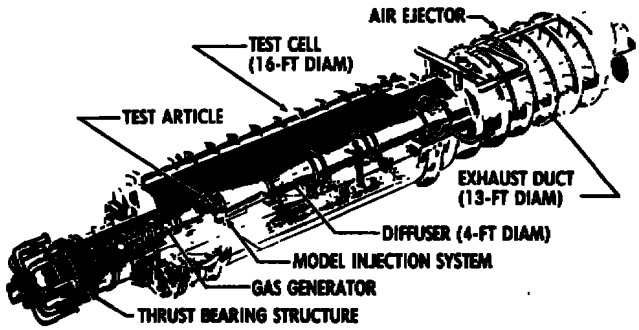

Figure 20. AEDC tunnel APTU.

COUNTRY	FACILITY WIND TUNNEL	TEST SECTION, DIAM, m	MACH NO.	TOTAL PRESSURE, ATMOSPHERES	TOTAL TEMP, °K	REMARKS
FRANCE	ONERA/S4MA	0.6-1.0	6, 10, 12	270	1,850	PEBBLE-BED BLOWDOWN, 90 SEC
FRANCE	CNRS.SR3	0.3-0.4	2-30	120	1,500	GRAPHITE BLOWDOWN LOW DENSITY
GERMANY	DLR/H2K	0.6	5-11	50	1,300	BLOWDOWN
U.K.	ARA.M7T	0.3	6-8	200	850	BLOWDOWN
JAPAN	NAL/HYPERSONIC	0.5 1.2	5, 7, 9, 10 11	100	1,500	BLOWDOWN, 120 SEC

Figure 21. Representative non U.S. hypersonic wind tunnels.

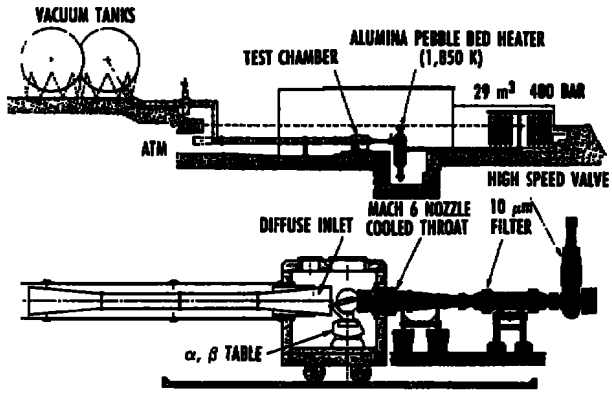

Figure 22. Schematic diagram of the S4MA wind tunnel.

1,250°K (2,250°R) in Tunnel C. Both tunnels have model injection systems which allow access to the model for configuration changes while the tunnel remains in operation.

AEDC APTU

The AEDC Aerodynamic and Propulsion Test Unit (APTU), Fig. 20, is a blowdown, free-jet wind tunnel with interchangeable, axisymmetric free-jet nozzles for Mach numbers from 2.2 to 4.1. A vitiated air heater (VAH) fueled by isobutane provides true-temperature flight conditions at altitudes ranging from 5,000 to 80,000 ft (1.5-24 Km). The tunnel exhausts to atmosphere using air ejectors, and an oxygen replenishment system is used to replace that consumed by the VAH. Although designed primarily for ramjet propulsion testing, the tunnel may also be used for aerothermal and thermo-structural type testing.

ONERA S4MA

The ONERA S4MA Tunnel (Fig. 22) is an blowdown hypersonic wind tunnel. The tunnel has a propane-heated alumina pebble bed heater. It has a Mach 6 nozzle with an 0.68-m diam exit and a Mach 10 to 12 nozzle with a 1-m-diam exit. The throat is water-cooled. The tunnel air supply vessel of 29 m^3 can be pressurized to 270 (3,900 psia) or 400 bar (5,800 psia). It exhausts either into atmosphere or into vacuum spheres (3,000 or 4,000 m^3). The heater provides a maximum temperature of 1,850°K (3,300°R). Run times are from 30 to 100 sec.

ONERA CNRS SR.3

The CNRS SR.3 Tunnel (Fig. 23) is a continuous-flow, low-density wind tunnel with an open-jet test section. An 80-KW graphite heater is used to heat the test gas (air or N_2) to 1,500°K (2,700°R) at a pressure up to 120 bars (1,740 psia). The SR.3 covers an extensive range of conditions from continuum to near free molecular flow at speeds from Mach 2 to 30. Nozzle exit diameters are 15 to 30 cm for Mach 2 to 7 and 36 cm for Mach 15 to 30.

DLR-H2K

The DLR Hypersonic Tunnel 2 is an blowdown tunnel with five nozzles of 0.6 m exit diameter for Mach numbers from 4.8 to 11.2. The maximum total pressure is 50 bar (725 psia), and total temperature

from a 2,500-KW heater is 300 to 1,300°K (2,340°R). The tunnel exhausts to a vacuum sphere and has typical run times of 30 sec.

N.A.L. 50-cm Tunnel

The NAL 50-cm Hypersonic Tunnel (Fig. 24) is an blowdown wind tunnel exhausting to a vacuum sphere. The tunnel has four interchangeable, contoured nozzles, 50-cm diameter, for Mach numbers 5, 7, 9, and 11, and a 1.2-m exit diameter nozzle for Mach 10. The tunnel has an alumina pebble bed heater providing temperatures to 1,500°K (2,700°R); the total pressure range is 10 to 100 bar (1,450 psia). Maximum run time is 120 sec.

ARA Bedford M7T

The ARA Bedford M7T is a hypersonic blowdown tunnel with an atmospheric exhaust. The tunnel has three contoured nozzles for Mach 6, 7, and 8. The tunnel total pressure is 100 to 200 bar (2,900 psia) at total temperatures up to 850°K (1,530°R).

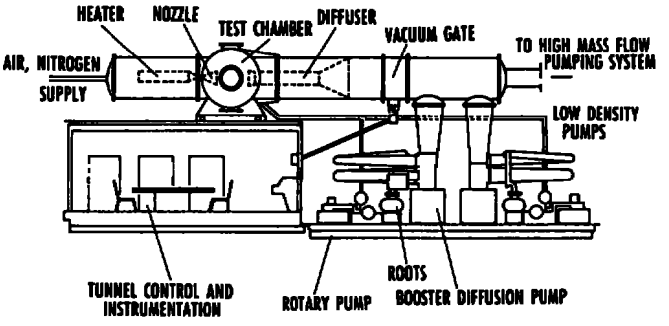

Figure 23. Schematic diagram of the CNRS SR.3 wind tunnel.

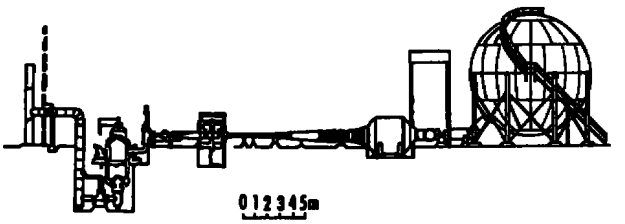

Figure 24. Schematic drawing of the NAL 50 cm hypersonic wind tunnel.

WIND TUNNEL TEST CONDITIONS

In considering a wind tunnel test two fundamental questions arise (Fig. 25): (1) how will the tunnel data be extrapolated to flight; and (2) can the tunnel provide the desired test conditions? In the first question, for example, the tunnel results may require modification for real-gas effects, and static stability coefficients may need corrections for tunnel values of model inlet internal flows and base drag. The tunnel test conditions problem may be a lack of sufficient pressure to generate the test Reynolds numbers desired or being unable to provide the maximum Mach number desired.

Flight Temperature Duplication.

Stream temperature simulation is not a basic aerodynamic simulation parameter for the wind tunnel. The duplication of flight temperature is extremely important for the development of structural components to withstand the aerothermal environment; however, providing this capability in the conventional hypersonic tunnel is extremely difficult except at low Mach numbers ($M \leq 5$), because of the high temperatures required. Figure 26 shows the total temperatures required as a function

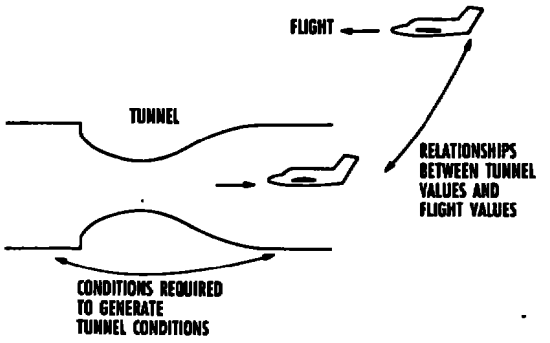

Figure 25. Two fundamental problems of wind tunnel testing.

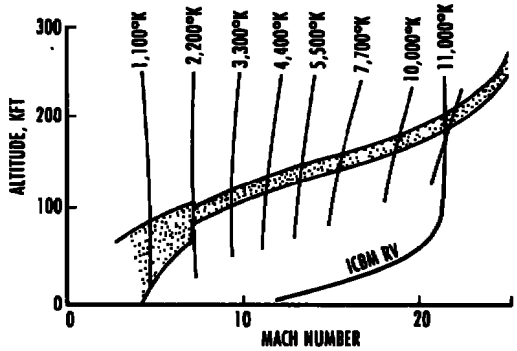

Figure 26. Typical temperatures for flight duplication.

of Mach number and altitude. This shows that a total temperature of about 1,000°K (2,000 °R) is required at Mach 5, which is about the limit available from a conventional electric heater. Temperatures up to about 2,000°K (3,600°R) can be obtained by storage heaters such as the pebble bed which are used for blowdown tunnels. Higher temperatures available from arc heaters and compression heating will be discussed later in regard to impulse-type tunnels.

Wind Tunnel Flow Quality

The calibration of a hypersonic tunnel generally consists of axial surveys through the test section with a rake of pitot-pressure probes. In tunnels where a probing mechanism is not available and in short-duration blowdown tunnels the rake may be positioned at different axial stations for separate test runs. The rake may include a corresponding number of total-temperature probes; however, in many cases the uniformity in total temperature indicated by a fixed rake of probes in the stilling chamber is accepted as evidence of the temperature uniformity in the test section.

A basic requirement for good wind tunnel data is a well-calibrated and documented test section airflow. Because of the current advanced state of instrumentation and data acquisition systems, a primary cause of uncertainties in test data is the flow nonuniformities present in all wind tunnels. Whether from nozzle fabrication imperfections, nozzle joints, etc., small disturbances are present which produce expansions/compressions throughout the flow field.[4] Nozzle boundary-layer growth, which may not always be symmetrical, produces changes in Mach number level with changes in tunnel Reynolds number. An example of the downstream progression of a disturbance from a nozzle wall discontinuity is given in Fig. 27. These pitot-pressure profile data are from the initial Mach 8 calibration of the AEDC Magnetic Suspension Tunnel, Tunnel E (now dismantled), (Fig. 27a) which had a rearward facing step in a nozzle joint. The data show the centerline focusing of disturbances, which is a disadvantage of axisymmetric nozzles. Because of the variables in accuracy of data from any wind tunnel, major new flight vehicles such as the space shuttle orbiter have repetitive tests conducted on the same model in different tunnels to arrive at the best com-

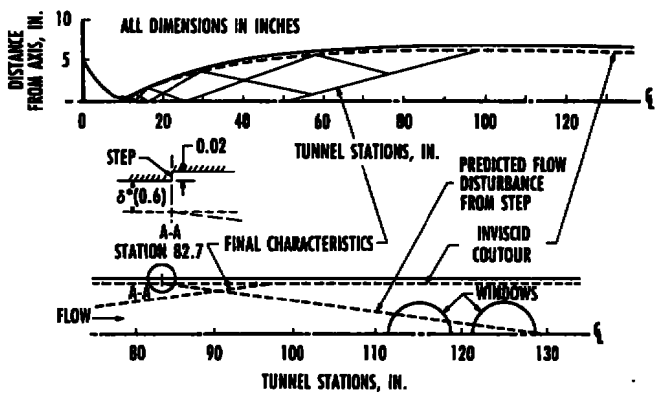

a. Nozzle joint step and predicted disturbance.

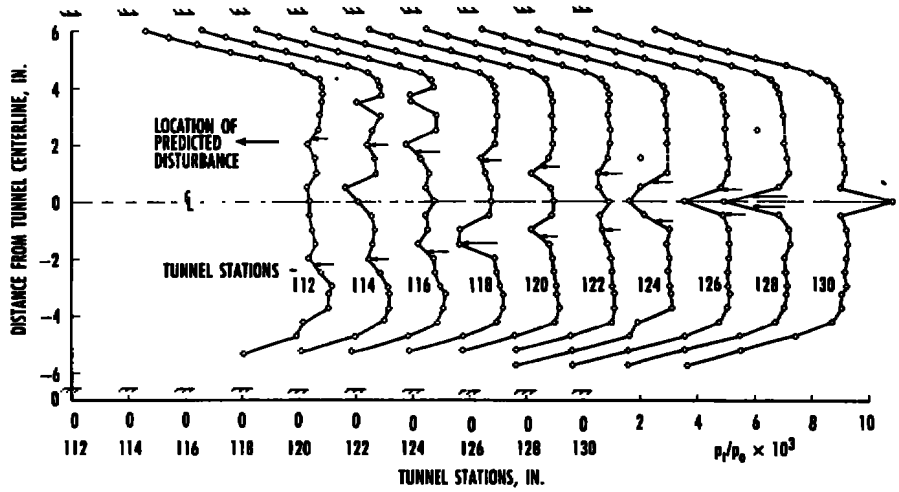

b. Test section pitot pressure profiles.

Figure 27. Test section flow disturbance from a nozzle joint.

promise value for the bounds of uncertainty on flight performance parameters.

Pitot-pressure measurements are used to define the test section flow uniformity because of problems involved in obtaining accurate measurements of stream static pressure. Cone-cylinder and disc probes can be used with good results at low to moderate supersonic speeds (M $\leq$ 3), but are not used at higher speeds because of viscous effects. Unfortunately, pitot-pressure is relatively unaffected by the presence of the nonisentropic effects of air liquefaction and water-vapor condensation, and other means should be employed to verify the test section flow properties. At the AEDC, this has been done since the early 1970s by using pressure distributions measured on a slender cone (5-deg half-angle) at α = 0 compared with CFD solutions.

Calibration results obtained recently (1992) in the AEDC Tunnel B at M = 8 are shown in Figs. 28 and 29. Figure 28a gives results from the pitot-rake surveys showing the variation in the average test-section Mach number with Reynolds

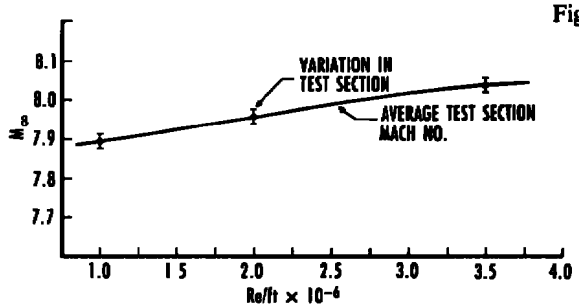

a. Variation of average M_∞ with Re from pitot rake data

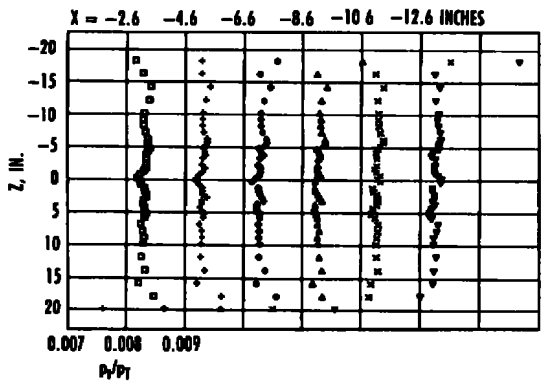

b. Test section pitot pressure profiles

Figure 28. AEDC tunnel B calibration data at Mach 8.

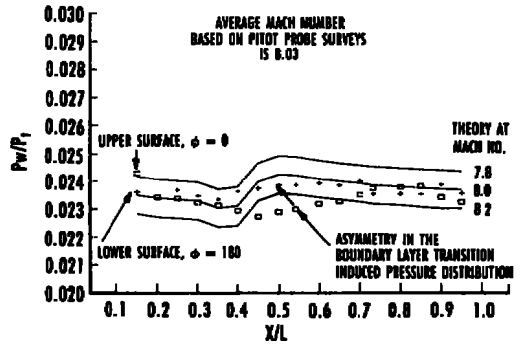

a. P_w/P_t versus X/L

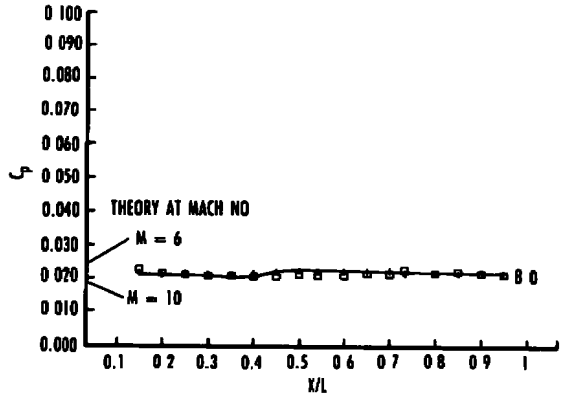

b. C_p versus X/L

Figure 29. Mach number inferred from the 5-deg cone.

number and vertical pitot-pressure profiles at several axial stations along the test section are presented in Fig. 28b. The probe mechanism used in Tunnel B also provides remotely driven lateral movement so similar profiles were obtained in the lateral axis. Figure 29 shows pressure distributions on the 5-deg cone at α = 0 compared to theoretical solutions. The theory is a CFD code[5] which is a space marching algorithm which includes the induced pressure effects of boundary-layer growth from laminar to turbulent flow provided the transition location is specified. The cone pressure distributions (Fig. 29a) presented as the ratio of local surface pressure, P_w to the local pitot pressure, P_t at the cone nosetip are considered in satisfactory agreement with theory for the average Mach number from the pitot surveys. The data in the form of pressure coefficient, C_p show (Fig. 29b) how one could easily mask any nonisentropic effects by such a presentation.

Air Liquefaction

For Mach numbers above about M = 4, the stilling chamber air must be heated above ambient

temperature to ensure that air liquefaction does not occur during the expansion process. Figure 30 shows the equilibrium-saturated expansion curve for air along with experimental results from a number of U.S. hypersonic tunnels. The data fairing for the onset of liquefaction from experiments shows that most tunnels attain an amount of supersaturation, which varies with stagnation pressure, which allows operation at lower stagnation temperatures than indicated by the saturated expansion theory. In general, a low rate of expansion in a long nozzle will minimize the degree of supersaturation obtained.

The generally accepted method of detecting the onset of liquefaction is illustrated by the results shown in Fig. 31. These are data from the AEDC Tunnel B at Mach 8 and show that pitot pressure is essentially unaffected by the stagnation temperature change; consequently, the normal flow calibration technique using pitot probes will not show any effect of air liquefaction. The onset of liquefaction, that is, the minimum allowable stagnation temperature, is determined by test section measurements of wall static pressure.

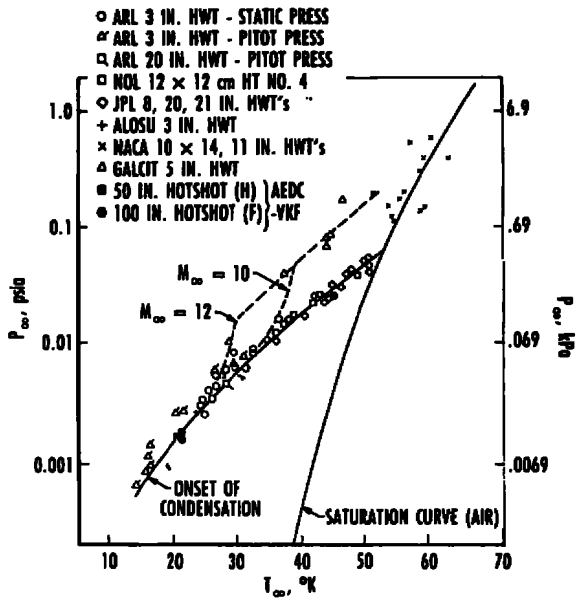

Figure 30. Phase diagram for air.

Water Vapor Condensation

Water vapor condensation and air liquefaction, although different phenomena, have the same type of effects on the test section flow properties, i.e., a decrease in stream Mach number and an increase in stream static pressure. As was the case with air liquefaction, pitot pressure is relatively unaffected and the local properties of static pressure and pitot pressure are used to define the test section Mach number and detect the effect of water vapor condensation. Unlike air liquefaction, however, where the needed air temperature can be predicted (expansion theory) and easily verified, the requirement for "dry" air is not easily predictable nor easily verified.

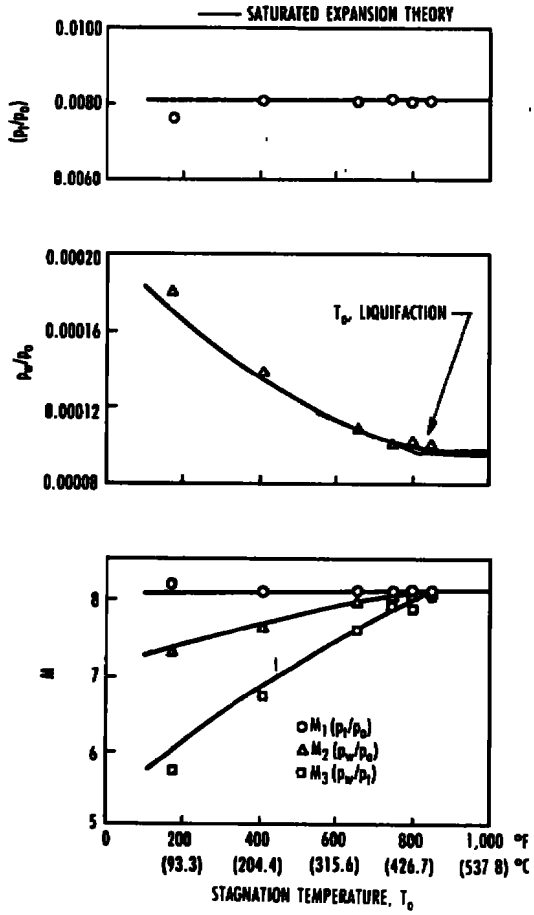

Figure 31. AEDC tunnel B, Mach 8 test results showing the onset of air liquifaction.

The water vapor condensation shock theory[6] provides only estimates of the effects of condensation on test section flow properties; consequently, the maximum allowable dewpoint (frost point) temperature for any wind tunnel must be verified by experiment. Experimentally determined results for the AEDC Tunnels A, B, and C are shown in Fig. 32. As you can see, hypersonic tunnels require very dry air. The −60°C frostpoint requirement at

Mach 10 represents a specific humidity of 13 ppm of water vapor to air. This −60°C requirement was determined from the test results shown in Fig. 33.

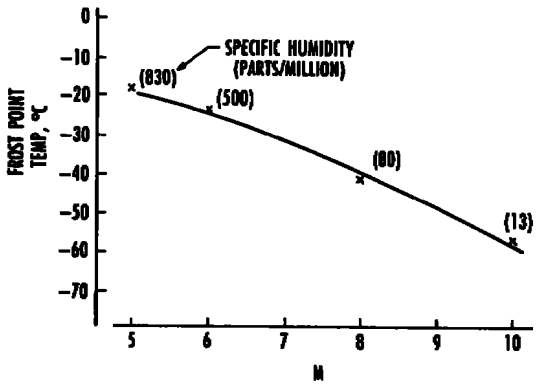

Figure 32. Maximum frost point temperatures for "isentropic" flow in AEDC/VKF hypersonic tunnels.

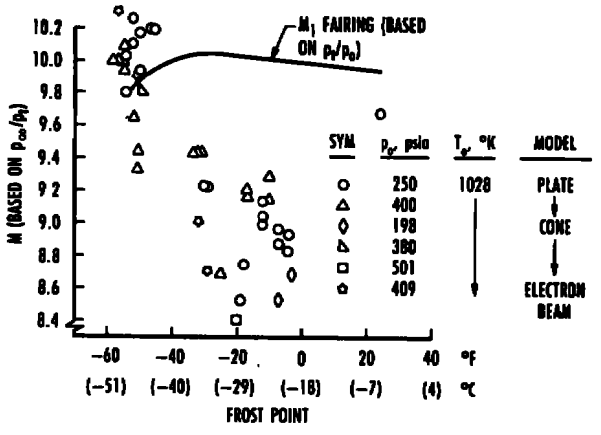

Figure 33. Effect of air moisture content on calculated Mach numbers based on the ratios (p_t/p_o), and (p_∞/p_t).

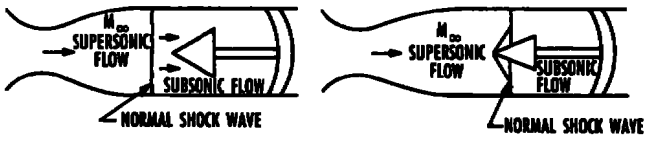

a. Flow blocked - model frontal area too large

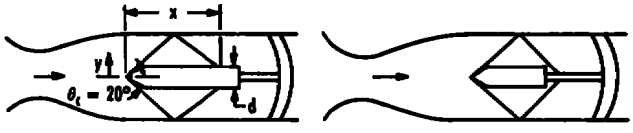

b. Model too long c. Proper size model

Figure 34. Model size restrictions.

The efficiency of air driers decreases as the desiccant bed nears saturation, and the tunnel frostpoint temperature must be continually monitored during operation. Air humidity problems are particularly severe in continuous flow tunnels because of possible inleakage of humid atmospheric air in low-pressure areas of the tunnel ducting, and the potential for water leaks in compressor plant coolers.

The nonisentropic effects on test section flow properties previously noted as an increase in local static pressure and decrease in Mach number are compensating such that dynamic pressure is minimally affected. Consequently, static stability data show little effect of air liquefaction or water vapor condensation. The primary area of concern is in defining specifically the tunnel freesteam conditions in terms of Mach number and static pressure which are key parameters needed for code validation test.

Model Size Considerations

The allowable model size; i.e., frontal area as well as model length, is a critical facility decision. One generally wants the largest model possible because of maximizing space for onboard instrumentation and for best similitude of surface features. However, a wrong choice and the tunnel user has built an expensive model which cannot be tested. Model length is rarely critical because model shock wave angles and reflected shock angles can be estimated to locate the reflected shock impingement at a satisfactory distance downstream of the model base (~3 diam) as illustrated in Fig. 34. Model blockage, however, is very dependent on model shape, and tunnel characteristics such as the starting pressure ratio and whether or not the tunnel has a model injection system. Each tunnel, therefore, will have its own guidelines established from experience as to allowable model frontal area. Tunnel choking can occur for reasons other than model size; an example shown in Fig. 35a is a wedge model tested in the AEDC Tunnel B at Mach 8. This model frontal area was well within the blockage criteria for this tunnel, but was totally destroyed (Fig. 35b) upon the first injection into the airstream. The inferred process involved in the flow breakdown (Fig. 36) is believed to start when the wedge initially deflects flow down into the tank, which then induces pressures to locally separate the tunnel boundary layer. Sequential shadowgraph pictures (Fig. 37)

illustrate the flow complexity during this process. Tests with a rebuilt model showed that clean injections could be made with the wedge model set at a reduced incidence angle to the flow. It should be emphasized that this was a very unusual case and is not the way a facility likes to add to its model blockage criteria. In most cases, a flow breakdown situation is determined without losing a model by testing suspected problem models at a reduced pressure level.

SUMMARY

Hypersonic wind tunnel facilities provide a wide range of Mach number, Reynolds number, run time, and size. However, it is extremely important to emphasize that these facilities are only tools and like any tools their use and correct application determine how effective they are in solving a specific problem.

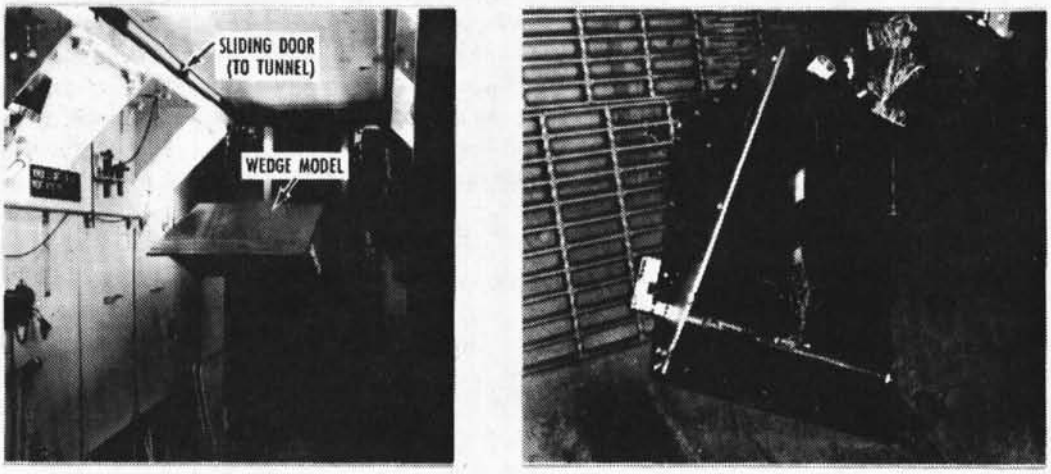

a. Wedge model prior to injection into tunnel b. Wedge model after flow breakdown

Figure 35. Results of flow breakdown on wedge model.

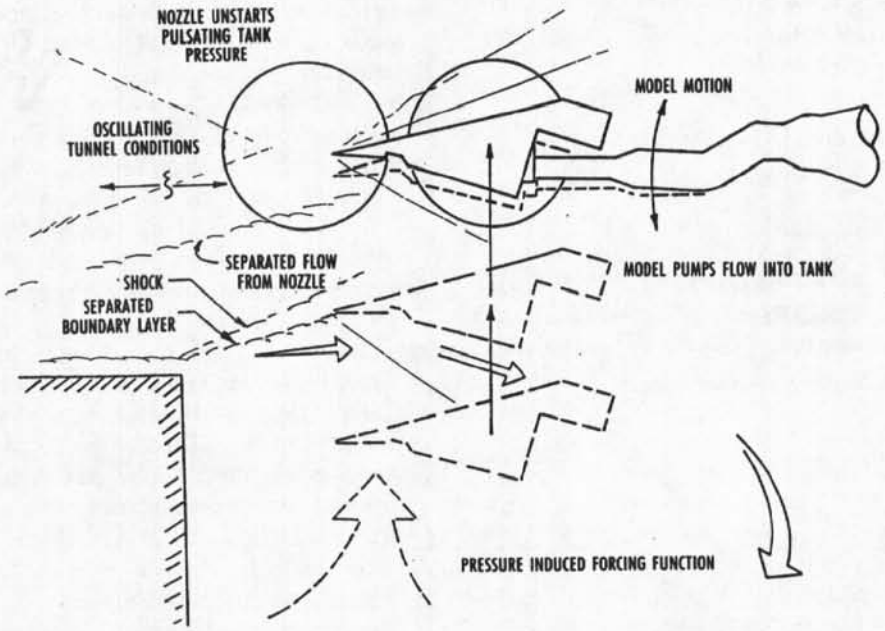

Figure 36. Pictorial concept of flow breakdown process.

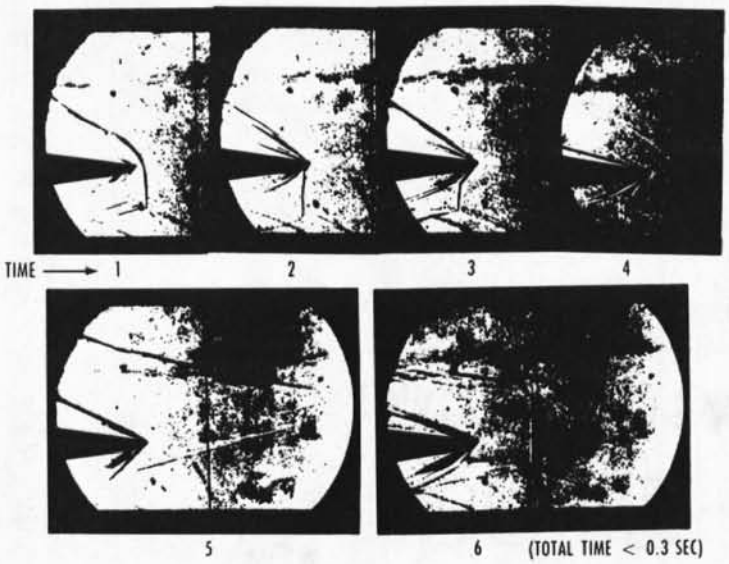

Figure 37. Sequencial shadowgraph of flow breakdown.

REFERENCES

1. Sivells, J. C. "A Computer Program for the Aerodynamics Design of Axisymmetric and Planar Nozzles for Supersonic and Hypersonic Wind Tunnels." AEDC-TR-78-63, December 1978.

2. NASA RP-1132 Aeronautical Facilities Catalogue. January 1985, Vol. 1, Wind Tunnels.

3. Wendt, J. F. "European Hypersonic Wind Tunnels." paper presented at the AGARD Symposium on Aerodynamics of Hypersonic Lifting Vehicles at Bristol, U. K., April 1987.

4. Fitch, C. R. "Flow Quality Improvement at Mach 8 in the VKF 50-inch Hypersonic Wind Tunnel B." AEDC-TR-66-82, May 1966.

5. Molvick, G. A. and Merkle, C. L. "A Set of Strongly Coupled Upwind Algorithms for Computing Flows in Chemical Nonequilibrium." AIAA Paper 89-0199, Presented at the 27th Aerospace Science Meeting, Reno, Nevada, January 9-12, 1989.

6. Wegener, P. P. and Mack, L. M. "Condensation in Supersonic and Hypersonic Wind Tunnels." *Advanced in Applied Mechanics*, Vol. 5, Academic Press, 1958.

AERODYNAMIC AND AEROTHERMAL FACILITIES II SHORT-DURATION, HIGH-ENTHALPY FACILITIES

by
JAMES R. MAUS
Principal Engineer
Calspan Corporation/AEDC Operations
Arnold Engineering Development Center

ABSTRACT

A brief survey of short-duration facilities primarily used for aerodynamic or aerothermal testing is presented. This paper deals with facilities which have useful run times ranging from a few hundred microseconds to a few hundred milliseconds. The review addresses the following types of facilities: arc-heated hot shot tunnels, shock-heated devices, compression-heated wind tunnels and, aeroballistic ranges. Examples are given of both US and European facilities. The review emphasizes principles of operation, facility performance, and strengths and weaknesses of the various types of facilities.

INTRODUCTION

Hypersonic facilities that attempt to simulate the high-temperature gas dynamic phenomena that occur in flight tend to be short duration facilities for two basic reasons: (1) The enormous levels of energy that are required to produce the flow (gigawatt levels) can only be sustained for short durations, and (2) Extended exposure of the facility and/or test article to the environment associated with these energy levels will cause severe damage to the hardware. The trend shown in Fig. 1 where various types of facilities are displayed in terms of run time and stagnation enthalpy reflects these constraints. This paper presents a brief survey of short-duration, high-enthalpy facilities employed primarily for aerodynamic and aerothermal testing. A companion lecture will deal with high-enthalpy facility types of longer test duration. The paper will emphasize principles of operation, performance envelopes, and strengths and weaknesses of the various facility types.

HOT SHOT TUNNELS

In hot shot tunnels, a fixed volume of test gas is heated to high pressure and temperature by an electric arc discharge and then expanded through a nozzle into an evacuated test chamber. AEDC operated several hot shot tunnels in the 1960s and 70s. The last of these was AEDC Tunnel F,[1] which was decommissioned in the late 1970's. A view of the Tunnel F plant and a layout of the facility as it existed in 1970 is shown in Fig. 2. There were several different arc chambers, ranging in volume from 1.0 ft^3 (28.32 liters) to 4.0 ft^3 (113.28 liters). Two of the smaller chambers that were available for the facility are shown in Fig. 3. The 4.0 ft^3 arc chamber was a scaled up version of the chamber shown in Fig. 3b. In the operation of this tunnel, nitrogen (N_2) or air was confined in the arc chamber by a diaphragm located near the nozzle throat. The gas was heated and compressed by the arc discharge, causing the diaphragm to rupture and initiating flow in the nozzle. The nozzle was a 4-deg half-angle conical

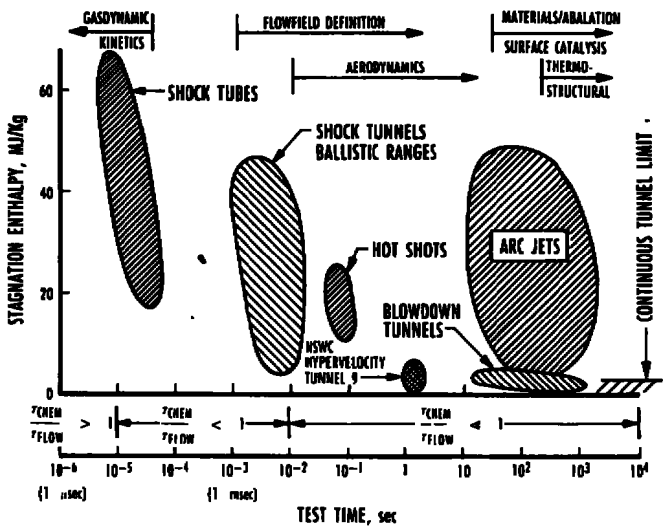

Figure 1. Stagnation enthalpy and flow duration domains for hypervelocity simulation facilities.

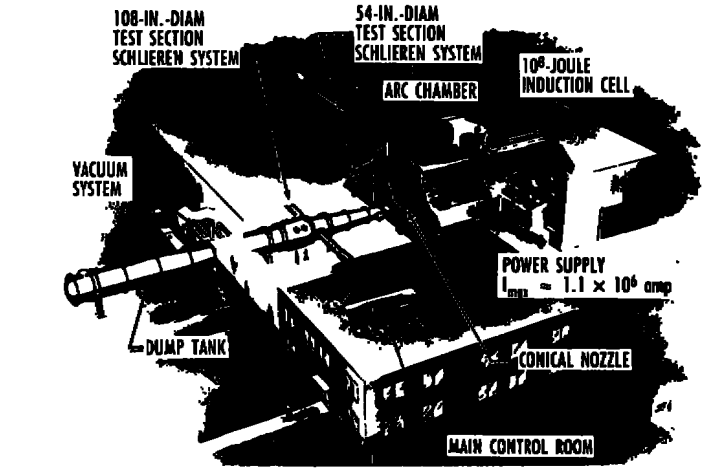

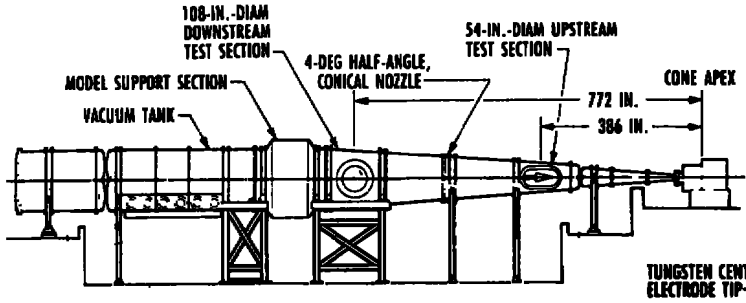

Figure 2. Tunnel F assembly.[1]

nozzle and contained two test stations at 54 in. (1.37 m) diameter, and 108 in. (2.74 m) diameter. Figure 4 gives the test envelope at these two stations in terms of Mach number and unit Reynolds number (L = 0.305 m). The maximum test section velocity achieved in Tunnel F was about 3,000 m/sec.

For aerodynamic testing, the usual test gas for Tunnel F was nitrogen. The maximum design conditions for the 4.0 ft^3 arc chamber were 1,400 bar (P_0) and 4,000 K (T_0) or 2,800 bar and 2,500 K. Under these conditions, nitrogen behaves as a perfect gas. Thus, Tunnel F was basically a perfect-gas aerodynamic test facility with performance somewhat similar to NSWC Tunnel 9. The useful run time for Tunnel F was between 50 and 200 msec. Figure 5 shows another characteristic of hot shot tunnels, the gradual decay of stagnation pressure over the useful test time. It is possible to obtain data for several test conditions in a single shot.

Tunnel F was a very productive facility at AEDC for many years. It was used predominantly for aerodynamic and aerothermal testing, but on occasions was employed for combustion studies using air as a test gas. Over the period of operation, a wide variety of testing techniques were developed for this tunnel; a partial list of these is given in Fig. 6.

The ONERA hot shot tunnel,[3] F4, at Le Fauga in Toulouse is currently undergoing shakedown and calibration tests. This arc-heated facility is designed to operate at stagnation pressures up to

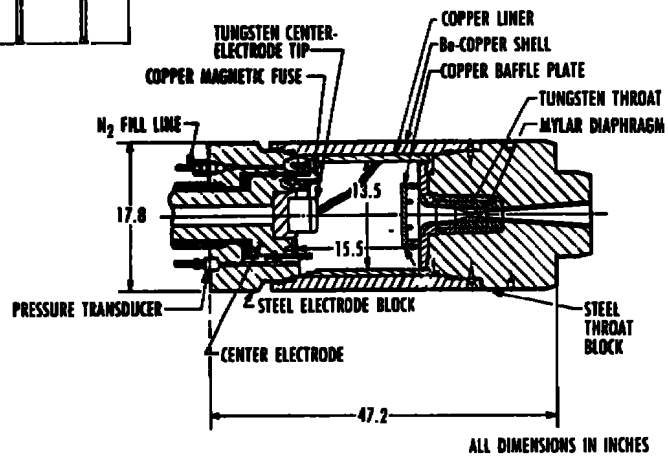

a. 40,000 psia arc chamber

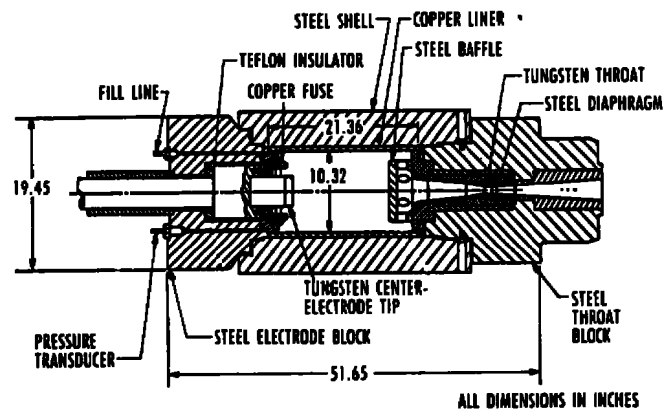

b. 75,000 psia arc chamber

Figure 3. Tunnel F arc chambers.[2]

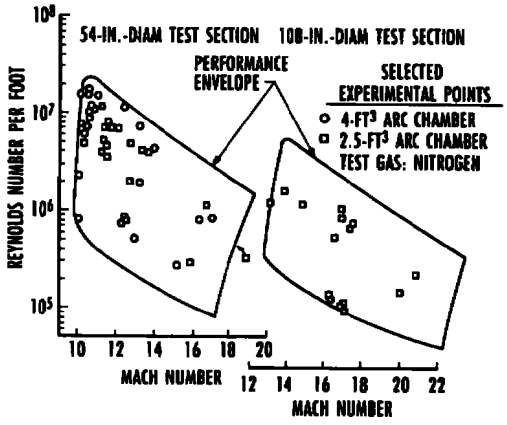

Figure 4. Reynolds and Mach number ranges for tunnel F.[1]

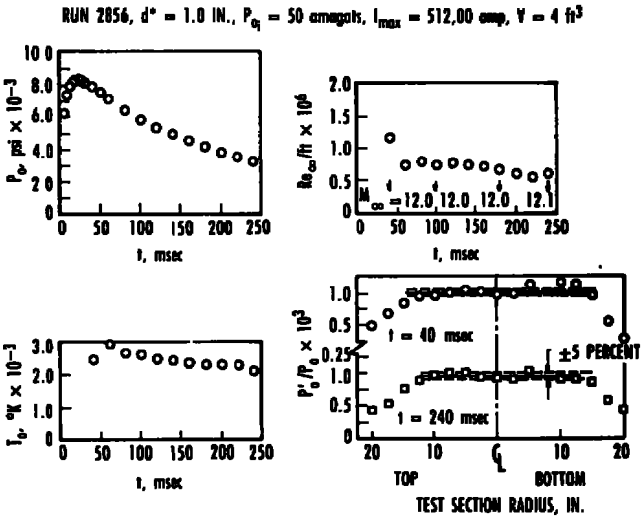

Figure 5. Calibration run for AEDC Tunnel F.[2]

2,000 bar and produce velocities in excess of 5,000 m/sec. This will represent a dramatic improvement in performance over previous hot shot facilities. Figure 7 shows a sketch of the ONERA hot shot

TEST TECHNIQUES

- FORCE AND MOMENT
- HEAT TRANSFER
- TRANSITION STUDIES
- COMBUSTION EXPERIMENTS
- DYNAMIC STABILITY
- SCRAMJET INLET STUDIES
- FREE FLIGHT EXPERIMENTS
- WAKE STUDIES (OPTICAL INSTRUMENTATION)

Figure 6. Test techniques in tunnel F.

tunnel, F4. A projected performance envelope for F4 is given later (Fig. 21), along with other European high-enthalpy faciilities.

A summary of the advantages and limitations of hot shot facilities in general, and Tunnel F in particular, is given in Fig. 8. The uncertainties in free-stream conditions, uncovered in Tunnel F, have been discussed in a previous paper in this series.[4] The lack of certainty about the free-stream Mach number in this tunnel was one of the factors that eventually led to its demise.

SHOCK HEATED FACILITIES

Heating a gas by processing it with a shock wave has long been recognized as an effective way, producing very high temperatures in the fluid. Shock tubes have long been a fundamental tool for the study of chemical kinetics. The pioneering work at the Cornell Aeronautical Laboratory[5,6] in the 1950s and 60s gave impetus to an important high-enthalpy wind tunnel for aerodynamic and aerothermodynamic testing.

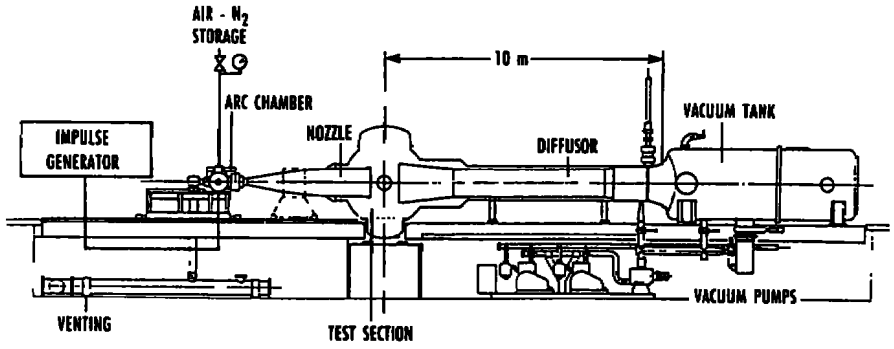

Figure 7. Sketch of ONERA facility, F4.

ADVANTAGES	LIMITATIONS AND CONCERNS
• LARGE MACH NUMBER REYNOLDS NUMBER MAP	• TIME VARYING TEST CONDITIONS
• MODERATELY LONG TEST TIME	• FLOW CONTAMINANTS
• MODERATELY HIGH ENTHALPY	• PRODUCTIVITY
• CHOICE OF TEST GASES	• LIMITED AIR CHEMISTRY
• WIDE RANGE OF TEST TECHNIQUES AVAILABLE	• COLD WALL CONDITIONS ONLY
	• FREE-STREAM UNCERTAINTIES

Figure 8. Advantages and limitations of hot shot tunnels.

Reflected Shock Tunnels

Figure 9 shows a schematic of a reflected shock tunnel along with graphs indicating the operating cycle for the device. Initially, a high-pressure driver gas is separated from the low-pressure test gas by a diaphragm. Rupture of the diaphragm at t = 0 starts the process with shock propagating along the shock tube, followed by the interface between the driver gas and the test gas. At the same time, an expansion wave system is propagating through the driver gas. Part b of Fig. 9 at t = t_1 shows the theoretical pressure distribution along the tube at this point in the process. The incident shock reflects from the end of the shock tube and processes the test gas a second time, bringing it to rest. The test gas stagnation pressure and temperature, p_5 and T_5 can be driven to very high levels if the incident shock Mach number is high.

The impingment of the incident shock on the end of the shock tube causes a second diaphragm at the nozzle entrance to rupture and initiates flow through the nozzle into the test chamber. A number of factors may limit the test time in a reflected shock tunnel. One of these is the interaction of the reflected shock wave with the driver gas interface. The three situations that can occur as the reflected shock intersects the contact surface between the driver gas and test gas are illustrated in Fig. 10. The under-tailored case results in a drop in stagnation pressure as soon as the expansion reaches the end of the shock

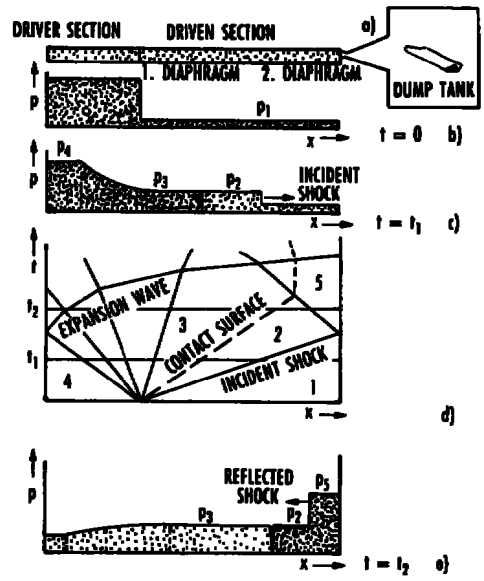

Figure 9. Shock tunnel operating diagram.

tube, and results in a reduced test time. The tailored interface,[6] where the shock wave propagates through the interface with no resistance, is the ideal case and produces maximum run time.

Other factors that can limit test time are arrival of the expansion wave reflected from the end of the driver tube at the end of the shock tube, and arrival of driver gas in the test section. The available test time for reflected shock tunnels is less than ten milliseconds at low enthalpy. In general, the higher the total enthalpy of the test gas, the shorter the test time.

The total enthalpy generated in the test gas is primarily a function of the incident shock Mach number, Figure 11 shows the effect of increasing diaphragm pressure p_4/p_1 on the incident shock Mach number. This figure clearly shows the limited

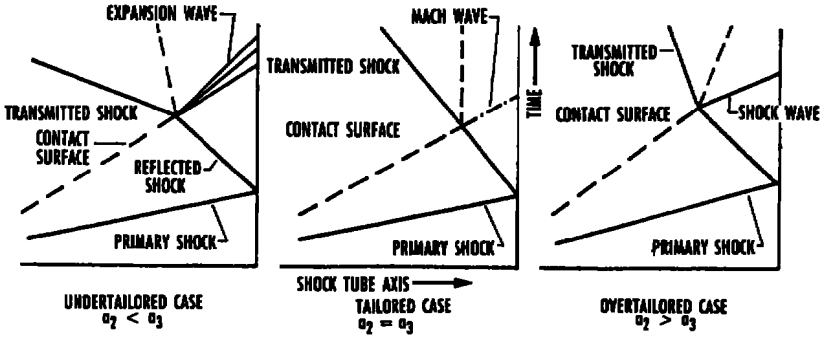

Figure 10. Interaction of reflected shock with contact surface.

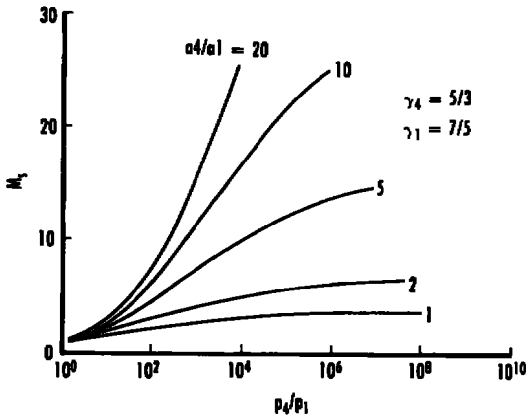

Figure 11. Ideal gas shock tube theory.[7]

number. Figure 11 shows the effect of increasing diaphragm pressure P_4/P_1 on the incident shock Mach number. This figure clearly shows the limited effect of high driver gas pressure on shock Mach number. Only by increasing the speed of sound ratio, a_4/a_1, as well as the driver gas pressure can high enthalpy conditions be produced in the test gas. The speed of sound of the driver gas can be increased by using a light gas (helium or hydrogen) for a driver and increasing its temperature. The conventional reflected shock tunnels at Calspan ATC and Technical University at Aachen use electrical resistance heaters to increase the temperature of the driver gas up to a few hundred degrees Kelvin. Other facilities use more exotic techniques to heat the driver gas and obtain higher enthalpy levels.

Figure 12 shows an elevation view of the Aachen shock tunnel,[8] TH2, and Fig. 13 shows a schematic drawing of the basic components. A performance envelope of the facility in terms of Mach number and length Reynolds number (L = 0.25 m) is presented in Fig. 14. A similar facility in the US is the Calspan 96-in. shock tunnel. A sketch of this unit, along with a performance diagram, is shown in Fig. 15.

Another useful way to display the characteristic of a reflected shock tunnel is on a Mollier diagram as shown in Fig. 16. This figure, which was computed air in equilibrium, shows explicitly the relationship between shock Mach number and total enthalpy. The right ordinate is test section velocity, assuming

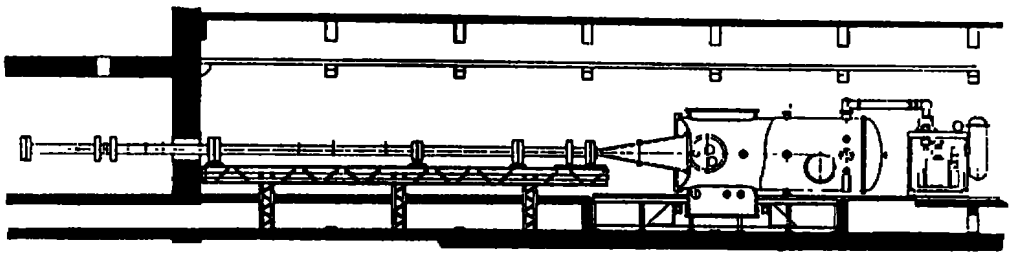

Figure 12. Side view to scale of the Aachen shock tunnel.[8]

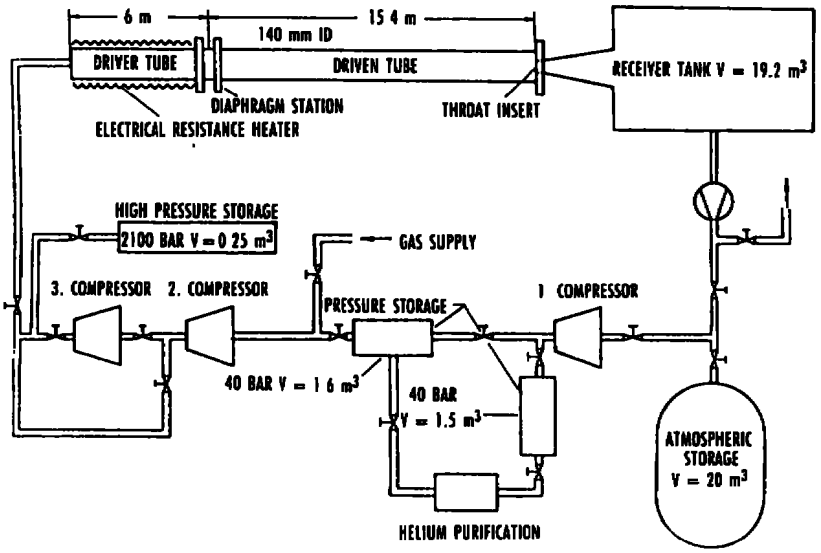

Figure 13. Basic components of the Aachen shock tunnel TH2.[8]

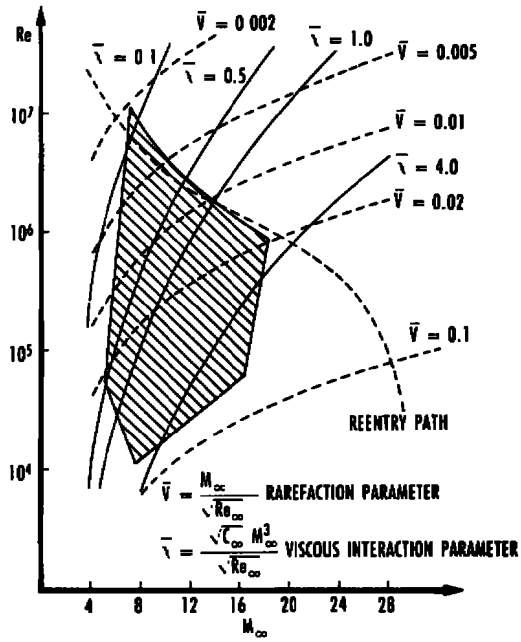

Figure 14. Performance envelope of Aachen shock tunnel, TH2.[8]

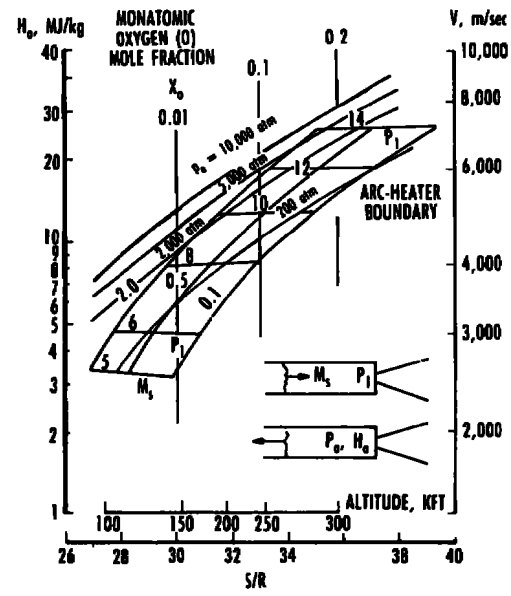

Figure 16. Reflected shock tunnel stagnation conditions.

complete conversion of total enthalpy to kinetic energy. At the high enthalpy levels shown in this figure, oxygen begins to dissociate in the stagnation region. As the test gas expands in the hypersonic nozzle, the composition freezes so that the test stream is partially dissociated. The frozen composition can be correlated with the stagnation entropy so that mole fractions of monatomic oxygen present in the test stream can be displayed in this figure. The altitude scale on this figure assumes an isentropic expansion of the test gas to the corresponding pressure.

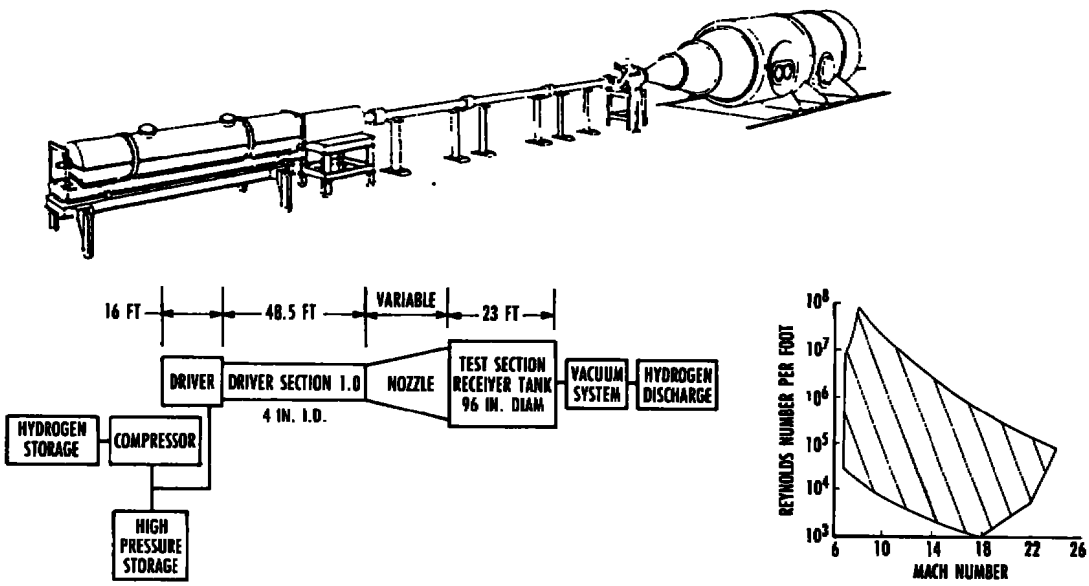

a. Facility sketch

b. Performance envelope

Figure 15. The Calspan 96 in. shock tunnel.[7]

Expansion Tubes

A expansion tube is a shock-heated device that uses an unsteady expansion rather than a nozzle to accelerate the test gas to high velocity. An operating diagram for an expansion tube is shown in Fig. 17. The unsteady expansion is more efficient in converting thermal energy to kinetic energy than a nozzle and can thus achieve higher velocities. Also, by not bringing the gas to rest prior to expansion, the expansion tube avoids the high static temperatures that produce a dissociated test stream. Since the test gas is processed by only one shock, the test gas entropy is less than in the corresponding reflected shock tunnel, and the total pressure of the test gas is higher. Very high total pressures are theoretically possible in expansion tubes.

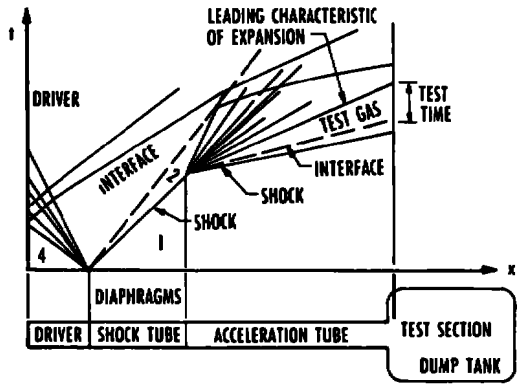

Figure 17. Expansion tube operation.[9]

The disadvantages of the expansion tube are that the run times tend to be very short (a few hundred microseconds), and the exit diameter of the acceleration tube where the test gas enters the test section is small. Langley experience with the expansion tube found that the operating envelope of the device is limited. The Langley expansion tube is currently being operated by GASL under the label HYPULSE. The device is currently directed toward supersonic combustion experiments.[10]

High Performance Drivers

A number of techniques are used to increase the temperature of the driver gas and to produce higher enthalpy of the test gas. The Boeing shock tunnel in Seattle, Washington, USA introduces a stoichiometric mixture of hydrogen and oxygen into the helium driver gas and ignites the mixture to heat the test gas. A shock tunnel at NASA AMES uses an electric arc discharge to heat a driver gas. Compressive heating of the driver gas has been shown to be a particularly effective way of generating high-enthalpy test streams.

Free-Piston Shock Tunnels

One of the most successful of the high-enthalpy shock tunnels is the free-piston shock tunnel developed primarily by Ray Stalker in Australia.[11] The operating diagram for the free-piston shock tunnel is shown in Fig. 18. The main advantage of the free-piston driver is the use of compression heating to increase the driver temperature to very high levels. The principal parameter affecting this temperature rise is the volume compression ratio of the compression process. With adiabatic compression, it is not difficult to achieve driver gas temperatures exceeding 4,000 K, and to produce shock Mach numbers above 15. All of the free-piston shock tunnels currently in operation use high-pressure air to propel a reuseable piston that compresses and heats the driver gas.

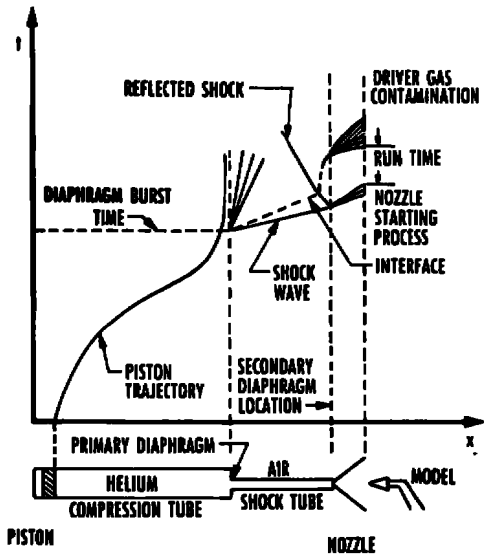

Figure 18. Free-piston shock tunnel operating diagram.

Figure 19 shows the series of free-piston shock tunnels designed and built by Prof. Stalker. The first three of these were built at Australian National University in Canberra. Experiments in T3 began in the mid 1960 and continue to the present time. The latest Australian facility,[12] T4, which began operation in the mid-1980s, is located at The University of Queensland. There is a fifth facility in the T series, T5, located at Caltech in the US. This tunnel, which is somewhat larger than T4, is operated by Prof. Hans Hornung, a long-time colleague and associate

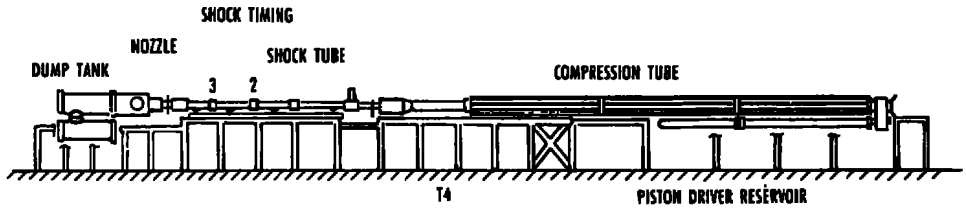

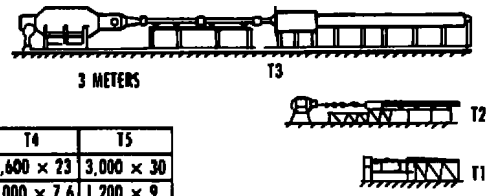

	T1	T2	T3	T4	T5
COMPRESSION TUBE, cm	150 × 5 1	300 × 7 6	600 × 30	2,600 × 23	3,000 × 30
SHOCK TUBE, cm	135 × 1.2	200 × 2 1	600 × 7 6	1,000 × 7.6	1,200 × 9
NOZZLE EXIT DIA , cm	5 1	11	30	30	31
PISTON MASS, kg	0 8	1 2	90	92	150

Figure 19. 'T' series free piston shock tunnels.[12]

of Prof. Stalker. The Caltech facility[13] became operational early in 1991. A second US facility, RHYFL, that was being built by Rocketdyne and would have been the world's largest, has been discontinued.

The European free-piston shock tunnel is located at DLR in Goettingen, Germany, and with a 15-cm shock tube is currently the world's largest.[14] A sketch of the layout of this facility, along with projected near-maximum operating conditions is given in Fig. 20. This facility came on line in 1991 and is currently undergoing calibration tests. Figure 21 shows a projected performance envelope for HEG in terms of binary scaling parameter, ϱL, and velocity, along with the re-entry

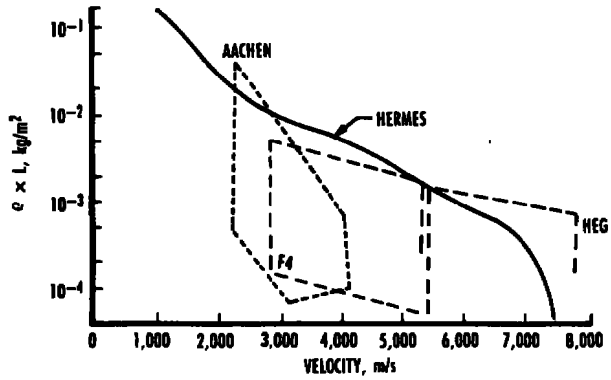

Figure 21. Performance envelopes for European high enthalpy facilities.[3]

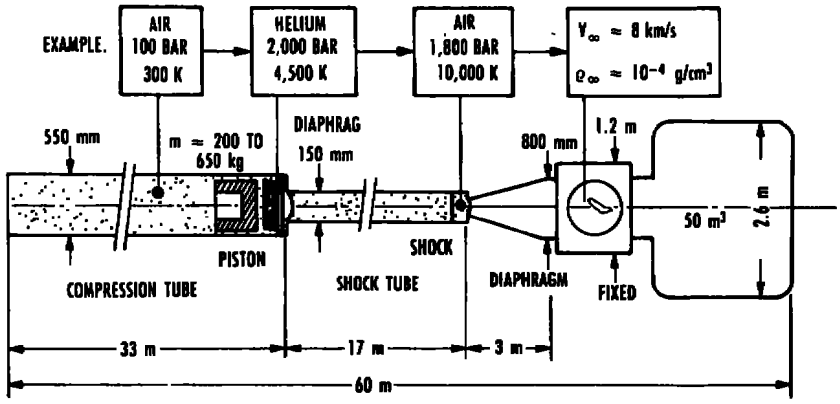

Figure 20. High enthalpy wind tunnel Göttingen.

trajectory of Hermes. Also shown on this figure are corresponding envelopes for the Aachen shock tunnel and the ONERA hot shot tunnel F4.

The extremely high enthalpies that can be generated with a free-piston driver introduce some severe materials problems for these facilities. This is particularly true for free-piston devices operating in a reflected shock mode. For these facilities, nozzle throat erosion and melting/burning of the shock tube in the stagnation region are factors that limit the stagnation pressures and temperatures that can be attained without incurring damage. Non-reflected shock tunnels and expansion tubes which do not stagnate the test gas are less susceptible to heating problems but tend to have much shorter run times. In this regard, nitrogen is a much more benign test gas for shock tunnels than air. Oxygen, at the temperatures produced, will destroy most of the high-strength materials available for shock tube and nozzle construction.

It is clear from this brief survey that many different types of shock-heated facilities have been developed. The common characteristics of these devices is that they have the ability to produce very high enthalpy flows for a very short duration. In general, the higher the enthalpy, the shorter the test time. The combination of short test time and high impulsive starting loads makes conventional aerodynamic force and moment testing in shock tunnels challenging. However, a wide variety of test techniques have been developed for use in these types of facilities. Figure 22 gives a summary of the advantages and limitations of shock heated facilities.

ADVANTAGES	LIMITATIONS AND CONCERNS
• HIGH ENTHALPY	• SHORT TEST TIMES
• WIDE RANGE OF FREE-STREAM CONDITIONS	• FLOW CONTAMINANTS DISSOCIATED FREE STREAM
• CHOICE OF TEST GASES	• PRODUCTIVITY
• WIDE RANGE OF TEST TECHNIQUES AVAILABLE	• FREE-STREAM UNCERTAINTIES
	• COLD WALL CONDITIONS ONLY

Figure 22. Advantages and limitations of shock-heated facilities.

COMPRESSION-HEATED FACILITIES

This class of facilities uses adiabatic compression to compress and heat a test gas and thus are related to the free-piston shock tunnels just described. In theory, the use of a nearly isentropic process to compress the test gas should be much more efficient than the highly nonisentropic shock wave. Practically, however, the compression heated devices have not been able to achieve the total temperature levels generated by shock tunnels. Figure 23 shows some of the characteristics and operating conditions of the principal western European gun and piston tunnels. Prominent among these is the VKI Longshot.

A compression-heated facility that is perhaps not as well known to westerners is the TsNIIMASH Piston Gas Dynamic Unit (PGU) U-11[16] illustrated schematically in Fig. 24. The upstream portion of this facility is a free-piston compressor consisting of a

	PLACE	P_0 MN/m²	T_0 °K	M_∞	Re_d MILLIONS	NOZZLE DIA d cms	TEST TIME mS
GUN TUNNEL	IC	67	1,000	9 3	25	45	5
GUN TUNNEL	RAE	≤ 17	1,100	11 + 13	0.25 TO 2	25	30 TO 50
GUN TUNNEL	SU	30	1,300	8.5 TO.11	0.5	25	20 TO 40
SHOCK TUNNEL	RAE	2-40	800 TO 4,000	9	15 TO 0.04	38	3 TO 10
LONGSHOT	VKI	≤400	≤2,480	14, 15 TO 20	4 – 2 5	42	10 – 15

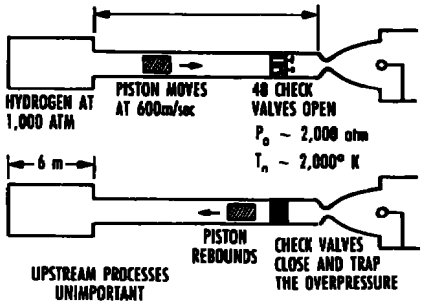

SCHEMATIC AND OPERATING CYCLE OF THE LONGSHOT TUNNEL

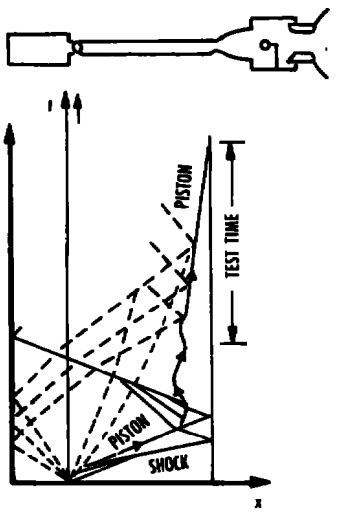

SCHEMATIC OF THE GUN TUNNEL AND OPERATING CYCLE

Figure 23. Characteristics of compression heated facilities.[15]

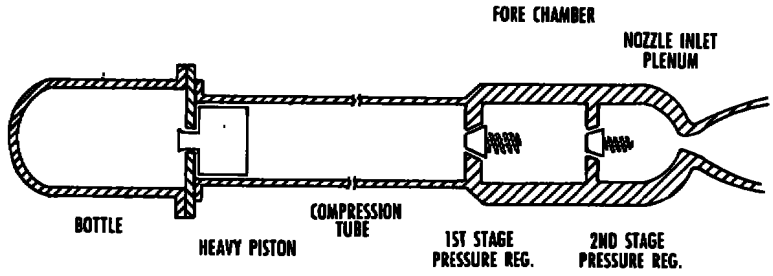

Figure 24. TSNIIMASH piston gas dynamic unit U-11.[16]

reservoir chamber, a heavy, 1,500 kg piston and an 18-in.-diam compression tube. In this compression process, a diatomic test gas (air or nitrogen) is compressed to approximately 2,500 bar and 2,000 K.

The two chambers at the downstream end of the compression tube are the most interesting feature of the facility. When the pressure of the test gas reaches some prescribed level, the quick-opening valve to the fore chamber or accumulator opens, and this chamber fills in an unsteady, nonisentropic process. In this process, the temperature of the test gas is increased by a factor of $\gamma = 1.4$.

When the pressure in the fore chamber reaches the level required for the test, the check valve closes. The gas remaining in the compression tube acts as a cushion for the piston. The second-stage regulator valve then opens introducing the test gas into the nozzle plenum and initiating flow through the nozzle and test section. The second stage regulator maintains the pressure in the plenum constant until the pressure in the accumulator falls below the required value. A diagram of the operating process of the TsNIIMASH facility is shown in Fig. 25. Run times for this facility are quoted as ranging from 0.1 to 1 sec.

A variety of nozzle assemblies are available for this facility, permitting the generation of hypersonic test section Mach numbers from 6 to 20. The nozzle exit diameter is 0.8 m. The facility is also equipped with a transonic nozzle. A performance envelope for this facility in terms of Mach number and Reynolds number is given in Fig. 26.

AEROBALLISTIC RANGE/TRACK

Figure 27 shows a cutaway drawing of the AEDC Hypervelocity Range/Track G.[1] The major components shown are a 6.35-cm bore light gas gun and a 300-m-long, 3-m-diam environmental chamber. The first 20 m of the chamber are separated from the rest by a bulkhead and quick-acting valve to form a blast tank. The vacuum plant is used to pump down the environmental chamber to simulate the desired altitude. The 300-m range is equipped with 50 orthogonal spark

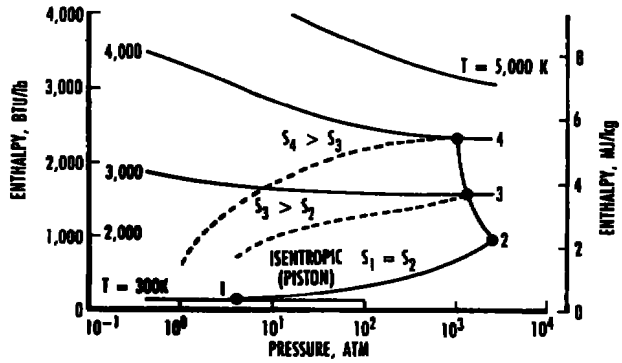

Figure 25. Mollier-type diagram of PGU compression process.[17]

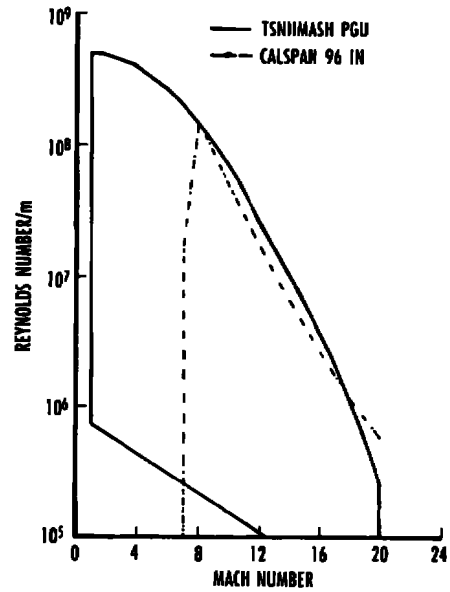

Figure 26. Operating envelope for aerodynamic/aerothermal testing.[17]

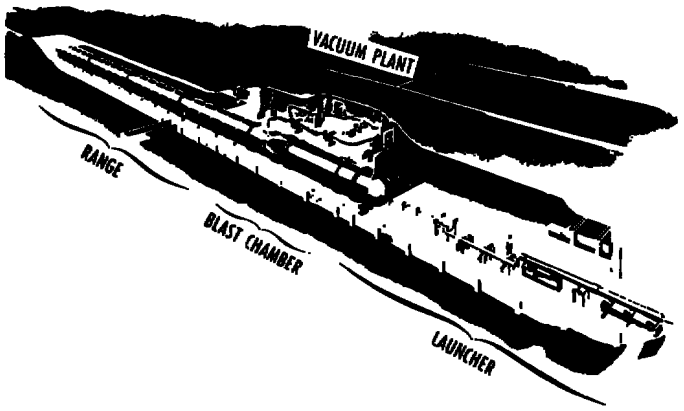

Figure 27. AEDC hypervelocity range/track G.[1]

shadowgraph stations, 13 X-ray stations, and 7 laser photographic stations, as well as many other special instruments.

The operation of the 2-stage light-gas gun is illustrated in Fig. 28. A gunpowder charge accelerates the piston down a pump tube, compressing and heating the light gas (usually hydrogen) to high pressure

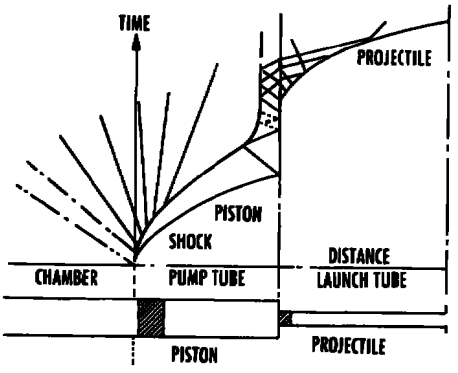

Figure 28. Two stage light-gas gun.[7]

and temperature. At some prescribed pressure, a diaphragm separating the pump tube from the launch tube ruptures, causing the projectile to be accelerated down the launch tube. With this method, projectile velocities in excess of 5,000 m/sec can be achieved. Figure 29 shows the launch capability of the Range G gun.

The facility is used in two modes. The first mode is called the free-flight mode. In this mode, a model and sabot package are launched out of the light gas into the blast chamber, where the sabot is aerodynamically separated from the model and trapped in the blast chamber. The model is allowed to pass through the blast chamber and into the test environment, where the necessary data are taken as the model flies to the end of the chamber, where it is destroyed. Figure 30 shows a typical Range G model for the free-flight test mode and its sabot. The main restriction of the free flight models is that they be aerodynamically stable so they can fly the length of the range without significant flyoff. Typically, free-flight models are axisymmetric.

The second mode of testing, the track mode, is illustrated in Fig. 31. In this test mode, the model is launched out of the light-gas gun onto a four-rail track which guides the model through the test chamber and into a recovery tube. In the recovery tube, the model is brought to rest without incurring significant damage. Figure 32 shows a typical Track G model. The major requirement here is that the model has a cylindrical base made of an appropriate material such as Lexan® . The base is used to mate the model with the gun and the four-rail track system. Aerodynamic stability is not an important consideration for track models.

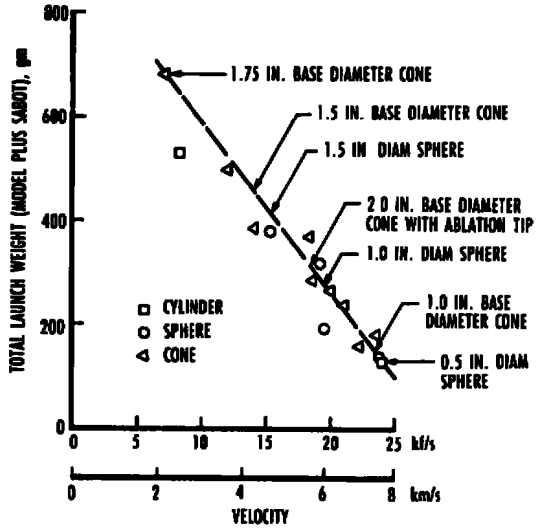

Figure 29. G-range launch capability.[1]

The significant advantage of the ballistic range is that it can duplicate the stagnation pressures and enthalpies at Mach numbers corresponding to the peak heating portions of reentry trajectories. In effect, ballistic ranges permit flight testing in a controlled environment. Figure 33 gives a partial list of types of tests that can be carried out in Range/Track G. The major disadvantages of an aeroballistic range are that only small axisymmetric

Figure 30. Typical range G free-flight model.

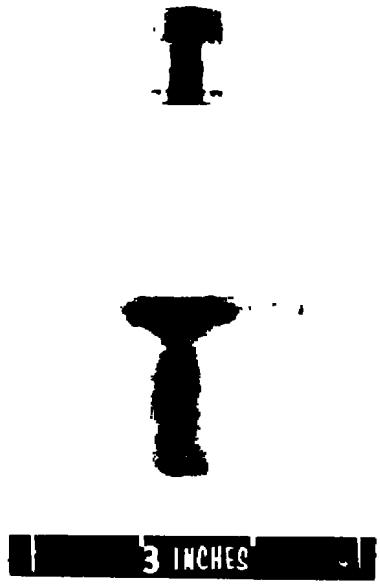

Figure 32. Typical track G model.

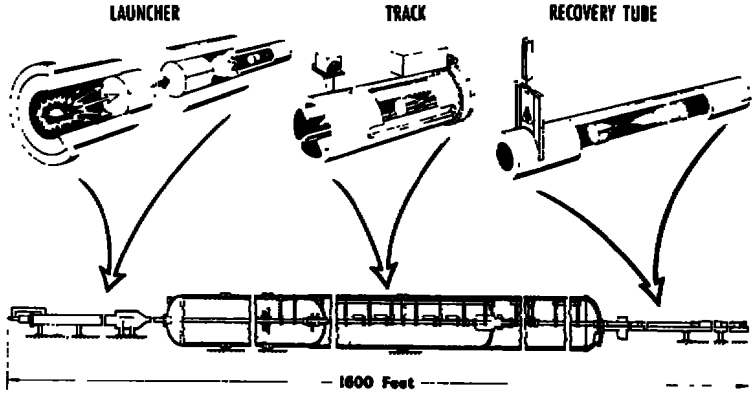

Figure 31. AEDC track G.

models normally can be tested, and that data acquisition, other than photographic data, is difficult because there is no physical data link. The advantages and limitations of ballistic ranges are summarized in Fig. 34.

RANGE G UPGRADE

AEDC is currently renovating and upgrading several test units in the Hypervelocity Range Complex.[18] Figure 35 is an artist's sketch showing the improved G-Range as it will appear at the end of this year (1993). The centerpiece of this renovation is a new, large (8.38-cm bore) two-stage light-gas gun capable of launching larger projectiles with substantially lower peak acceleration. The softer launch anticipated with the larger gun is illustrated in Fig. 36. A primary role of the new gun will be to launch slender models of low bluntness for the purpose of studying their wake signature characteristics.

An important ancillary device in this enhancement is a dual-purpose impact/impulse facility that will be placed adjacent to the new large gun. In its impact role, the dual facility will be a

- ABLATION/EROSION
- TCNT
- NOSETIP TRANSITION
- HEAT TRANSFER
- AERODYNAMICS
- ROCKET CONTRAIL
- REENTRY PHYSICS
- IMPACT
- PROJECTILE
- WAKE SIGNATURE

Figure 33. Range/track G test techniques available.

ADVANTAGES	LIMITATIONS AND CONCERNS
• FREE FLIGHT IN A CONTROLLED ENVIRONMENT	• SHORT TEST TIMES
• HIGH VELOCITY ATTAINABLE	• NO PHYSICAL DATA LINK
• WIDE RANGE OF FREE STREAM DENSITY	• SMALL SCALE AXI SYMMETRIC AERODYNAMICALLY STABLE MODELS
• UNCONTAMINATED FREE STREAM	• 1 MODEL - 1 HOT SHOT
• CHOICE OF TEST GASES	• HIGH ACCELERATION LOADS ON MODEL
• POSSIBLE SNOW, DUST, WATER DROPS	• UNCONTROLLED MODEL ATTITUDE

Figure 34. Advantages and limitations of ballistic range/track facilities.

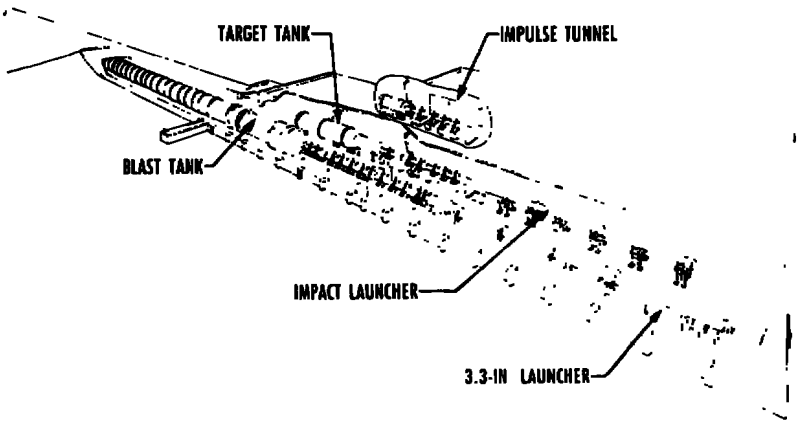

Figure 35. G-range enhancements.[18]

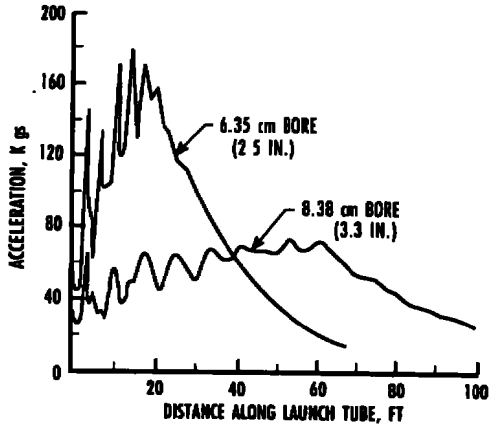

Figure 36. Launch acceleration comparison.[18]

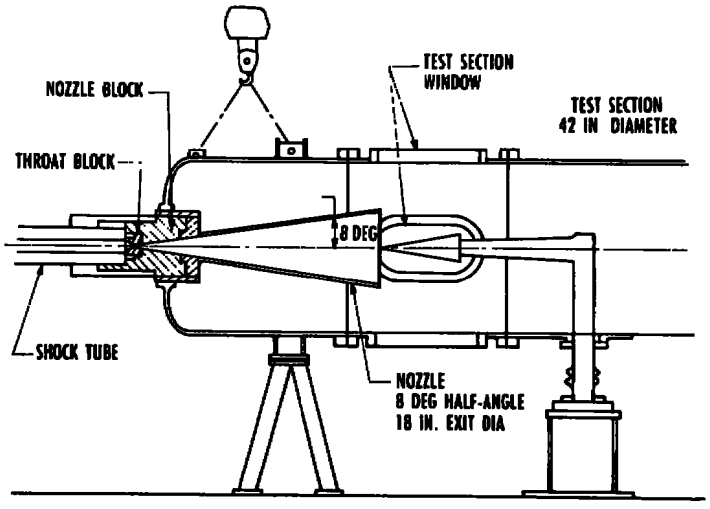

Figure 37. Nozzle/test section detail.[19]

copy of the existing launch gun with a 6.35-cm bore. The gun will be used to launch projectiles to impact targets located in the existing target/dump tank. In addition to the impact role, it is planned to operate this leg of the facility as a free-piston-driven reflected shock tunnel. In this mode of operation, the launch tube will be replaced with a 7.62-cm diam shock tube, nozzle, and test section. The nozzle and test section of this shock-heated impulse tunnel is shown in Fig. 37. The free-piston shock tunnels built previously use high-pressure air to drive a reusable piston. It is anticipated that by using a gun-powder-propelled dispos-able piston to compress and heat the driver gas, higher performance may be achieved by this facility than other free-piston shock tunnels. Figure 38 presents an anticipated performance map of this facility in terms of velocity and binary scaling parameter, ϱL.

CURRENT AERODYNAMIC SIMULATION DEFICIENCIES

The current deficiency in aerodynamic ground test capability can be illustrated by comparing the trajectories of various vehicle with a composite envelope of existing facilities. This comparison can be made in terms of different parameters depending on what phenomenon is of principal concern. Perhaps the most fundamental is in terms of velocity and pressure altitude, the basic vehicle trajectory parameters. This comparison is shown in Fig. 39 and dramatically reveals the inability of ground test facilities to duplicate the flight conditions of hypersonic vehicles. When plotted in terms of classical aerodynamic simulation parameters, Mach number and Reynolds number, the comparison of vehicle trajectory and composite envelope of US facilities shows less disparity. Much of the facility performance map shown in Fig. 40 is provided by the Calspan Shock Tunnels. Even in terms of classical aerodynamic simulation, however, there are difficulties that are not apparent in terms of this figure. One of the major influences of flight Reynolds number is its effect on the location of

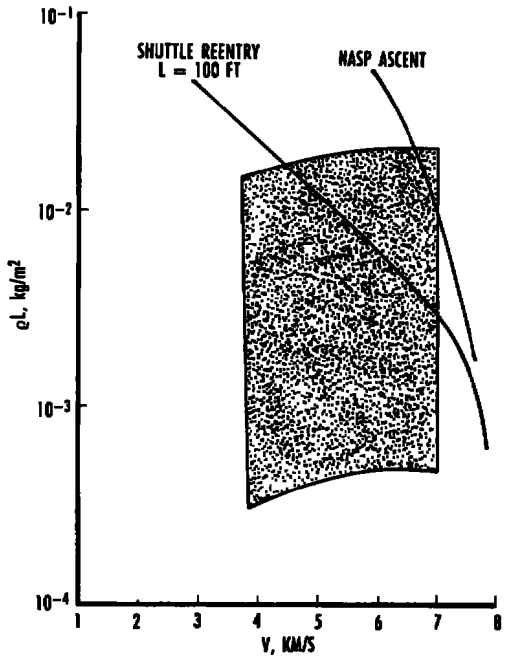

Figure 38. Projected performance envelope for AEDC free piston shock tunnel.

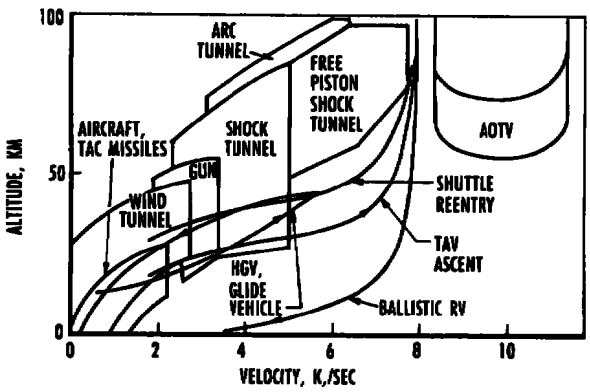

Figure 39. Comparision of facility envelops and vehicle trajectories.

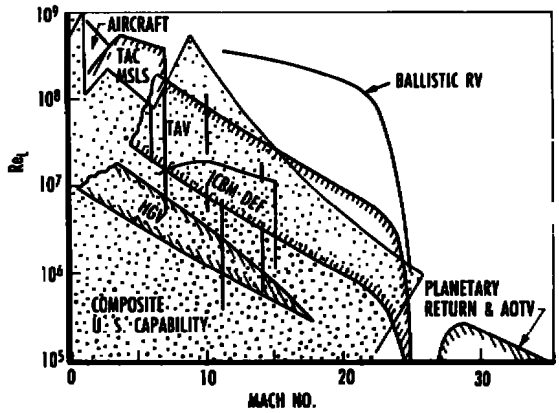

Figure 40. Aerodynamic simulation capability.

boundary-layer transition. No large, high Mach number facility currently exists that is sufficiently quiet to reasonably simulate this phenomenon.

The ability to simulate chemical kinetic effects is best represented by comparisons of facility performance and vehicle trajectory on an ρL-V plot. Such a plot is shown for some European high-enthalpy facilites in Fig. 21 and for the AEDC free-piston shock tunnel in Fig. 38. Generally, ultra-high enthalpy facilities which introduce chemical kinetics into the flow do not expand the test gas to the correct ambient temperature. Thus, a duplication of ρL and velocity do not imply a duplication of Mach number and Reynolds number.

The major shortcomings of the ballistic range are primarily associated with small-scale models and data quality problems rather than the inability to match flight conditions.

CONCLUDING REMARKS

A short survey of various types of short-duration, high-enthalpy facilities has been presented and examples given. No attempt has been made to provide a complete list of the active high-enthalpy facilities in the world. The types of facilities considered in this paper are primarily employed for aerodynamic and aerothermal testing, but many of them have been and are being used for combustion experiments. Examples have been chosen from US and European facilities. Of the examples presented, only Tunnel F, the AEDC Hot Shot Tunnel, is no longer in operation.

REFERENCES

1. *Test Facilities Handbook*, 12th edition, Arnold Engineering Development Center, Arnold Air Force Base.

2. Pate, S. R. and Eaves, Jr. R. H. "Recent Advances in the Performance and Testing Capabilities of the AEDC-VKF Tunnel F (Hotshot) Hypersonic Facility." AIAA Paper No. 74-84.

3. Muylaert, J. et al. "Standard model test in the new European High Enthalpy Facility F4 and Exrapolation to Flight." to be published.

4. Boudreau, A. H. "Characterization of Flow Fields in Hypersonic Ground Test Facilities." Paper No. 4 VKI Lecture Series on Methodology of Hypersonic Testing, Feb. 1993.

5. Resler, E. L., Lin, S. C., and Kantrowitz, A. "The Production of High Temperature Gases in Shock Tubes." J. App. Physics, v. 23, n.12, 1952.

6. Witliff, C. E., Wilson, M. R., and Herzberg, A. "The Tailored-Interface Hypersonic Shock Tunnel." J. Aerospace Sci, 1959.

7. Lukasiewicz, J. *Experimental Methods of Hypersonics*. Marcel Dekker, Inc, 1973.

8. Technical Staff. "Description of the Aachen Shock Tunnel TH2." The Technical University at Aachen, Jan. 1991.

9. Trimpi, R. L. "A Preliminary Theoretical Study of the Expansion Tube, a New Device for Producing High-Enthalpy, Short-Duration Hypersonic Gas Flow." NASA-TR-R-133.

10. Tamagno, J. Bakos, R., Pulsonetti, M. and Erdos, J. Hypervelocity Real Gas Capabilities of GASL's Expansion Tube (HYPULSE) Facility." AIAA-90-1390, June 1990.

11. Stalker, R. J. "The Free-Piston Shock Tube." The Aeronautical Quarterly, November, 1966.

12. Stalker, R. J. and Morgan, R. G. "The University of Queensland Free Piston Shock Tunnel T4 - Initial Operation and Calibration." Fourth National Space Engineering Symposium, Institution of Engincers, Australial, July 1988.

13. Hornung, H "Performance Data of the New Free-Piston Shock Tunnel at GALCIT." AIAA Paper 92-3940, July 1992.

14. Eitelberg, G., McIntytre, T. J., Beck, W. H., and Lacey, J. "The High Enthalpy Shock Tunnel in Goettingen." AIAA 92-3942, July 1992.

15. Stollery, J. L. and Stalker, R. J. "The Development and Use of Free Piston Wind Tunnels." Proceedings of the 14th International Symposium on Shock Tubes and Shock Waves, August 1983.

16. Anfimov, N. A., Kislykh, V. V. and Krapivnoy, K. V. "Nonisentropic Multicascade Gas Compression in Piston Gas Dynamic Units (PGU) U-11 and RHYFL - Development Outlooks." Z. Flugwiss. Weltraumforsch, v16, 1992.

17. Roffe, Gerald, Erdos, John, and Tamagno, Jose "Description of a Unique Hypersonic Blowdown Wind Tunnel and Evaluation of its Capabilities." GASL-0TM 245, October 1991.

18. Cable, A. J. "Upgrade of the Ballistic Range Facilities at AEDC." AIAA Paper 92-0565, January 1992.

19. Maus, J. R., Laster, M. L., and Hornung, H. G. "The G-Range Impulse Facility - A High Performance Free Piston Shock Tunnel." AIAA-92-3946, July 1992.

AERODYNAMIC and AEROTHERMAL FACILITIES
CONTINUOUS FLOW HIGH ENTHALPY FACILITIES

by
Roger Crawford, PhD
Professor Mechanical and Aerospace Engineering
University of Tennessee Space Institute

Introduction

There are hypersonic test requirements which can not be satisfied by short duration or pulsed high enthalpy facilities. Thermal equilibrium in structures and propulsion systems is required for accurate evaluation of temperature and performance. Reference 1 contains a summary of both continuous and pulsed hypersonic simulation capability for application to hypersonic propulsion system testing. Combustion-heated facilities and electric arc-heated concepts are presented in Reference 1 and will be reviewed in this paper. Also MHD augmented arc-heated facility performance will be presented for very high Mach number simulation above 10. Propulsion system test and simulation requirements include; true enthalpy, correct entropy, freestream total pressure and clean air for correct combustion kinetics. Exact simulation requires flight test, however each of the high enthalpy facilities reviewed meets most of the requirements for a range of Mach numbers.

Combustion-Heated Facilities

Combustion-heated facilities produce a test flow by burning a mixture of fuel, air and oxygen in a high pressure combustor to yield a test gas with the correct total temperature and oxygen content. However the products of combustion, CO_2, CO, H_2O, OH - - - are present as contaminants, and their impact on combustion kinetics and wall heat transfer must be analytically evaluated. Facilities of this type include the NASA Langley Combustion-Heated Scramjet Test Facility which burns hydrogen, the NASA Langley 8-foot high temperature tunnel which burns methane (Ref. 2), and the Aerojet Engine Test Facility which uses monomethylhydrazine and nitrogen tetroxide.

The major advantage of these facilities is that the energy input to the test gas due to combustion can be much greater than electrically heated facilities allowing much greater mass flow. The Langley Combustion Heated Facility is nominally operated at 912° K, six atmospheres with a mass flow of 14 Kg/s (Ref. 2). Approximately 0.1 Kg/s of hydrogen produces energy release of 10 MW of power. The maximum test total temperature is limited to the adiabatic flame temperature of an ideal mixture of fuel and oxidizer. (Figure 1.) The level of water vapor becomes a significant contaminate as the total temperature is increased in a hydrogen-air-oxygen facility. The maximum Mach number simulation in a hydrogen heated facility is approximately 7. Thus combustion-heated facilities have a limited Mach number application in development of hypersonic systems.

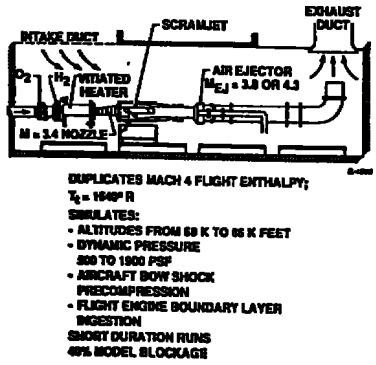

Figure 1. Langley Combustion-Heated Scramjet Test Facility (Ref. 2)

Since a stoichiometric mixture of oxygen and hydrogen will produce a total temperature near 4000°K (Mach 10), a combustion-heated storage (convection-heated) facility can provide clean air at Mach 8 conditions. The NASA Lewis Hypersonic Tunnel Facility (Ref. 3) uses a carbon storage heater to heat nitrogen followed by oxygen mixing ahead of the test section. Figure 2 shows the HTF configuration, and Figure 3 presents the operating simulation range. High operating costs, low test frequency, and flow contamination by heater "dust" limit the application of combustion-heated storage heaters. However very large mass flow rates may be obtained from storage heaters for several minutes of test time. Table 1 provides performance of the HTF

at Mach numbers 5, 6 and 7.

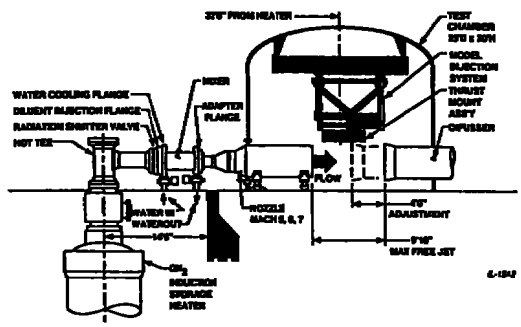

Figure 2. HTF Schematic View. (Ref. 3.)

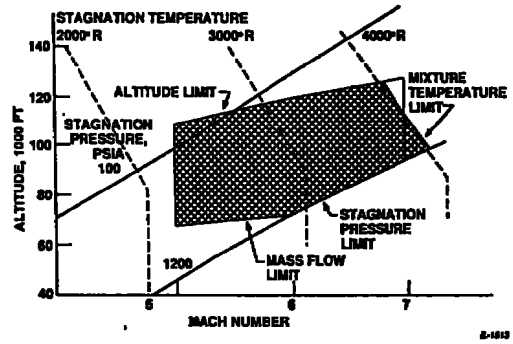

Figure 3. HTF Operating Envelope. (Ref. 3.)

TABLE I
HTF FLOW SUMMARY

	NOZZLE					TEST SECTION					
MACH NO.	PRESSURE (PSIA)	TEMP (°F)	FLOW (LB/SEC)	THROAT DIA (INCHES)	EXIT DIAMETER (INCHES)	STATIC PRESS (PSIA)	STATIC TEMP (°F)	ALTITUDE (1000)	DYNAMIC PRESS (PSFA)	RUN TIME	
5	410	2200	188	7.2	42	0.740	394	68	1852	103 SEC	2
	70.5	2420	30.9	7.2		0.210	428	100	291	4.9 MIN	1
6	1200	2965	222	4.9		0.510	398	72	2157	42 SEC	2
	144	3310	25.4	4.9		0.071	451	120	220	4.8 MIN	1
7	1200	3630	104	3.5		0.210	412	68	1835	69 SEC	2
	430	4180	36.19	3.5	7	0.071	451	120	220	3 MIN	3

1 Based on Steam Availability at 150 PSIG
2 Based on Maximum Gas Temp. Change of 200° F
3 Based on Diffuser Temp. Limits

Electric Arc-Heated Facilities

The requirements for higher test enthalpies lead researchers to develop electric arc heaters. Early research was directed toward small high temperature materials testing and low density hypersonic wind tunnels. As the size and power levels of arc heaters increased they were adopted for large hypersonic aerothermal and propulsion facility applications. The following presentation "Electric Arc Heaters" is taken from Reference 4, AGARD High Enthalpy Facility Study Group Report by, Laster, Arnold, Nichols and Horn. (Ref. 4.)

The electric arc heater is a means of directly heating test gases including air to much higher temperatures than by indirect means. Enthalpies as high as 40,000 BTU/lb may be possible at relative low pressures. A maximum practical operating chamber pressure for continuously operating electric arcs is believed to be about 200 atm for heating air. Currently, continuous electric arcs are routinely operated to approximately 120 atm. At this condition the average total enthalpy is limited to about 3000 to 4000 BTU/lb, depending upon the type of arc heater used.

Aerothermal materials testing for shuttle and atmospheric entry (earth and planetary) vehicles has been conducted extensively in arc heated facilities using both blunt body and panel testing modes. Aerothermal materials testing has been by far the most extensive application of large electric arcs. Some experience exists in heating air for combuster research and development and simulated products of combustion for nozzle research and development. Electric arcs also have been used to heat air and other gases to study high speed low density flow phenomena.

Arc Heater Types

Two basic types of electric arc heaters are normally used in high enthalpy wind tunnels. These, the Huels type and the segmented (or constrictor type), are illustrated in Figures 4 and 5.

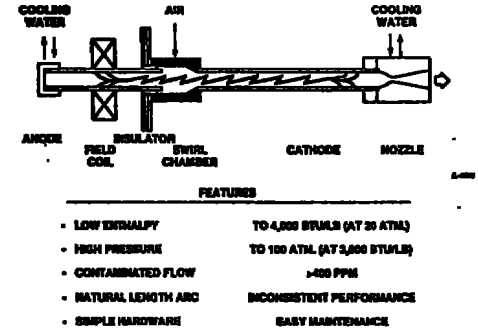

Figure 4. Illustration of Heuls Arc-Heater Concepts and Features (Ref. 4.)

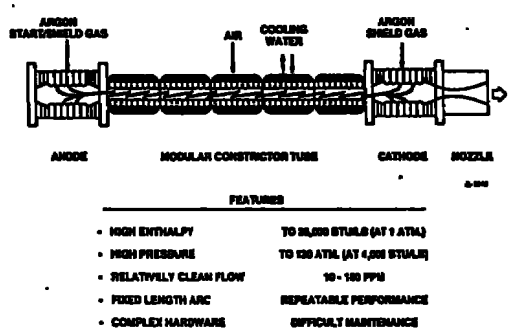

Figure 5. Illustration of Segmented Arc-Heater Concept and Features (Ref. 4.)

Huels Arc Heater. The Huels arc heater is a relatively simple unit where the electrodes are long coaxial tubes separated by a swirl chamber and a single large insulator that takes the entire voltage drop across the arc heater. Air is introduced tangentially into the swirl chamber and the strong vortex formed is largely responsible for stabilizing the arc in the downstream electrode. The upstream electrode has a large magnetic field coil to enhance arc termination and rotation. In some cases a similar field coil is used on the downstream electrode to prevent the arc from blowing through the nozzle. The geometry of this arc heater results in relatively simple device with few components, but the arc is also free to select its own operating length and characteristics since there is little constraint on its termination. Because the arc can select its own "natural" operating length in a Huels arc heater the operating characteristics of this type arc heater are somewhat erratic since the arc does not necessarily attach in the downstream electrode in a repeatable fashion from one run to another. The Huels arc heater can be designed to operate at very high pressure, but the unit is limited to low enthalpy (2,000-4,000 BTU/lb in air) operation since the current density must be kept at a reasonably low level to maintain the integrity of the electrodes. However, the simplicity of the unit allows for easy maintenance and short turn around times during testing. The basic Huels arc heater design has been in existence for many years, predating 1940. The Huels electric arc design is used extensively in industrial applications as well as high enthalpy wind tunnel applications.

Segmented Arc Heater. The segmented design is more commonly used for the wind tunnel applications. This type arc heater is usually quite complicated with many components and precisely machined parts. The electrode packages often contain multiple rings that are the actual electrodes and each active electrode is isolated from the others and is individually ballasted. Each ring electrode has a given current rating, therefore, the number of electrode rings required is determined by the total current expected in the arc column. With proper adjustment of the individual ballasts the electrode rings can be made to share current more or less equally. To assure sufficient ionization in the vicinity of the electrodes a small amount of argon gas may be used to sheath each electrode ring. Since the electrode rings share the current load, the arc attachment produces less thermal load in the material than does the attachment point in the Huels arc heater resulting in less material contamination for the segmented arc heater flow. The stream contamination produced from the electrode material in a segmented arc heater is less than 10 parts per million of the stream mass flow. The constrictor tube separates the anode and cathode electrode packages and is made up of a series of water cooled disks (or segments) that are electrically isolated from each other. The disks are individually water cooled and the test gas (usually air) is introduced between the disks along the entire length of the constrictor channel. The distribution of air along the constrictor can be changed to tailor the performance of the arc heater. Since each segment is insulated from the others the voltage is dropped incrementally along the constrictor from one electrode package to the other. This is in sharp contrast to the design of the Huels arc heater. The disk segments and their associated insulators and seals can be packaged into modules of several disks for ease of handling. The length of the constrictor is tailored to the performance desired with due consideration for the operating pressure, mass flow, and arc current. The arc length is fixed once the length of the constrictor has been determined and the arc column can not achieve its " natural" length as in the Huels arc heater. As a result the segmented arc heater operates in a very predictable fashion with excellent repeatability. The segmented arc heater can produce very high enthalpy levels, but it does so at relatively low pressures. It can be operated at high pressures, but arc instabilities associated with high pressure operation are formidable, because of the high voltage gradients of the long constrictor.

For all types of electric arc heaters contamination of the air stream from electrode particles and thermal and chemical nonequilibrium expansion poses issues which are not fully resolved or addressed. The development of electric arc heaters, especially the segmented type, is not fully matured for the array of test applications envisioned for the future. Much more R & D is needed relative to design, contamination assessment (and possible reduction), scaling, and performance improvements.

Existing Arc Heater Capabilities

Electric arc heaters for high enthalpy wind tunnel testing are operated in China, France, Germany, Israel, the USSR and the United States. Interest is known to exist for development of this capability in India, Japan, and Italy. Capabilities known to exist in the NATO community are discussed in more detail below. France, Germany, and the United States all have arc heater development activities. The existing large electric arc test facilities are predominately used for aerothermal material and structural testing although some usage of them is made for hypersonic combuster and nozzle research in the United States. In France the center of electric arc development for continuous running arcs is at Aerospatiale, Establishment D'Aquitaine. A new "hot shot" electric arc tunnel, F-4, is under construction by ONERA at

LeFagua, France. This new facility will be the only known operating "hot shot" facility in the NATO community. AEDC mothballed their "hot shot" facility (Tunnel F) in 1980. European Space Agency is participating in the planning of a new arc driven wind tunnel to be built at Capua, Italy. Germany has electric arc heater research and development activities at DLR-Koln, University of Stuttgart, and the University of Munich. In the United States the NASA Ames Research Center, NASA Langley Research Center, NASA Johnson Space Center, AEDC, and numerous industrial organizations (most all in the 5-10 MW class) have electric arcs in operation. A summary of existing arc heater capabilities in France, Germany, and the United States is presented in Table 2.

Table 2.a
High Enthalpy Arc Facilities

LOCATION	NAME	TYPE	NOMINAL POWER, MW	MACH RANGE	CHAMBER PRESSURE, atm	REDUCED BULK ENTHALPY, MJ/KG	USE	STATUS
Aerospatiale, Bordeaux	SIMOUN	H	5	3.5-4.5	1-14	16-140	Thermal Protection System	Operational - 1990
"	SAM	I	20		10	230	"	Under Development
"	IP200	I 4 Pkr	20	1.7-2.4	5-60	80-170	"	Operational - 1970
"	MWAH	H	5		130	70	"	Operational - 1988
Capua, IT	SCIROCCO	5	70	-	10.3	250	"	Proposed - Study
CNRSA Le Fauga	P4	Hot Shot		8-15	200-3000	50-300	Aero Heat Transfer	In Construction
DLR Koln	LBK	H H	5 1	3-10 3-10	100 10	45-420 77-152	"	Planned Upgrade Operational
U. of Stuttgart	PWK 1		0.3		1	131-1314	Low Density, Rarefied Flow	Operational
"	PWK-2		6	1.3-3	20		"	Under Construction
AEDC	DET	H	5				Dust Erosion	Stand by
"	H5	H	20	1.5-2.5	100	60-150	Thermal Protection	Operational - 1966
"	H3	5	20	1.5-2.5	115	60-300	"	Operational - 1977
"	H2	H	20	3.1-5.0	100	60-150	Thermal Protection, Aerothermal	Operational - 1969

H - HUELS
S - SEGMENTED

Table 2.b
High Enthalpy Arc Facilities

LOCATION	NAME	TYPE	NOMINAL POWER, MW	MACH RANGE	CHAMBER PRESSURE, atm	REDUCED BULK ENTHALPY, MJ/KG	USE	STATUS
NASA - ARC	Aero Heating	H	20	3.5-12	40	45-120	Aerodynamic Heating	Operational - 1965
	"	S	20	3.5-7	10	120-450	"	Operational - 1970
	3' x 3'	H	20	3.5	20	60-120	Thermal Protection	Operational - 1964
	Panel Test Facility	S	20	3.5	10	120-450	"	Operational - 1970
	Aero-Assisted Hosting Facility	S	60	3.5-7.5	10	120-370	Aerodynamic Heating	Operational - 1974
	Hi-Enthalpy Entry	S	100	5.7	10	200-450 H gMix	Entry Entry	Operational - 1985
	Transition Flow Facility	H	20-100	1.7-2.5	100	60	Propulsion	Under Development
NASA - LRC	Aerothermal	Double Ended Hotch	10	4.5-4.3	6-10.5	To 170	Thermal Protection	Stand by
"	"	AC	5	2.5-3.2	2	10-157	"	"
"	Semiglet Test Facility	H	12	"	40	To 45	Combustor Research	Operational - 1974
NASA-JSC	ARAMJET	S	10		5-10	To 240	Thermal Protection	Operational (2 Test Stands)

France. Three active electric arc facilities exist and are operated by Aerospatiale at Establishment D'Aquitaine. One is a 5 MW Huels type operating at pressures to 14 atm. A second facility uses four 5 MW Huels heaters operating in parallel into a common manifold to 60 atm pressure. The third facility, a Huels type, operates to 9 MW and 130 atm. A fourth facility using the segmented design is under development and will operate to 20 MW and up to 10 atm pressure. All of these facilities are used or are to be used for aerothermal materials testing. The SCIROCCO facility in Italy will have a 70 MW segmented heater operating to 16 atm pressure and is also to be used for aerothermal materials testing.

Germany. DLR-Koln has an arc heated wind tunnel, designated LBK. This facility currently is powered to one megawatt but is proposed for improvement to 5 MW and to be used for Hermes aerothermal testing. The University of Stuttgart is proposing a new 6 MW, one atmosphere total pressure arc facility, designated PWK-2, for materials testing and also has a goal of low density, rarefied flow, aerodynamic testing. They currently have a 500 KW arc driven facility (PWK-1). They have considerable long term experience with operation of low pressure plasma generators.

United States. Government owned electric arc heater test facilities are located at NASA centers and the US Air Force's Arnold Engineering Development Center.

1. NASA Ames Research Center. Currently all of the Ames electric arc facilities are contained within the Arc-jet Complex which has nine available test bays. The Huels arc heater has been used to drive a variety of nozzles in different test bays and exists in three different sizes: a 5 MW unit, a 20 MW unit, and a 100 MW unit. Each of the units is available with various downstream electrode lengths which allow the operator to select a tube length that will best match the expected "natural" arc length. Current designs are for power levels of 100 MW with pressure capabilities to 100 atm and above. With operational capability in this realm the arc heater can be used to drive large hypersonic nozzles. However, consistent operation at these power levels and pressures have not yet been demonstrated for the Ames 100 MW Huels arc heater. The Ames segmented arc heaters are used to drive a variety of nozzles (both semi-elliptic and conical) in different test bays and exist in two sizes: one has a 6 cm bore constrictor and is operated up to 20 MW with air as the test gas; the other has an 8 cm bore constrictor and operates up to 60 MW also with air as the test gas. Both arc heaters use the same basic electrode package, but with a different number of active electrode rings in the package depending on the arc column current required. Another configuration exists which operates at power levels in the 100 MW range using an 8 cm bore constrictor with hydrogen/helium mixtures as the test gas, but this arc heater utilizes carbon rod downstream electrodes rather than the electrode package illustrated in Figure 5. In addition the arc column passes through the nozzle to reach the carbon rod electrodes. This configuration was selected to insure the maximum possible energy transfer to the gas and the attainment of extremely high enthalpy levels for simulation

of entry into the atmosphere of the giant planets. The arc-jet complex uses a variety of axisymmetric nozzles in the facilities, but all of them are conical with 8 degree half-angle expansion. No axisymmetric contoured nozzles are in use. All of the Ames electric arc facilities are pumped by a large 5 stage stream ejector vacuum system. The primary Ames power supply can operate 30 minutes at 75 MW and 15 seconds at 150 MW. The open circuit voltage is 33,000 volts and maximum currents is 16,000 amps. A 20 MW power supply also exists which has an open circuit voltage of 25,000 volts and maximum current of 6,000 amps.

2. NASA Langley Research Center. NASA Langley has three electric arc facilities, one AC and two DC arc powered facilities. The 3-phase AC, 5 MW, arc facility operates at low pressure (2.0) atm with enthalpy levels to 3,500 BTU/lbm and is used for material evaluation. The 20 MW Aerothermal Tunnel is used for structural and material evaluation. It uses a double ended Huels type arc operating up to 18.5 atm chamber pressure and 5,500 BTU/lbm enthalpy. The 20 MW Arc heated Scramjet Test Facility operates to 40 atm chamber pressure and at enthalpies up to 1500 BTU/lb (3500 BTU/lb at 5 atm). This facility is powered by two 10 MW DC power supplies. Figure 6 shows the configuration of the Langley Arc-Heater Scramjet Test Facility including vacuum sphere. Figure 7 details the 20 MW arc heater. Figure 8 compares the performance differences between the combustion-heated and arc-heated scramjet test facilities. Note that Mach number 8 is a simulation limit at a single altitude point.

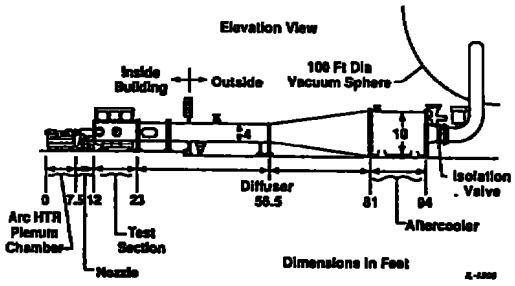

Figure 6. Langley Arc-Heated Scramjet Test Facility (Ref. 2.)

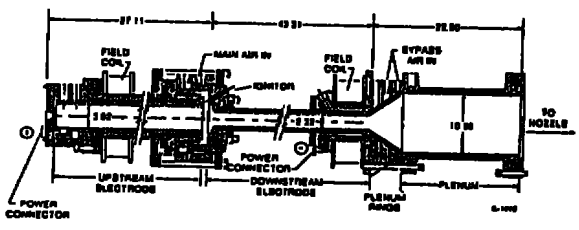

Figure 7. Arc Heater and Plenum Chamber (Ref. 2)

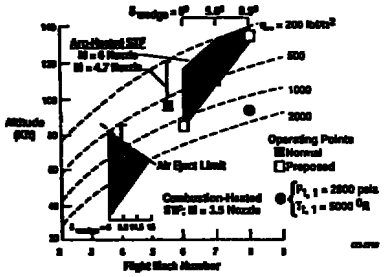

Figure 8. Langley Scramjet Test Facilities Flight Simulation Capabilities (Ref.2.)

3. Arnold Engineering Development Center (AEDC). The AEDC has four test units driven by electric arcs. Three of these units are driven by Huels arcs and one by a segmented arc. One cell, driven by a 5 MW Huels arc with a 7 MW dc power supply, is called the Dust Erosion Tunnel and is used to simulate dust particle impact phenomena. The AEDC High Temperature Laboratory contains the other three test units. Two of these, called HEAT-HR and H2, are driven by a 50 MW Huels type arc, capable of operating at pressure levels to 100 atm with average bulk enthalpy ranging from 2000 to 5200 BTU/lbm. Test unit H1 is driven by a 30 MW segmented arc heater capable of operating at pressure levels to 115 atm and average bulk enthalpy ranging from 2000 to 8500 BUT/lbm. These three arcs are powered by a 60 MW dc power supply with an open circuit voltage of 50 kv and maximum rated operating current of 3000 amps. Both the HR and H1 units are used for aerothermal material testing, primarily re-entry nose tip testing. The H1 test unit also has dust erosion test capability. The H2 unit is a new hypersonic arc driven wind tunnel which currently is driven by a 50 MW Huels type arc. It is anticipated that both aerothermal materials testing and aerodynamic real gas phenomena studies will be conducted with this facility. Both the HR and H1 test units use contoured nozzles with a variety of throat sizes and exit Mach numbers ranging from 1.8 to 3.5. The H2 facility has a variety of conical nozzles and throat sizes which provides Mach numbers ranging from 3.1 to 8.0

The price which is paid in most propulsion test facilities for heating the test gas to enthalpies representative of high flight Mach numbers is some sort of flow contamination. Therefore, the actual test gas is not really air. In the case of H_2 combustion-heated flow, the contaminant is water vapor. Although the oxygen consumed in the heater combustion process is replenished to the proper air mass fraction, the mass fraction of nitrogen is less because of the presence of the extraneous water vapor. The amount of water vapor increases dramatically as higher flight

Mach numbers are simulated. (See Figure 9.)

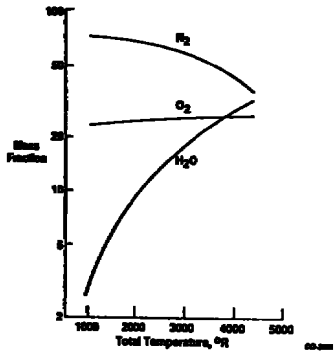

Figure 9. Contaminants in Combustion Heated Scramjet Test Facility (Ref. 2.)

In Langley's Arc-Heated Scramjet Test Facility, the contaminant which is generated in heating the test gas is NO_X. The NO_X is stable as it flows through the facility nozzle. Its concentration has been determined from gas samples over a range of simulated flight Mach numbers and arc power. (Figure 10.) At present, the oxygen lost to NO_X formation is not replenished in the arc-heated flow and, thus, a deficiency of oxygen exists. The existence of these contaminants in the engine and component test facilities has raised questions about their effect on the engine combustion process.

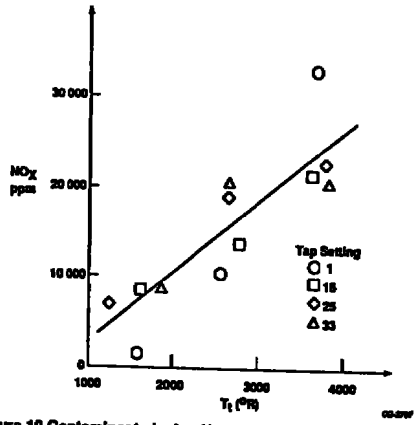

Figure 10 Contaminants in Arc-Heated Scramjet Test Facility (Ref. 2.)

Heating gases with electric arcs is one of the most practical techniques for use in high enthalpy facilities. This is the only viable means of heating air to high temperatures in excess of 3000 deg K for test durations of several minutes. Magnetohydrodynamic acceleration has potential but has had very little development. Hypersonic testing requirements exceed existing capabilities and dictate an aggressive test facilities development program. Critical needs for propulsion, materials, structural, and aerothermodynamic testing dictate high pressures and temperatures not attainable by conventional means. Propulsion and aerothermodynamic testing establish the high pressure and high power requirements. Aerothermal testing defines the high enthalpy and long run time requirements. (See Figure 11.)

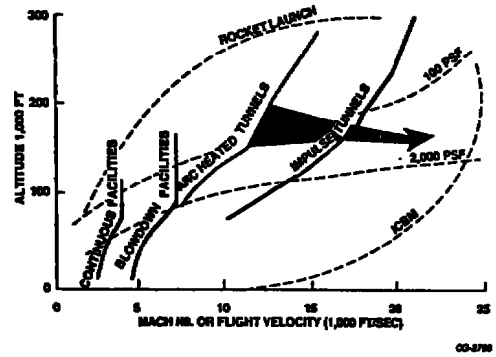

Figure 11. Typical Performance Limits For Facilities Assumes True Simulation of Flight

MHD Augmented, Arc-Heated Facilities

The development of hypersonic flight vehicles has been handicapped and frustrated by a continuing long term lack of experimental simulation facilities. This national shortage of hypersonic test capability includes the range of test facilities from small, basic flow physics research tunnels to large environmental simulation facilities for testing scaled airframe and propulsion systems. The recent renewal of national interest in development of hypersonic flight vehicles for both military and civilian application has directed attention to the critical simulation limitations of test facilities in this flight regime. Facilities based on heating a gas to stagnation conditions in a reservoir by combustion or electrical resistance techniques and expansion in a nozzle to hypersonic Mach number, are limited to true temperature simulation in the Mach 7.0 to 8.0 range. Advances in arc heater technology hold promise for air-breathing propulsion simulation to Mach 12 and higher Mach numbers. The most promising technology for simulation of flight Mach numbers in the 10.0 to 25.0 range utilizes magnetohydrodynamic forces to accelerate the test gas to the required stagnation enthalpies.

The MHD accelerator utilizes the Lorentz force, $J \times B$ body force, to increase gas velocity and thus the total pressure and temperature. Since the energy is added to a supersonic flow, the operating static pressures and temperatures in the accelerator are lower than the corresponding stagnation conditions which should result in reduced wall heat transfer and test gas dissociation. (Figure 12.)

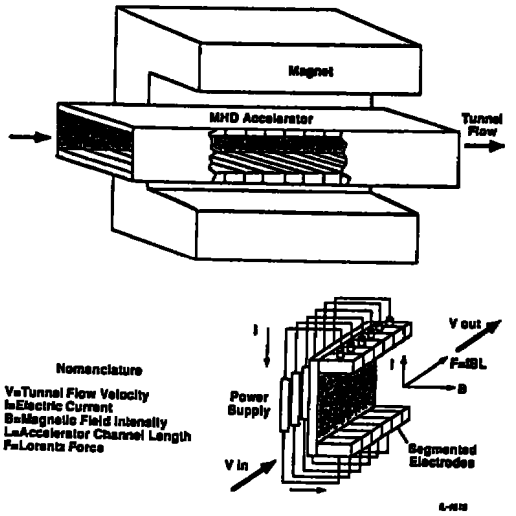

Figure 12. General Concept for the MHD Air Accelerator, With Major System Components (Top) and a Schematic of the MHD Accelerator Process (Bottom)

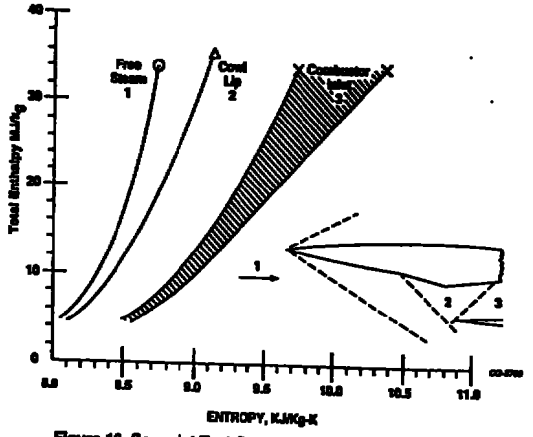

Figure 13. Scramjet Test Conditions, q=1000 psf (Ref. 8.)

Studies and small scale experiments at AEDC in the 1960's (Ref. 5) demonstrated the feasibility of MHD acceleration for high enthalpy flow simulation. Although the United States did not pursue this technology, Russian scientist V.I. Alfyorov published results from an MHD accelerator in 1978. (Ref. 6.) (Alfyorov, 1992) describes an arc-heated, MHD augmented test facility for aerodynamic testing. This facility has produced velocities of 7.5 km/s in a flow cross section of 180 mm X 180 mm for a duration of 1.5 seconds.

A design study conducted by UTSI and supported by AEDC evaluated the technology required to build a large scale MHD augmented, arc-heated hypersonic test facility. (Ref. 7.) The baseline facility performance was evaluated for application to hypersonic propulsion system testing. (Ref. 8.) The key results from this investigation are presented in the following sections.

This study evaluates MHD accelerator performance on the total enthalpy vs entropy map which also contains three hypersonic flight vehicle simulation conditions: free stream, cowl lip and combustor inlet. Figure 13 shows these three simulation requirements for the $q = 1000 Lbf/ft^2$ flight path. The cowl lip envelope and combustor inlet envelope on the enthalpy/entropy map are dependent upon vehicle forebody compression and inlet external compression. Typical values of NASP type inlet losses were used to estimate these envelopes.

Simulation requirements include; correct free-stream velocity, density, hypersonic Mach number, and low dissociation level. Mach number and density can be traded in the nozzle expansion, thus the total enthalpy and entropy are the better simulation parameters for comparison. The MHD augmented facility can be expected to provide correct total enthalpy, and the entropy will be determined by the required accelerator inlet conductivity and accelerator inefficiencies. The influence of accelerator exit entropy on Mach number, Prandtl number, Reynolds number and hypersonic scaling must be evaluated. The MHD augmented facility may provide significant environmental test capability without complete duplication of free-stream conditions.

The performance of the MHD accelerator channel was computed by a series of codes which are routinely used by the UTSI MHD group. The primary code is a one-dimensional accelerator model which accounts for wall heat flux, wall friction and variable thermodynamic properties. The code provides a solution to the energy equation, the momentum equation and the continuity equation with Ohm's Law used to express the electrical terms. A chemical equilibrium code originated by NASA is used to calculate the thermodynamic properties of air seeded with either potassium or cesium.

Accelerator Baseline Design and Performance

An arc-heater, gas generator was selected for the baseline channel design calculations and trade studies. The arc heater was considered for the baseline design due to the existing data base on arc heater performance and the potential for growth in arc heater performance. For the baseline definition of arc heater performance the 200 atm point on the limit line $HP\frac{1}{2} = 40{,}000\ \left(\frac{Btu}{Lbm}\sqrt{P_t}\right)$ was selected resulting in the following arc heater exit conditions:

$H = 6.65 MJ/Kg \quad T = 4751K \quad P = 200\text{atm}$
$S = 8.86 KJ/Kg - K$

The arc heater is connected to the accelerator channel by a convergent-divergent nozzle which is designed to provide a supersonic flow with uniform properties. For the baseline calculations the nozzle is assumed isentropic and provides the selected accelerator inlet pressure at the corresponding Mach number. A primary requirement for the inlet flow to the accelerator is that the gas has sufficient conductivity so that it can be accelerated to overcome friction effects, avoid deceleration and choking.

The baseline simulation design point was selected at Mach 20 along the $q = 1000$ psf flight envelope line. A design mass flow of 22.10 Kg/sec was selected based on projected requirements for a single hypersonic propulsion module. A baseline magnetic field strength of 8 Tesla was considered current state-of-art. Two percent potassium seed by weight was selected as the baseline seeding condition. Electrode current density was constrained to 50 amps/cm^2, and the channel cross-section was assumed square with 0.32 degrees divergence angle on each wall. Twenty atmospheres static inlet pressure was selected as the baseline operating pressure, which yielded an inlet Mach number of 2.161. The one- dimensional MHD math model was run in the design mode to determine channel length required to produce the design point total enthalpy of 22.65 MJ/Kg. The resulting baseline channel length was 3.59 meters with an inlet area of 44.75 cm^2 and an exit area of 118 cm^2. The resulting baseline channel operating envelope was investigated by running the math model at various electrode current density limits. It was found that the channel would simulate Mach 15 conditions at 25 amps/cm^2 and Mach 25 at 70 amps/cm^2. Figure 14 shows the three accelerator simulation results on the enthalpy vs entropy plot, and Table 3 presents the baseline channel definition and resulting operating conditions.

Table 3

Baseline Faraday Accelerator Performance Results

Parameter	inlet	exit M = 15	M = 20	M = 25
P atm	20 00	8.02	4.19	4.07
T K	3266	3406	4025	4689
U M/sec	2306.3	3721 9	5648.5	7168 4
h MJ/Kg	3.996	4.569	6 694	8 748
ρ Kg/m^3	2.141	0.504	0.332	0.262
γ	1.203	1.180	1.169	1.229
σ mhos/m	57.95	149.73	392.79	704.89
s KJ/Kg °K	8.87	9.43	10.06	10.54
H MJ/Kg	6.67	11.50	22.65	34.44
P_t atm	199.3	552.0	4066.8	7290.9
Mach	2.161	3.412	4.565	5.151
J amps/cm^2	____	25	50	70
Q Kw/cm^2	____	5.07	10 37	16.10
Total Power Mw	____	178	458	755

Two conclusions from the design trade study are significant to hypersonic propulsion system testing. Capability of a single accelerator channel geometry and primary magnet to provide a large Mach number simulation range (15-25) by varying only the applied electrode power and exit nozzle area, offers a cost effective test facility. In addition the potassium seed density study indicated that 0.5 to 1.0 percent potassium was adequate for most accelerator calculations made during the study.

Since the seed is a contaminate for propulsion simulation, minimum seed density is important. Figure 15 shows the results of the potassium seed density trade study for baseline accelerator case. The entropy increase with decreasing seed density result from reduced conductivity.

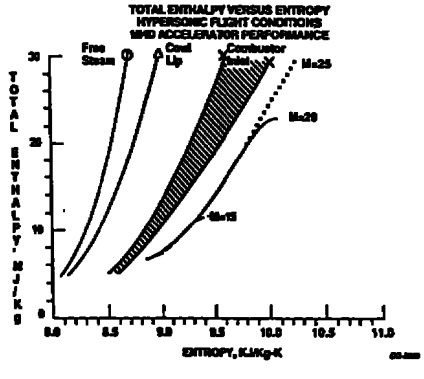

Figure 14. Total Enthalpy vs Entropy, MHD Accelerator Performance (Ref. 8.)

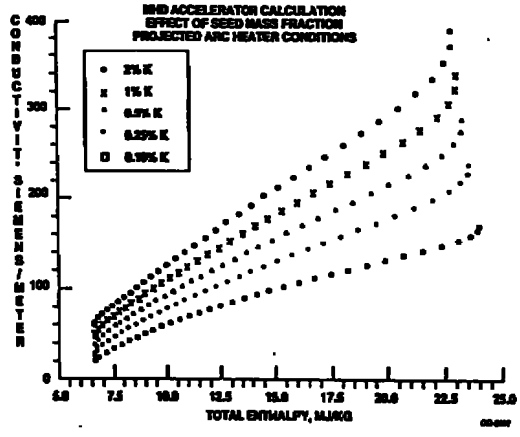

Figure 15. Base Case With Variation in Seed Fraction, (Ref. 8.)

Finite Rate Expansions

The non-equilibrium nozzle calculations were accomplished with a computer code derived from the LAPP code which was originally written to calculate the properties of rocket exhaust plumes. In addition, electromagnetic terms were added to the momentum and energy equation so that the effect of finite rate chemical reactions could be evaluated in an MHD channel. A typical MHD augmented, direct connect propulsion system test facility is shown in Figure 16.

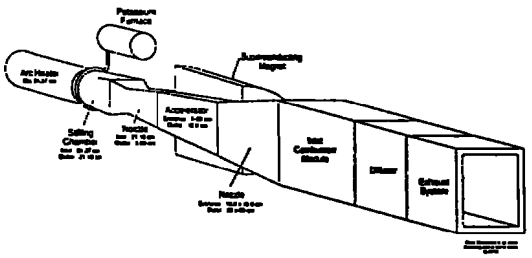

Figure 16. Hypersonic Flow Simulation Facility, Direct Connect (Ref. 8)

With the electromagnetic terms set to zero, this program is used to calculate the gas properties during the expansion through the nozzle which follows the MHD channel. It is also used to estimate the departure from equilibrium in an MHD channel by using the $J \times B$ force, the ohmic heating and the area from the equilibrium acceleration code calculation of the baseline case.

Hypersonic Simulation Results

The following conclusions summarize the results of the finite rate expansions from the accelerator design trade studies. All expansions were calculated for an assumed 15-degree half-angle nozzle. The data was presented as a function of static pressure instead of area or nozzle length. This method allows the simulation parameters to be evaluated over the complete simulation range from combustor inlet to free stream pressures.

- Velocity was well simulated because total enthalpy was correctly simulated and the kinetic energy term dominates (Figure 17).

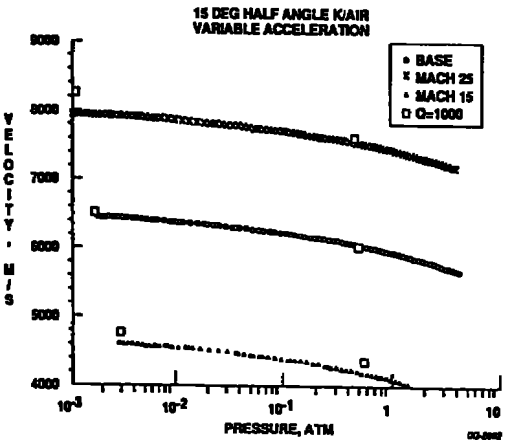

Figure 17. Finite Rate Expansion, Velocity vs. Pressure (Ref. 8.)

- Static temperature was properly simulated at combustor inlet pressures, but ranged 300 to 400° K too hot at free stream conditions. Finite rate effects were significant in reducing temperature as equilibrium calculations increased temperature about 500°K over finite rate calculations (Figure 18).

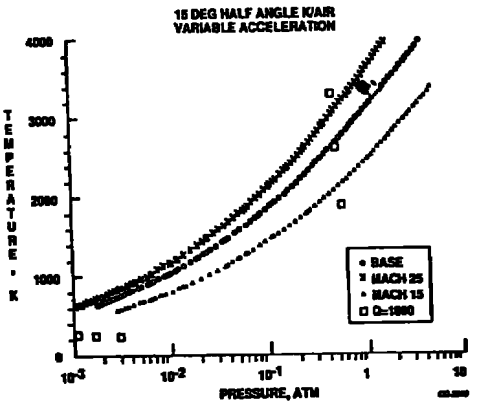

Figure 18. Finite Rate Expansion, Temperature vs. Pressure (Ref. 8.)

- Mach number simulation was influenced by the higher static temperatures which produced 10-percent low values at the combustor inlet and 50 to 60- percent low values at free-stream pressures. In hypersonic flow exact Mach number simulation is not required as long as the simulated Mach number is "High" (Figure 19).

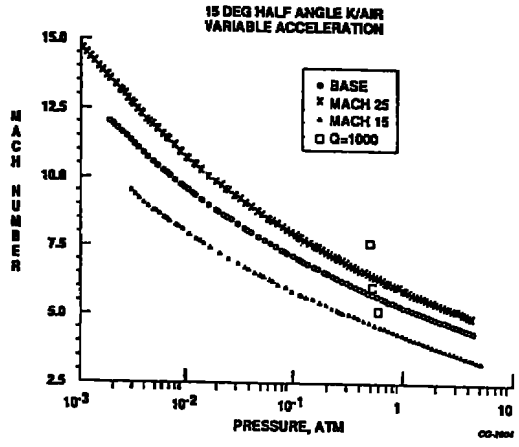

Figure 19. Finite Rate Expansion, Velocity vs. Pressure (Ref. 8.)

- Density followed the inverse of temperature with good simulation at combustor inlet conditions and low values at free stream (Figure 20).

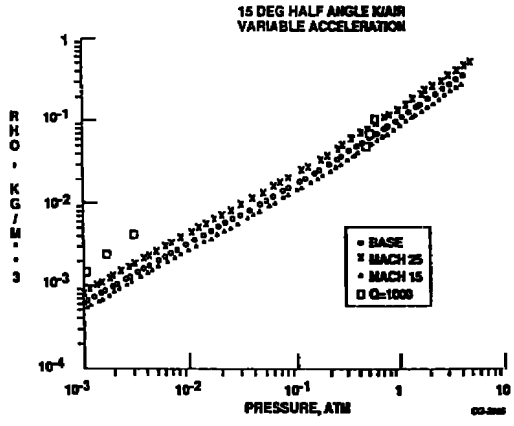

Figure 20. Base Cases, Finite Rate Expansions, Density (Ref. 8.)

- Reynold number simulation was again good at the combustor inlet but was only 20-percent of the desired free stream value (Figure 21).

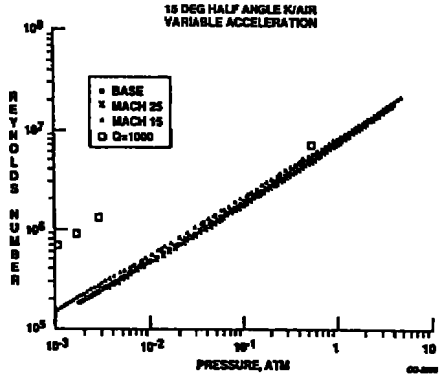

Figure 21. Base Cases, Finite Rate Expansions, Reynolds Number (Ref. 8.)

- The hypersonic similarity parameter Mach number squared divided by the square root of Reynolds number was very well duplicated over the expansion (Figure 22). Mach number divided by the square root of Reynolds number was well simulated at combustor inlet conditions and was higher than free stream values by 50-percent.

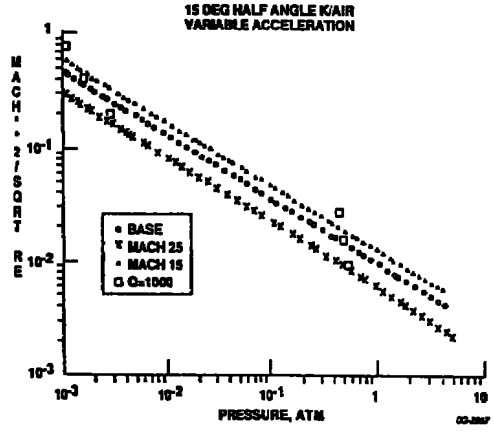

Figure 22. Base Cases, Finite Rate Expansions, $M^2/\sqrt{Re}$ (Ref. 8.)

Direct Connect Propulsion Testing Conclusions

The air-breathing hypersonic propulsion system is integrated into the air-frame to efficiently utilize the vehicle external compression of the capture airflow. Thus at the cowl lip, the start of internal compression, the flow has been compressed by oblique shock waves reducing the Mach number and raising the static temperature and pressure.

The higher entropies and lower Mach numbers down stream of the inlet structure are easier to simulate than the free-stream conditions. The only simulation properties that will not be exactly duplicated in a MHD augmented facility are species concentration. The levels of atomic oxygen, oxides of nitrogen, and potassium seed must be evaluated for possible impact on propulsion testing. The study results show that the MHD augmented facility will provide a good flow simulation for direct connect propulsion testing.

References

1. Thomas, S.R. and Guy, R.W., "Scramjet Testing from Mach 4 to 20 Present Capability and Needs for the Nineties." AIAA-Paper-90-1388, AIAA 16th Aerodynamic Ground Testing Conf., June, 1990.

2. Andrews, E.H., and Guy, R.W., "NASA Scramjet Test Facilities," Hypersonic Propulsion Short Course, UTSI, April, 1989.

3. Haas, J., Chamberlin, R. and Dicus, J., "New Hypersonic Facility Capability at NASA Lewis Research Center," AIAA Paper 89-2534, July, 1989.

4. Laster, M.L., Arnold, J.O., Nichols, F. and Horn, D., "Electric Arc Heaters" AGARD High Enthalpy Facility Study Group Report, 1990.

5. Ring, L.E., "General Consideration of MHD Acceleration for Aerodynamic Testing," Paper presented at the AGARD Specialist's Meeting ARC Heaters and MHD Accelerators, Sept., 1964.

6. Alfyorov, V.I., Labazkin, A.P., Rudakova, A.P. and Shcherbakov, G.I. "Application of MHD-Accelerators in Hyper-Velocity Experimental Aerodynamics," 11th Int. Conf. on MHD Elect. Power Gen., Vol. 4, October, 1992.

7. Crawford, R.A., Chapman, J.N. and Rodes, R.P., "Performance Potential and Technology Issues of MHD Augmented Hypersonic Simulation Facilities," AIAA Paper 90-1380, June, 1990.

8. Crawford, R.A. and Rhodes, R.P., "Hypersonic Propulsion Simulation Capability Utilizing MHD Augmented Arc-Heater Flow," AIAA Paper 90-2505, July, 1990.

CHARACTERIZATION OF FLOW FIELDS IN HYPERSONIC GROUND TEST FACILITIES

by
ALBERT H. BOUDREAU
Director for International Affairs
Arnold Engineering Development Center

ABSTRACT

This paper describes the fundamental differences between nonequilibrium encountered in flight and nonequilibrium phenomena encountered in ground test facilities. It then focuses on facility-induced nonequilibrium, describing the gross effects on bodies and the methods now available to characterize such flows.

It shows that hypersonic test facilities are inherently difficult to characterize. In the past, many hypersonic facilities were reputed to produce test data of inferior quality when, in fact, it was poor characterization of the flow-field principally at fault. With the renaissance in hypersonics at hand, experimentalists face new challenges in characterizing flow fields. The hypersonic test community has developed techniques to accurately determine free-stream conditions. After describing these "tools of characterization," the paper suggests a standard by which all hypersonic wind tunnels should be compared.

NOMENCLATURE

A	Nozzle cross-section area
C_A	Axial-force coefficient
C_N	Normal-force coefficient
C_p	Specific heat at constant pressure
d*	Wind tunnels throat diameter
e_v	Energy of molecular vibration
h	Enthalpy
k	Constant
ℓ	Model length
M	Mach number
MF	Mole fraction
P	Pressure
q	Heat addition term [Eq. (3)]
R	Gas constant
Re	Reynolds number
r	Model radius
s	Model surface distance
T	Temperature
t	Time
U	Velocity
X_{cpN}	Axial distance to center of pressure
x	Axial distance
α	Angle of attack
γ	Ratio of specific heats
ϱ	Density
ϕ	Circumferential angle on model
θ	Shock angle on model
τ	Vibration relaxation time

Superscripts

'	Conditions behind a normal shock
*	Sonic conditions at the throat

Subscripts

1	Conditions before a heat addition process
2	Conditions after a heat addition process
b	Model base
$\mathcal{L}$	Centerline
DP	Dew point
fv	Frozen vibration
N	Nozzle static
n	Model nose
o	Reservior conditions
TR	Translation
V	Vibrational
w	Wall
∞	Free stream

Introduction

Vehicles traveling at hypersonic speeds in the Earth's atmosphere encounter air which is in chemical and thermal equilibrium. Air crossing the nearly normal shock wave at the vehicle's nose will

change to a new thermal and chemical state, and the subsequent expansion of that stagnation-region gas around the body may or not be in equilibrium. Dr. Smith's lecture 1-16 indicated the flight regimes where natural nonequilibrium is encountered.

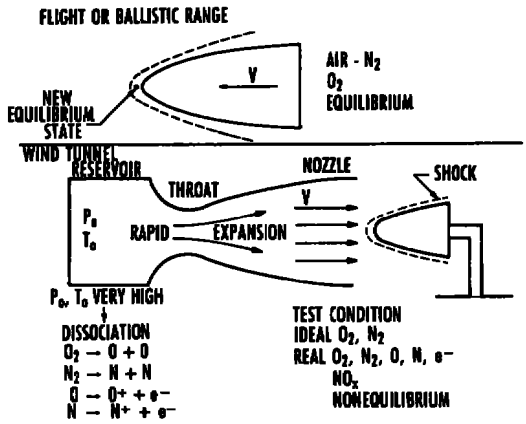

Figure 1. Nonequilibrium in flight and in wind tunnels.

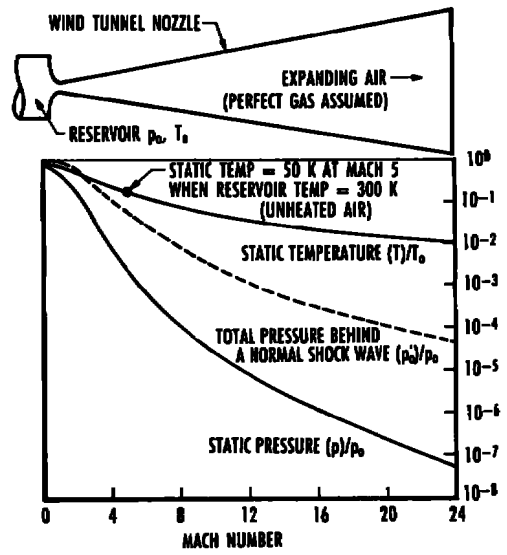

Figure 2. A perfect-gas expansion of air to hypersonic conditions.

In this lecture we will examine another form of nonequilibrium, a non-natural nonequilibrium created in the flow field of a hypersonic ground test facility (See Fig. 1). This form of nonequilibrium results from the heating of the test gas and the subsequent rapid expansion of that gas in a hypersonic nozzle. Assuming that the test gas was air before the heating and expansion process, the flow which exits the nozzle may be a mixture of oxygen and nitrogen molecules, plus a percentage of atomic oxygen, atmoic nitrogen, free electrons, and oxides of nitrogen (NO_x). These species are likely to be in either thermal or chemical nonequilibrium. Hence, the test body encounters a gas already in nonequilibrium to some extent.

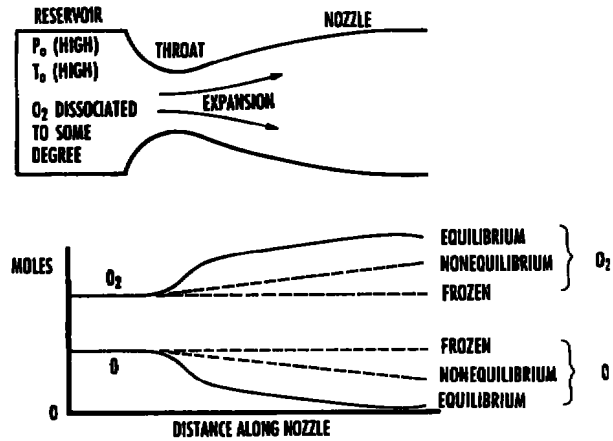

Figure 3. Equilibrium/non-equilibrium/frozen flow.

One can see from Fig. 2 that a gas such as air, when undergoing an expansion to hypersonic conditions, experiences a rapid decrease in static temperature and pressure (hence density). For example, the decrease in static pressure is four orders of magnitude at Mach 8. Recalling that reaction rates and the times required to reach thermal equilibrium are a function of the density of the gas, one can naturally expect that an expansion may not allow sufficient time for the gas to reach equilibrium as the expansion progresses.

An example for dissociated oxygen is shown in Fig. 3, where the test gas containing oxygen is initially contained in a reservoir at high temperature and pressure. In this case the temperature is above 2,400 K and a portion of the oxygen has dissociated. The rapid expansion after the throat is required to keep nozzle lengths within practical limits; hence, the expansion typically progresses at such a rapid rate that equilibrium cannot be maintained in the gas.

If the expansion is so rapid that the reactions (which bring the gas to equilibrium) are essentially stopped, the gas is said to be in a "frozen" state. If the reaction continues during the expansion, but cannot progress rapidly enough to reach equilibrium, the flow is said to be in "nonequilibrium." At

elevated temperatures, a nonequilibrium expansion from a wind tunnel reservoir will yield substantially different gas chemistry than that predicted by assuming an equilibrium process (as shown in Fig. 4).

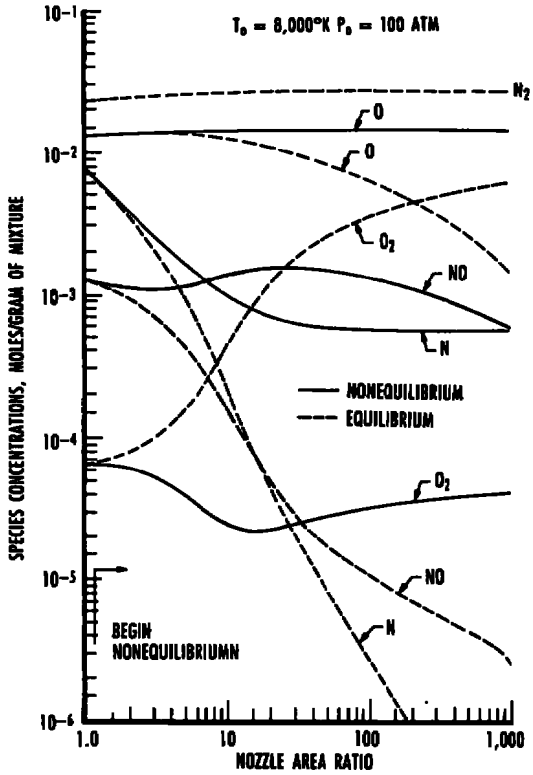

Figure 4. Nozzle flow species distributions, T_o = 8,000°K.

One of the most troublesome constituents of these high-temperature processes is oxides of nitrogen (NO, NO_2), commonly referred to as NO_x. Figure 5 shows that nitric oxide, NO, reaches a maximum mole fraction between 4,500 and 5,500 K, a region of great practical interest for hypersonic wind tunnels. When this gas is expanded through a typical nozzle, the reaction essentially ceases (frozen case) very close to the throat, as shown in Fig. 6. Hence, the experimentalist can expect a significant mole fraction of NO in the test gas exiting the nozzle.

Since the reactions which govern the state of the gas are functions of pressure, temperature, and time, every expansion will differ, being dependent upon the initial state of the gas and the particular geometry of the nozzle. One should expect, however, that the test gas does exhibit some degree of nonequilibrium as it exits a hypersonic nozzle. The experimentalist is therefore required to understand the degree of nonequilibrium and estimate its effects on the test article.

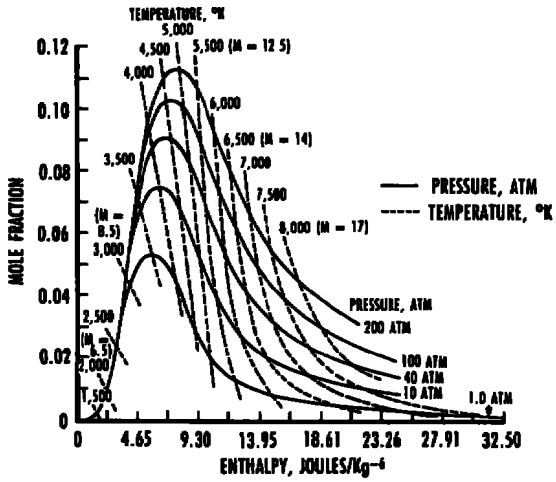

Figure 5. Nitric oxide in high temperature equilibrium air [NO] mole fraction versus enthalpy at constant pressure.

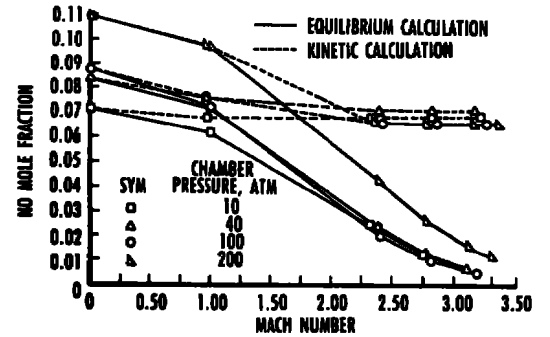

Figure 6. Nitric oxide concentration versus Mach number, equilibrium and kinetic calculations.

As shown in Fig. 7, these effects will vary according to the geometry of the model placed in the test section of the hypersonic wind tunnel. In this case we are assuming that the flow exiting the nozzle exhibits some degree of nonequilibrium. Let us examine the potential effects on four model shapes. Model number one is a very blunt body with a strong shock. Here the gas stagnates and time is sufficient for the gas to come to a new equilibrium state, hence there is a definite change in the gas chemistry.

Case number two considers a very sharp body were the shock waves are relatively weak. Here the transit time of a molecule across the shock wave and the temperature behind the shock are not sufficient to change the state of the gas, so the gas remains in nonequilibrium, i.e. no change. Aerodynamics are dicated by a nonequilibrium gas.

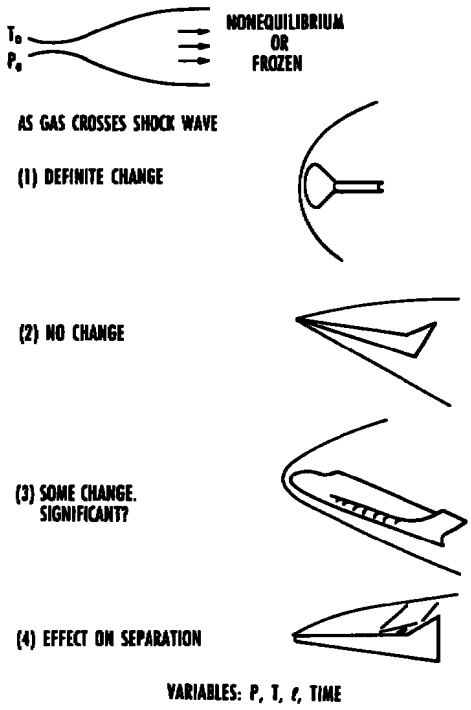

Figure 7. Effect on Models due to wind tunnel non-equilibrium.

The most common, and most difficult case, is example number three where a portion of the test gas penetrates a weak shock, but the remainder passes through a relatively weak shock. Obviously there will be a change only in the gas passing through the strong shock. The effects may or may not be significant.

Case number four deals with a non-equilibrium flow over a separated region. Experiments have shown repeatedly that such separation regions exhibit measurable changes between equilibrium and non-equilibrium flow.

Throughout these discussions one point is apparent: "time" in the form of reaction rates, must be considered as well as the normal aerodynamic parameters of temperature, pressure and geometry when estimating wind tunnel aerodynamics.

Example of Characterization Problems

In 1976 experimentalists working with AEDC's hypersonic wind tunnels discovered that the arc-driven hypersonic Tunnel F was operating at a lower Mach number than expected based on isentropic calculations. A task force was assembled to investigate errors as high as 25 percent in free-stream Mach number.

Generally, improper characterization of hypersonic tunnel flow fields manifests itself as an error in Mach number. Although Tunnel F is an extreme case because of its arc heater, all hypersonic wind tunnels, regardless of type, appear to have some Mach number characterization problems. For example, AEDC's Tunnel C, heated by conventional clean-air heaters, exhibits a Mach error of as much as 1.5 percent compared to that predicted by isentropic flow using the ratio of free-stream pitot to reservoir pressure (see Fig. 8).

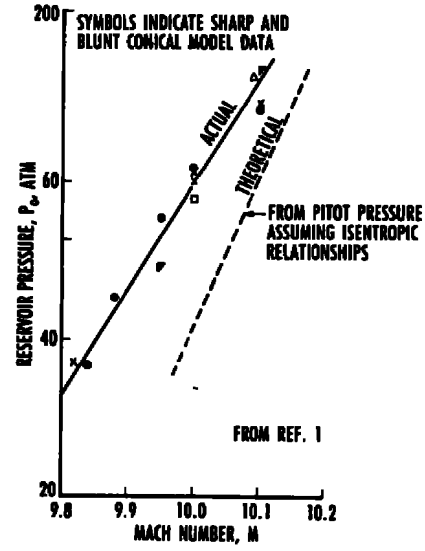

Figure 8. AEDC Tunnel C Mach number adjustment.

These relatively small errors in Mach number can have large effects on the test article. A. Martellucci of Science Applications International reported[2] that a 2-percent apparent Mach error produced a 20-percent error in static pressure measured on a model. Those tests were performed in a hypersonic wind tunnel at Mach 10.

The message distilled from these experiences is that any hypersonic wind tunnel operating at or above Mach 8 is likely to have flow-field characterization problems because of nonisentropic phenomena.

Hypothesis of Nonisentropic Processes

The mechanism believed responsible for the Tunnel F problem (and also observed in Tunnel C) is vibrational excitation, followed by vibrational freezing just downstream of the nozzle throat, and subsequent rapid relaxation in the downstream section of the nozzle. The de-excitation phenomenon is apparently enhanced by the presence of water vapor. It is hypothesized that condensed water vapor (and other contaminants) act as third bodies. Collision of vibrationally excited air molecules with these third bodies allows de-excitation to take place.

The reservoir gas of most hypersonic wind tunnels is excited to various energetic states, as shown in Fig. 9. Note that the vibrational state is excited beginning approximately at 800°K, which means that perfect-gas wind tunnels can experience the phenomenon when test section Mach numbers of eight or more are produced. Duplication facilities (where true temperatures are produced in the test section) encounter excitation at test section Mach numbers above three. Generally, only arc-heated facilities where arc electron temperatures approach 14,000°K can excite the higher energy states. Once free of the arc column, the molecules recombine in the order of 10^{-6} secs. The higher energy states thus decay to excited vibrational states which have relatively long relaxation times, so a significant amount of the vibrational energy remains excited as it passes through the wind tunnel throat.

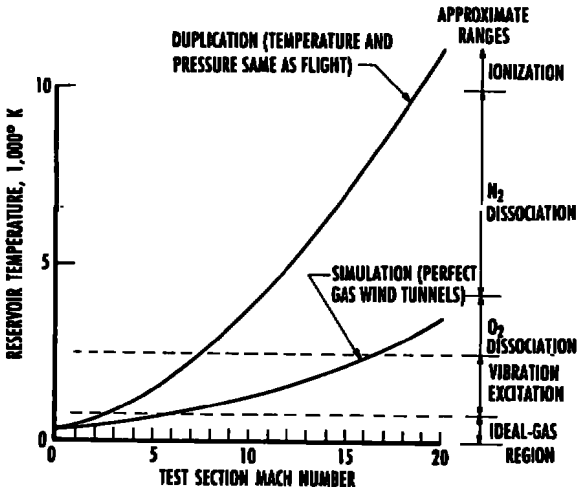

Figure 9. Energetic species in a wind tunnel reservoir.

The vibrational freezing downstream of the throat is predictable based upon available N_2 relaxation rates. The subsequent relaxation (or de-excitation) hypothesis was tested in Tunnel C by measuring the vibration temperature with various levels of water vapor using a Laser-Raman scattering technique. Mach number was experimentally determined from cone measurements.

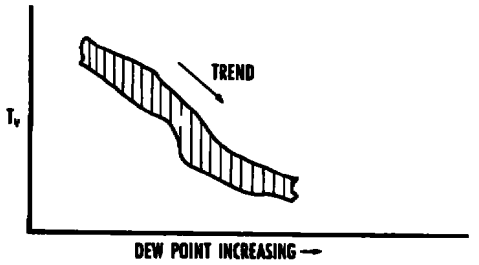

a. Effect on vibrational temperature, T_v

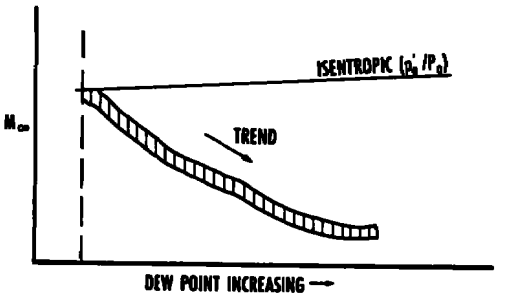

b. Effect on Mach number, M_∞

Figure 10. Effect of water vapor on T_v and M_∞.

Figure 10 indicates the strong correlation between water vapor (dew point) and vibrational temperature, and the subsequent effects on measured Mach number. Figure 11 illustrates this process in the wind tunnels where the downstream portion of the

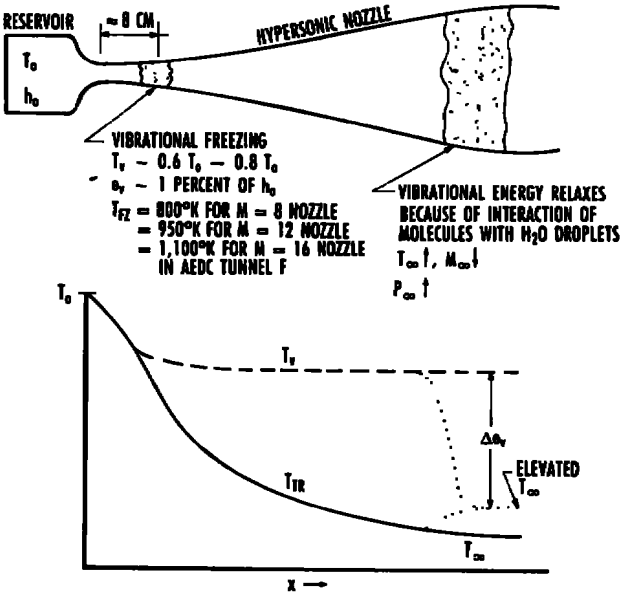

Figure 11. Hypothesis fo cause.

contoured nozzle approximates a constant area duct. When a mechanism is present to raise the static temperature in a constant area, supersonic flow (for $M \geq 8$), the free-stream static pressure also rises significantly with $\Delta P_\infty/P_\infty \approx \Delta T_\infty/T_\infty$. However, velocity and desnsity (hence pitot pressre) change very little.

This may be shown by considering a heat addition process in a constant area duct where condition "1" is prior to the addition and condition "2" is after it. The governing equations are

$$\varrho_1 U_1 = \varrho_2 U_2 \tag{1}$$

$$P_1 - P_2 = \varrho_2 U_2^2 - \varrho_1 U_1^2 \tag{2}$$

$$C_p T_1 + \frac{U_1^2}{2} + q = C_p T_2 + \frac{U_2^2}{2} \tag{3}$$

And rearranging Eq. (2),

$$\frac{\varrho_2 U_2^2}{\varrho_1 U_1^2} = \frac{P_1 - P_2}{\varrho_1 U_1^2} + 1 = \frac{P_1 - P_2}{P_1 \gamma M_1^2} + 1 \tag{4}$$

since

$$\varrho_1 U_1^2 = P_1 \gamma M_1^2 \tag{5}$$

Using the equations of state, continuity, and momentum,

$$\frac{P_2}{P_1} = \left[\frac{1 + \gamma M_1^2}{1 + \gamma M_2^2}\right] \tag{6}$$

and

$$\frac{\varrho_2 U_2^2}{\varrho_1 U_1^2} = \frac{1}{\gamma M_1^2} - \frac{P_2/P_1}{\gamma M_1^2} + 1$$

$$= \frac{1}{\gamma M_1^2} - \frac{1}{\gamma M_1^{\,2}}\left[\frac{1 + \gamma M_1^2}{1 + \gamma M_2^2}\right] + 1 \tag{7}$$

Simplifying,

$$\frac{\varrho_2 U_2^2}{\varrho U_1^2} = \frac{M_2^2}{M_1^{\,2}} \frac{[1 + \gamma M_1^2]}{[1 + \gamma M_2^2]} \tag{8}$$

but

$$\varrho U^2 = k P_o' \tag{9}$$

Therefore,

$$\frac{P_{o2}'}{P_{o1}'} = \frac{M_2^2}{M_1^2}\left[\frac{1 + \gamma M_1^2}{1 + \gamma M_2^2}\right] \tag{10}$$

A typical Mach change observed in Tunnel F was from M1 = 14 to M2 = 12.5. Solving for these values (assuming $\gamma = 1.4$), $P_{o2}'/P_{o1}' = 0.9991$, or for $M \gg 1$

$$\frac{P_{o2}'}{P_{o1}'} \approx 1 \tag{11}$$

With this relative insensitivity of pitot pressure to an entropy increase in the free-stream flow, it is obvious that measurement of pitot pressure alone cannot resolve even large changes in the upstream static temperature. Consequently, measurement of the ratio P_o'/P_o does not readily disclose the presence of real-gas effects that would lower $M\infty$.

Since the static pressure, P_∞, shows a large change, the simultaneous measurement of both P_∞ and P_o' is required to accurately determine free-stream conditions. The prediction of Mach number is, therefore, dependent upon precise determination of free-stream static pressure.

The vibrational de-excitation phenomenon noted here is strongly dependent upon both the species and concentration of impurities such as water vapor. Hence, it is extremely important to reduce these impurities to the lowest levels possible. Likewise, the rate of expansion is important in establishing the vibrational temperature at which that mode freezes. Contoured nozzles with high expansion rates are more prone to vibrational freezing problems than conical nozzles with lower expansion rates.

While other processes could be present to produce nonisentropic flow, the vibrational relaxation phenomenon appears to be widespread. Regardless of the mechanism producing nonisentropic expansions, it is extremely important to experimentally determine free-stream pressure and Mach number to accurately characterize the flow.

Theoretical Analysis

The theoretical analysis utilized in the present work quantifies the effects of nonisentropic (vibration) processes on a hypersonic nozzle expansion. Its objectives are to:

1. Apply the relations for a one-dimensional flow of an imperfect diatomic gas as develolped by Eggers.[3]

2. Perform an equilibrium vibration (isentropic) calculation.

3. Perform a sudden-freezing calculation in which the vibrational energy is instantaneously frozen at a specified point in the expansion downstream of the throat and continue the calculation with the vibration energy frozen at this value.

4. Assume that the frozen vibrational energy is instantaneously and totally released (i.e., local vibrational "melting" occurs) at a specified downstream Mach number in the expansion. Further assume that this vibrational melting occurs at constant area (consistent with the local Mach number specification above).

It is important to observe that this local vibrational "melting" approach is effectively a constant-area heat-addition process under supersonic conditions, which is weli-known from classical gasdynamics to result in the following:

Local Flow Property	Effect
Mach Number (M)	Decrease
Static Pressure (P_∞)	Increase
Static Temperature (T_∞)	Increase

Typical calculated results from the analysis defined above are presented below for the case of a nitrogen gas expansion through a hypersonic nozzle to specified Mach numbers in the range from 8 to 16 (with corresponding A/A^* area ratios from 200 to 5,000) assuming a nozzle reservoir (stagnation) temperature of 1,100°K. Figures 12a-g present solutions assuming that the vibrational energy is frozen at a local Mach number of 1.60 which corresponds to an local area ratio of 1.447. This freezing condition results in one percent of the reservior (stagnation) enthalpy being frozen in vibrational enthalpy i.e., $h_{fv}/h_o = 0.01$). As can be seen from Figs. 12a-f, the influence of local instantaneous vibrational melting on the local flow is

Local Flow Property	Effect
Mach Number (M)	Decrease
Static Temperature (T_∞)	Increase
Static Pressure (P_∞)	Increase
Static Density (ϱ_∞)	Insignificant
Velocity (V_∞)	Insignificant
Dynamic Pressure (q_∞)	Insignificant

Since P_o'/q_∞ = constant in hypersonic flow, the effect on P_o' is also insignificant.

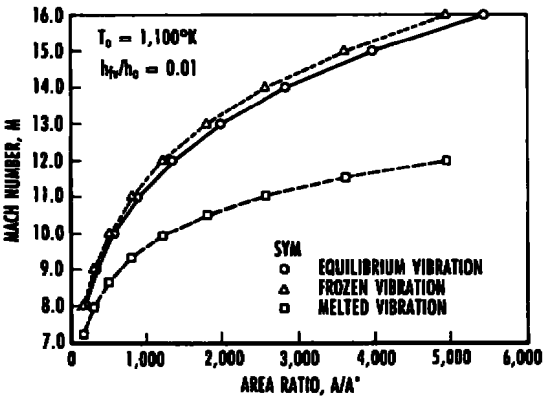

a. Mach number

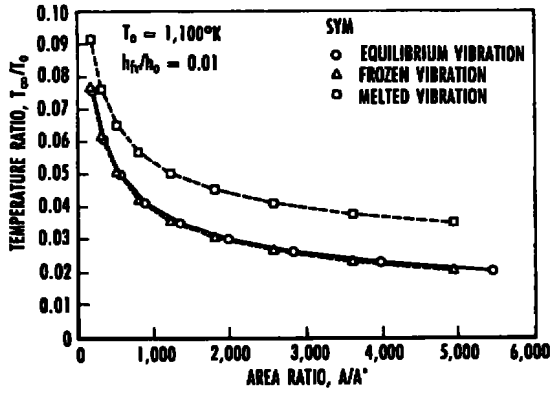

b. Static temperature

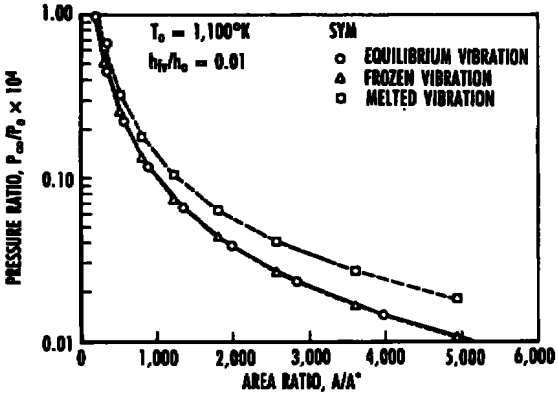

c. Static pressure

Figure 12. Effect of frozen vibration and melted vibration on flow properties (nitrogen gas nozzle expansion).

Figure 12g shows quite clearly the strong influence of the vibrational state on specific heat ratio (1.365 for frozen vibration and 1.40 for both equilibrium and melted vibration). The results presented above are consistent with the findings of Erickson[5] for the limiting cases of nitrogen flow through hypersonic nozzles with equilibrium and frozen vibration.

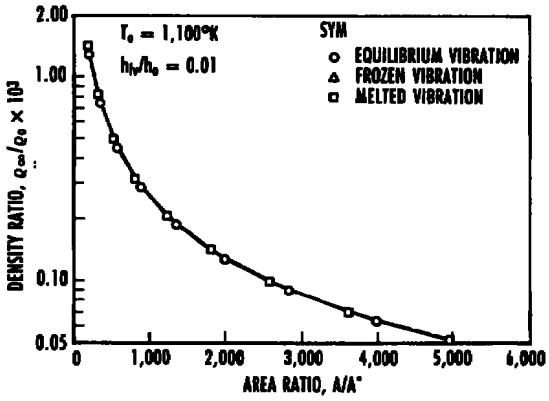

d. Static density

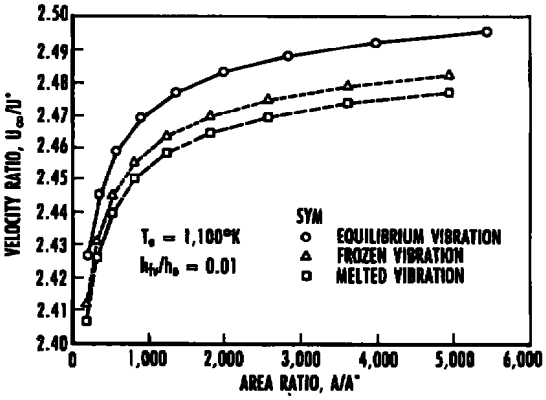

e. Velocity

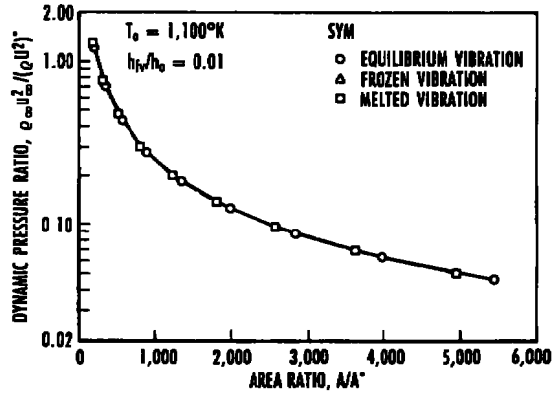

f. Dynamic pressure

Figure 12. Continued.

To better understand the influence of upstream vibrational freezing energy level on the resulting downstream flow and associated vibrational melting,

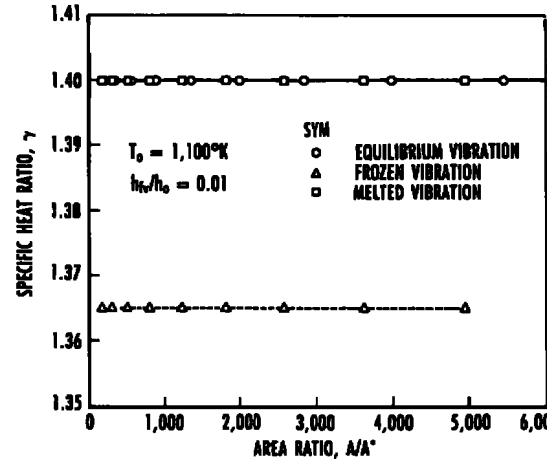

g. Specific heat ratio

Figure 12. Concluded.

calculations are presented in Figs. 13a-e for the following three freezing conditions:

Local Flow Property	Value at Freezing Point
M	1.945 1.600 1.115
A/A^*	1.641 1.447 1.129
h_{fv}/h_o	0.005 0.010 0.020
T_{fv}/T_o	0.595 0.689 0.813

Also shown on these figures for sake of reference is the line of perfect agreement whereby the frozen and melted vibration values are identical. As expected, the larger the amount of frozen vibrational energy, the larger the resulting of effect of vibrational melting on Mach number, static pressure, and static temperature. There is almost no effect on static density and only a very small effect on velocity.

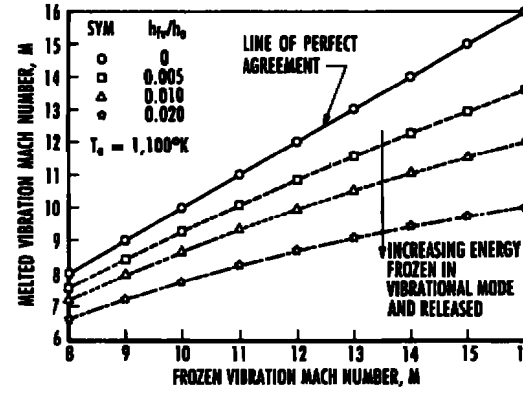

a. Mach number

Figure 13. Effect of frozen vibration energy level on melted vibration flow properties (nitrogen gas nozzle expansion).

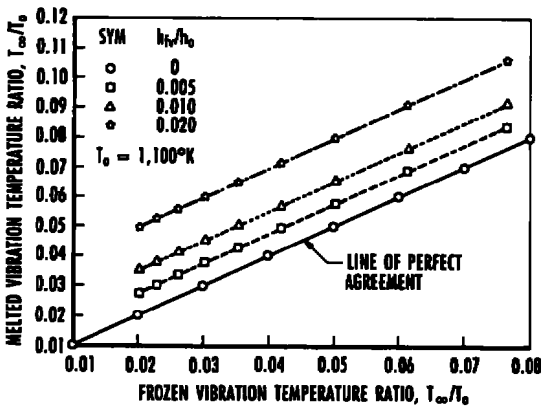

b. Static temperature

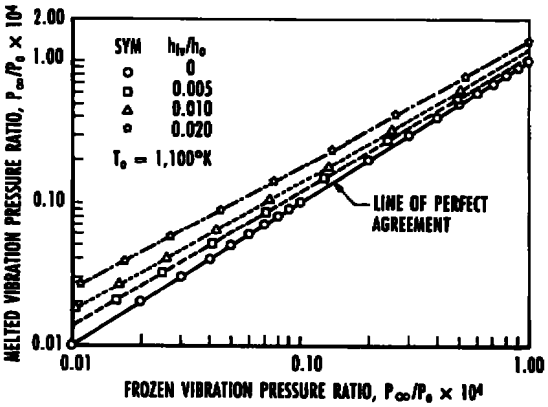

c. Static pressure

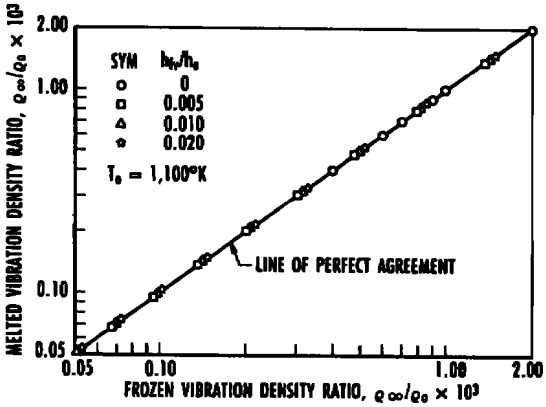

d. Static density
Figure 13. Continued.

It is of interest to review the influence of water vapor on vibrational relaxation phenomena based upon existing knowledge relative to gasdynamic laser applications. It is well known in carbon dioxide-nitrogen-water vapor gasdynamic laser theory[6] that nitrogen has the longest relaxation time of any diatomic molecule and that water vapor is used to

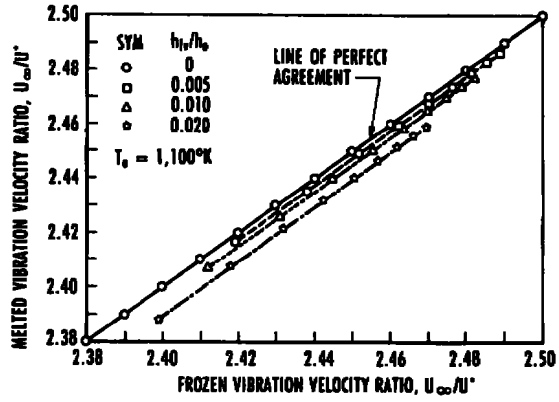

e. Velocity
Figure 13. Concluded.

speed up the slow mode equilibration, thus increasing the population inversion necessary for succesful laser operation. Presented in Fig. 14 are the vibrational relaxation times for nitrogen-water vapor molecules as taken from Appendix B of Anderson.[6] Also shown on this figure is the curve fit for pure nitrogen expansion in supersonic nozzles as recommended by Hall and Treanor.[7] Water vapor reduces the vibrational relaxation times by between two to three orders of magnitude in the temperature range from 1,100 to 670 K. Figure 15 presents the vibrational relaxation times for nitrogen-water vapor mixtures based upon the molecule vibrational relaxation times of Fig. 14 and the "parallel resistance" mixture rule given by Eq. (4.13) in Anderson.[6] Small water vapor content in the mixture (on the order of 1-percent mole fraction) has a strong effect on mixture vibrational relaxation times, especially at the lower temperature. It is not known how this information (for temperatures in the range from 670 to 1,100°K where vibrational freezing occurs) relates to downstream

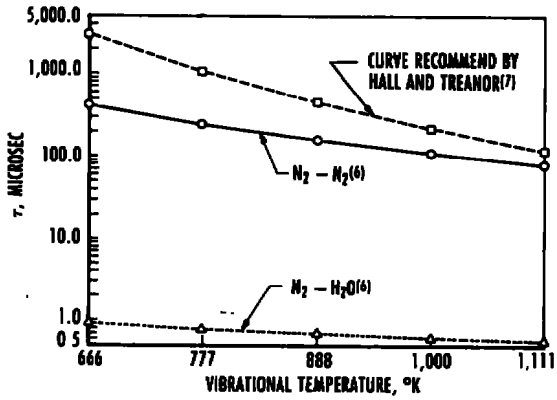

Figure 14. Molecular-molecule vibrational relaxation times (nitrogen gas nozzle expansion).

influence of water vapor on nitrogen gas nozzle ezpansion at hypersonic Mach numbers (where the static temperature is on the order of 28 to 83°K when vibrational melting occurs). However, it suggests the possibility that the presence of water vapor strongly influences the vibrational melting process through enhancement of the vibrational equilibration process.

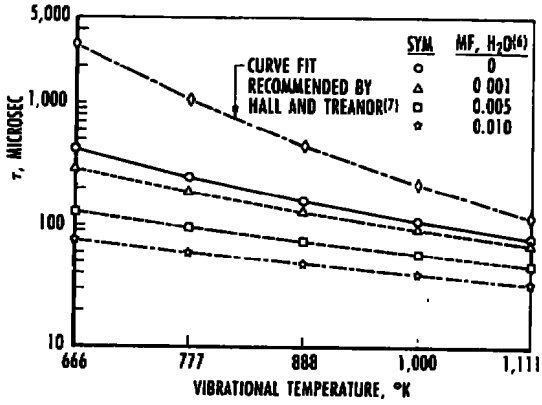

Figure 15. Influence of water vapor content on mixture vibrational relation times (nitrogen gas nozzle expansion).

Example Experiments

The AEDC Tunnel F investigation serves as an excellent example of flow-field characterization because of its depth of analysis and the wide variety of experimental techniques employed. In this section that investigation will be discussed as a practical example of the tools available for flow-field analysis.

It is important to note that the Tunnel F flow field has been characterized in the conventional style previous to the investigation described here. In fact, Tunnel F had operated for 15 years prior to these experiments. In addition to the standard pitot and heat-transfer surveys, sharp-cone models were used to demonstrate the validity of the calibrations. Figures 16 and 17 present some of those results which clearly leave the impression that no problems existed.

Sharp cones, however, are similar to pitot pressure measurements because they are relatively insensitive to entropy changes in the free stream. Hence, the experimentalist obtains a false sense of well being.

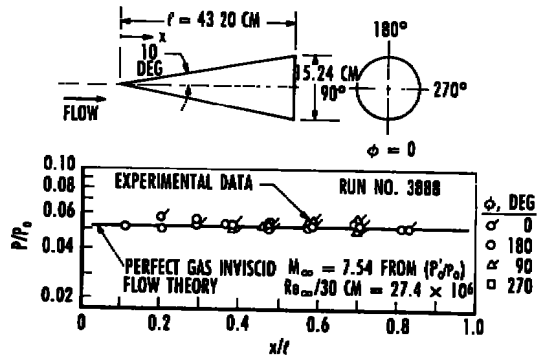

Figure 16. Peripheral pressure measurements on a 10-deg sharp cone (contoured nozzle) in Tunnel F.

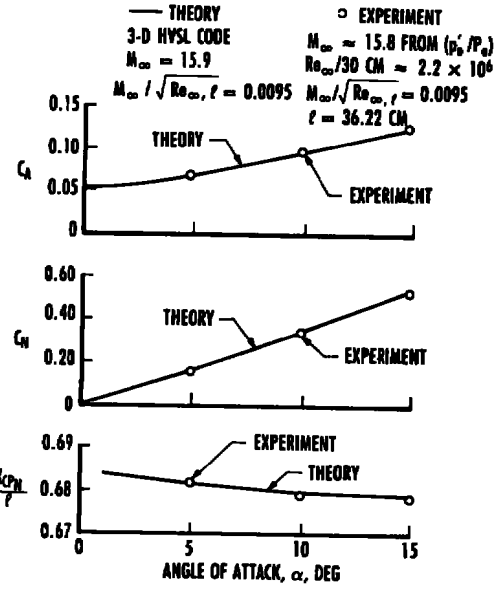

Figure 17. Mach 16 contoured nozzle force results-7-deg half-angle sharp cone.

Blunted, low-angle cones are aerodynamic configurations exhibiting extreme sensitivity to Mach number. Therefore, an r_n/r_b = 0.168, 5-deg half-angle cone was chosen for testing in Tunnel F. As noted in Fig. 18, the model was heavily instrumented with surface pressures and featured three nose pitot measurements for redundancy.

To interpret blunt-cone results, one must obtain high-quality predictions of surface pressure including the viscous-induced contribution. Figure 19 presents some solutions using the reliable Lubard Hypersonic

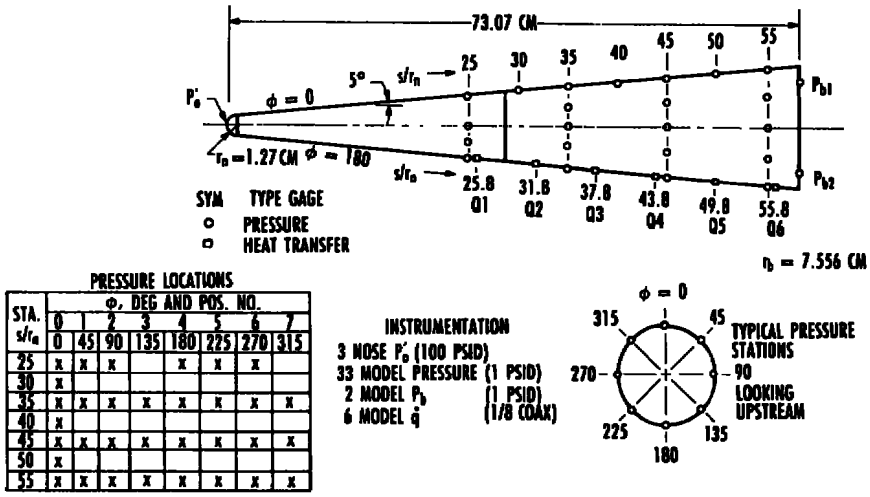

Figure 18. 5-deg cone pressure model.

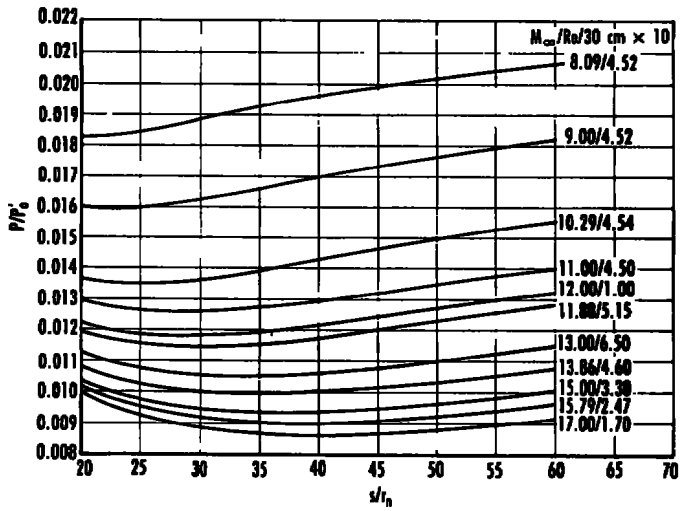

Figure 19. Blunt 5-deg cone solutions using the Lubbard HVSL Code.

Viscous Shock Layer (HVSL) Code. Experimental 5-deg cone measurements are compared to three of these solutions in Fig. 20. Note that the viscous contribution is relatively small at these Reynolds numbers. Hence the high sensitivity of wall pressure to Mach number makes this the best method of experimentally determining free-stream Mach number. In addition, surface pressures are relatively insensitive to changes in the ratio of specific heats, γ. Gamma varies from 1.4 at equilibrium to 1.365 for the $h_v/h_o = 0.01$ frozen case, and the calculated change in surface pressure is 1.3 percent (well within the measurement accuracy of the instrumentation). Since the relaxation (or "melting") process drives γ back to a value near 1.4, the error in surface pressure would be significantly below 1.3 percent, and hence unmeasureable.

The high-quality cone results (Fig. 20) permitted a mapping of the Mach errors present in Tunnel F. Figure 21 compares Mach numbers derived from the cone measurements with those calculated from pitot pressure measurements assuming isentropic relationships. Note that the amount of water vapor in the reservoir clearly influences the Mach error, lending credence to the relaxation hypothesis raised in the previous section. Likewise, the use of a 4-deg half-angle conical nozzle with lower expansion rate also indicates less Mach error.

The rise in free-stream temperature affects Reynolds number as well as Mach number. Hence, the standard Mach-Reynolds number map of wind tunnel performance will show a marked decrease in simulation capabilities as indicated in Fig. 22. The degradation is more severe at higher Mach numbers where the reservoir gas must be heated higher to prevent liquefaction. The higher reservoir temperatures are hypothesized to put more energy into the vibrational mode; hence, more energy is available for the relaxation process.

Of course, one cannot run a large 5-deg cone in the test section when other experiments are underway. Hence, the experimentalists at Tunnel F developed a correlation between measured nozzle

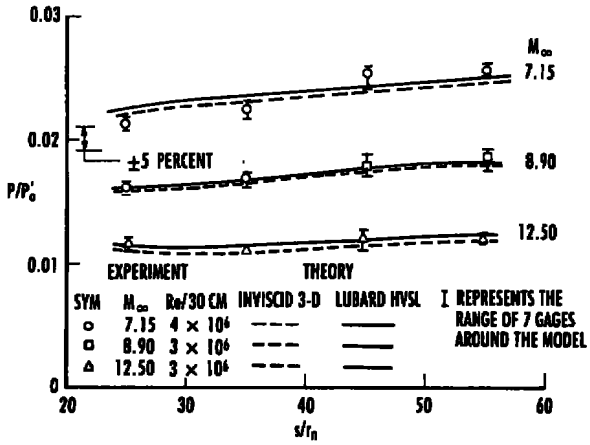

Figure 20. 5-deg blunt cone wall pressure measurements.

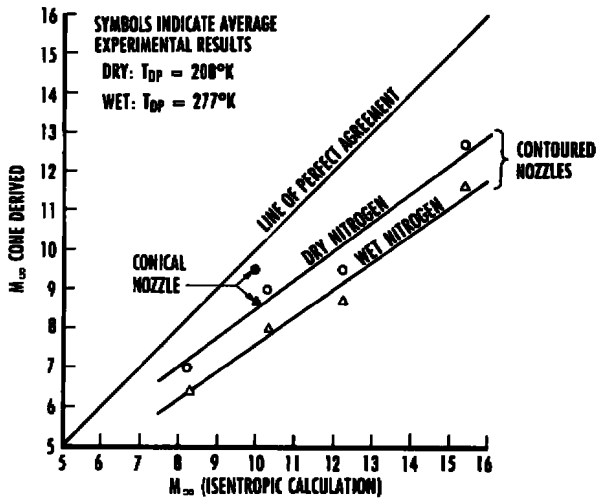

Figure 21. Comparison of mach numbers for Tunnel F.

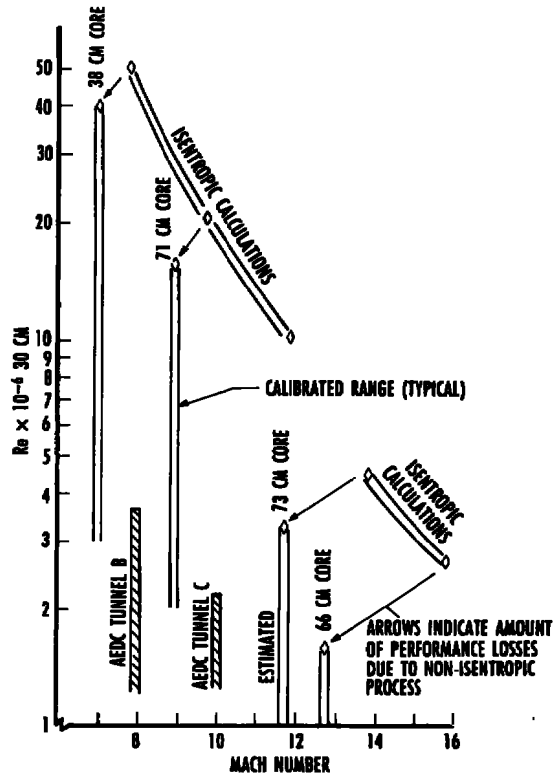

Figure 22. Tunnel F Mach-Reynolds number map.

static pressures (PN) and Mach number determined from the blunt 5-deg cone. That correlation is illustrated graphically in Fig. 23. With a family of such correlations for each nozzle and throat, free-stream conditions could be accurately determined. This method was extremely successful, and Tunnel F subsequently produced data with accuracies comparable to those obtained in AEDC's continuous wind tunnels, i.e., ± 5-percent uncertainty.

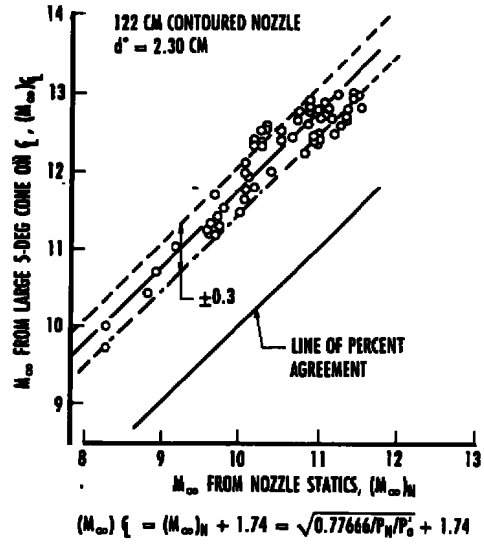

Figure 23. Mach number correclation for Tunnel F.

Other Experimental Methods

Wedges have been used often to check Mach number experimentally. While they may produce useful results, they are clearly inferior in sensitivity compared to a low-angle, blunted cone. Figure 24 compares the percentage change in measured pressure ratios between a wedge and the 5-deg cone used in the Tunnel F experiments. Not only is the blunted cone a factor of two more sensitive, but it eliminates

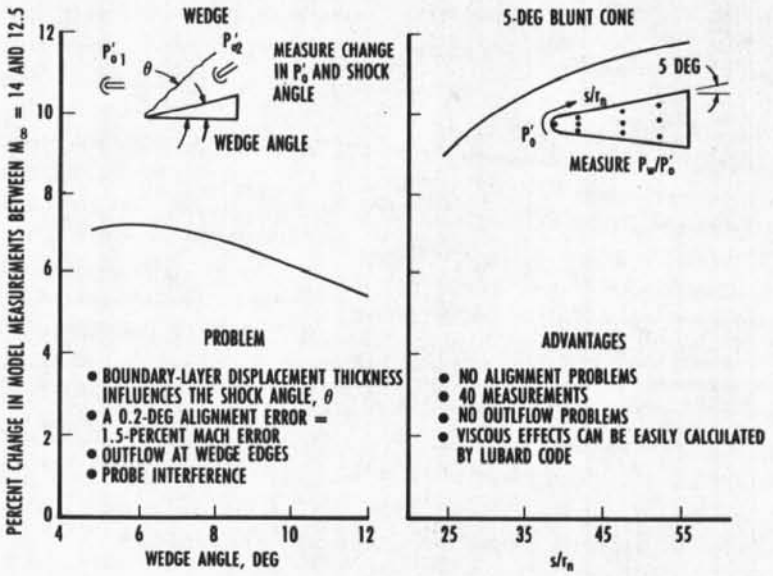

Figure 24. Comparison of a low-angle wedge and a 5-deg cone for determination of Mach number.

many practical problems encountered with the wedge such as viscous sensitivity, alignment sensitivity, outflow problems, and probe interference problems. These can be critical consderations in hypersonic facilities since times are relatively short; hence, instrumentation accuracies are often inferior to those realized in continuous wind tunnels. In short, the factor of two increase in sensitivity may be required simply to make the measurements meaningful.

Free-stream velocity measurements were made in the course of the Tunnel F experiments. Figure 25 illustrates smear photography of free-stream density fluctuations as viewed through a narrow slit on the tunnel window. This extremely simple, yet highly accurate technique essentially produces a distance versus time plot on the film from which velocity is easily calculated. These measurements are compared with calculated velocity in Fig. 26. Note the excellent agreement. This agreement further reinforces the conclusion previously drawn: velocity and density are insensitive to a heat-addition process in the free-stream. The hypothesized relaxation of vibrational energy will be observed primarily as an increase in free-stream temperature and pressure, not a change in velocity.

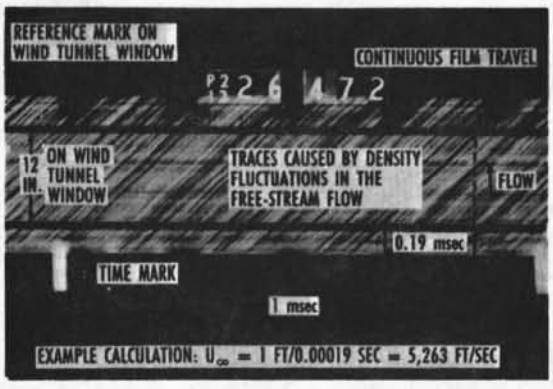

Figure 25. Enlargement of a 16-mm film segment used to determine free-stream velocity in Tunnel F.

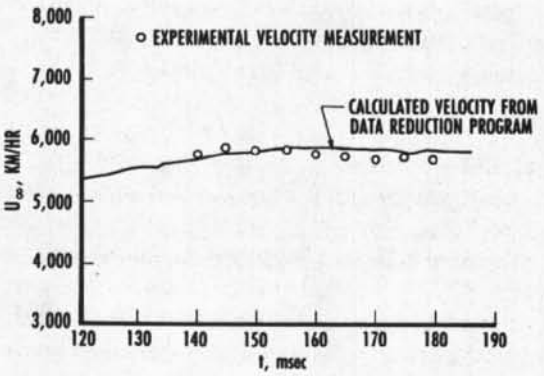

Figure 26. Tunnel F velocity measurements at $M_\infty \approx 12.5$ (run 5604).

This can be shown by considering the equation of state written as

$$P = \varrho RT \text{ or } \varrho = \frac{P}{RT} \qquad (12)$$

But for the heat-addition process in a constant-area duct previously discussed, Eq. (6) yeilds

$$\frac{P_2}{P_1} = \frac{1 + \gamma M_1^2}{1 + \gamma M_2^2} = > 1.25 \qquad (13)$$

for the case $M_1 = 14$ and $M_2 = 12.5$.

Likewise,

$$\frac{T_2}{T_1} = \frac{M_2^2}{M_1^2}\left[\frac{1 + \gamma M_1^2}{1 + \gamma M_2^2}\right]^2 = > 1.25 \qquad (14)$$

Hence,

$$\frac{\varrho_2}{\varrho_1} = \frac{P_1/RT_1}{P_2/RT_2} = \frac{P_1}{P_2}\frac{T_2}{T_1} = 1 \qquad (15)$$

and considering the conservation of mass [Eq. (1)],

$$U_1 = U_2 \qquad (16)$$

Vibrational temperature of the free-stream flow was measured using the Laser-Raman method in both AEDC's Tunnels C and F. The Tunnel C results are more complete and hence are presented here in Fig. 27. They clearly show the sensitivity of vibrational temperature to water vapor content of the free stream. Note that the measured Mach number closely follows the trend in vibrational temperature decay. The Tunnel F results were consistent with the Tunnel C measurements.

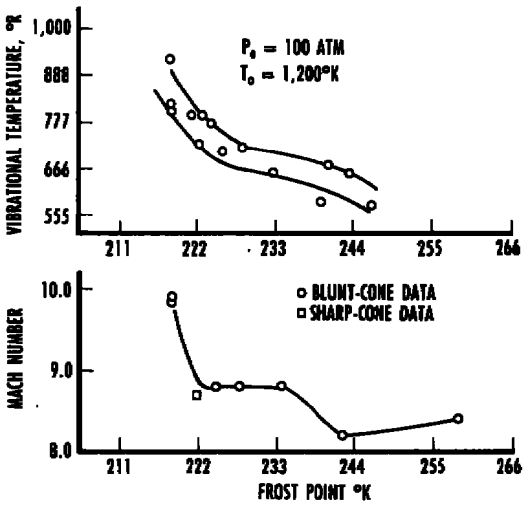

Figure 27. The effect of water vapor on vibrational temperature and M_∞ measured in the test section of AEDC Tunnel C.

In Tunnel F the free-stream flow contained, in addition to water vapor, vaporized copper and tungsten from the arc chamber. These impurities undoubtedly further exacerbate the situation. In general, one should expect nonisentropic processes to be enhanced in proportion to the amount of contamination present in the free stream. As reservoir temperatures increase to satisfy the requirements for hypersonic simulation, clean, unadulterated flow will be increasingly more difficult to produce. Since perfectly clean flow is impossible to achieve in most hypersonic facilities, steps must be taken to account for the inevitable nonisentropic processes. Local test section measurements must be used to characterize free-stream test conditions.

Conclusions

1. Most hypersonic wind tunnels operating at or above Mach 8 appear to suffer a loss of free-stream Mach number because of nonisentropic processes occurring in the expansion nozzles.

2. It is hypothesized that the principal nonisentropic process consists of a rapid, nonequilibrium, vibrational relaxation which raises free-stream temperature and pressure. This relaxation phenomenon is associated with impurities such as water vapor in the free-stream flow which act as third bodies.

3. Theoretical calculations support this hypothesis and suggest that as little as 1 percent of the reservoir enthalpy need be frozen and subsequently released to produce the effects observed.

4. Conventional methods of determining free-stream Mach number (i.e., pitot pressure measurements) are insensitive to such nonisentropic processes and hence are poor indicators of true Mach number. Blunt, low-angle cones, on the other hand, have been shown to be excellent indicators of free-stream Mach number.

Recommendation

The hypersonic wind tunnel testing community should adopt a standard Mach-sensitive model, such as a blunted 5-deg cone, by which all operating and newly calibrated hypersonic facilities can be compared.

References

1. Boudreau, A. H. "Performance and Operational Characteristics of AEDC/VKF Tunnels A, B, and C." AEDC-TR-80-48 (AD-A102614), July 1981.

2. Martellucci, A. Science Applications International, Private Communications, 4 September 1986.

3. Eggers, A. J., Jr. "One Dimensional Flows of an Imperfect Diatomic Gas." NACA Report 959, 1950.

4. Shapiro, A. H. The Dynamics and Thermodynamics of Compressible Fluid Flow. Vol. 1, Ronald Press, New York, 1953.

5. Erickswon, W. D. "Vibrational-Nonequilibrium Flow of Nitrogen in Hypersonic Nozzles." NASA TN D-1810, June 1963.

6. Anderson, J. D., Jr. *Gasdynamic Lasers: An Introduction*. Academic Press, New York, 1976.

7. Hall, J. G. and Treanor, C. E. "Nonequilibrium Effects in Supersonic Nozzle Flows." CAL Report No. CAL-163, March 1968.